JOINT TRANSPORTATION
RESEARCH PROGRAM
INDIANA DEPARTMENT OF TRANSPORTATION
AND PURDUE UNIVERSITY

Removing Obstacles for Pavement Cost Reduction by Examining Early Age Opening Requirements: Material Properties

Federico C. Antico, Hadi S. Esmaeeli, Igor De la Varga, Wesley Jones,
Timothy Barrett, Pablo Zavattieri, W. Jason Weiss

SPR-3403 • Report Number: FHWA/IN/JTRP-2015/18 • DOI: 10.5703/1288284316003

RECOMMENDED CITATION

Antico, F. C., Esmaeeli, H. S., De la Varga, I., Jones, W., Barrett, T., Zavattieri, P., & Weiss, W. J. (2015). *Removing obstacles for pavement cost reduction by examining early age opening requirements: Material properties* (Joint Transportation Research Program Publication No. FHWA/IN/JTRP-2015/18). West Lafayette, IN: Purdue University. http://dx.doi.org/10.5703/1288284316003

AUTHORS

Federico C. Antico
Graduate Research Assistant
Lyles School of Civil Engineering, Purdue University

Hadi S. Esmaeeli
Graduate Research Assistant
Lyles School of Civil Engineering, Purdue University

Igor De la Varga
Graduate Research Assistant
Lyles School of Civil Engineering, Purdue University

Wesley Jones
Graduate Research Assistant
Lyles School of Civil Engineering, Purdue University

Timothy Barrett
Graduate Research Assistant
Lyles School of Civil Engineering, Purdue University

Pablo Zavattieri, PhD
Associate Professor of Civil Engineering
Lyles School of Civil Engineering, Purdue University

W. Jason Weiss, PhD
Jack and Kay Professor of Civil Engineering and
Director of Pankow Materials Laboratory
Lyles School of Civil Engineering, Purdue University
(541) 737-1885
jasonweiss99@gmail.com
Corresponding Author

JOINT TRANSPORTATION RESEARCH PROGRAM

The Joint Transportation Research Program serves as a vehicle for INDOT collaboration with higher education institutions and industry in Indiana to facilitate innovation that results in continuous improvement in the planning, design, construction, operation, management and economic efficiency of the Indiana transportation infrastructure. https://engineering.purdue.edu/JTRP/index_html

Published reports of the Joint Transportation Research Program are available at: http://docs.lib.purdue.edu/jtrp/

NOTICE

COPYRIGHT

Print ISBN: 978-1-62260-368-8
ePUB ISBN: 978-1-62260-369-5

TECHNICAL REPORT STANDARD TITLE PAGE

1. Report No.	2. Government Accession No.	3. Recipient's Catalog No.
FHWA/IN/JTRP-2016/18		

4. Title and Subtitle	5. Report Date
Removing Obstacles for Pavement Cost Reduction by Examining Early Age Opening Requirements: Material Properties	August 2015
	6. Performing Organization Code

7. Author(s)	8. Performing Organization Report No.
Federico C. Antico, Hadi S. Esmaeeli, Igor De la Varga, Wesley Jones, Timothy Barrett, Pablo Zavattieri, W. Jason Weiss	FHWA/IN/JTRP-2016/18

9. Performing Organization Name and Address	10. Work Unit No.
Joint Transportation Research Program Purdue University 550 Stadium Mall Drive West Lafayette, IN 47907-2051	11. Contract or Grant No. SPR-3403

12. Sponsoring Agency Name and Address	13. Type of Report and Period Covered
Indiana Department of Transportation State Office Building 100 North Senate Avenue Indianapolis, IN 46204	Final Report
	14. Sponsoring Agency Code

15. Supplementary Notes
Prepared in cooperation with the Indiana Department of Transportation and Federal Highway Administration.

16. Abstract

The risk of cracking in a concrete pavement that is opened to traffic at early ages is related to the maximum tensile stress, σ_1, that develops in the pavement and its relationship to the measured, age dependent, flexural strength of a beam, f_r. The stress that develops in the pavement is due to several factors including traffic loading and restrained volume change caused by thermal or hygral variations. The stress that develops is also dependent on the time-dependent mechanical properties, pavement thickness, and subgrade stiffness. There is a strong incentive to open many pavements to traffic as early as possible to allow construction traffic or traffic from the traveling public to use the pavement. However, if the pavement is opened to traffic too early, cracking may occur that may compromise the service life of the pavement. The purpose of this report is two-fold: 1) to examine the current opening strength requirements for concrete pavements (typically a flexural strength from beams, f_r) and 2) to propose a criterion based on the time-dependent changes of σ_1/f_r which accounts for pavement thickness and subgrade stiffness without adding unnecessary risk for premature cracking. An Accelerated Pavement Testing, APT, facility was used to test concrete pavements that are opened to traffic at an early age to provide data that can be compared with an analytical model to determine the effective σ_1/f_r based on the relevant features of the concrete pavement, the subgrade, and the traffic load. It is anticipated that this type of opening criteria can help the decision makers in two ways: 1) it can open pavement sections earlier thereby reducing construction time and 2) it may help to minimize the use of materials with overly accelerated strength gain that are suspected to be more susceptible to develop damage at early ages than materials that gain strength more slowly.

17. Key Words	18. Distribution Statement
accelerated pavement testing, concrete pavement, cracking, early age concrete, opening criteria	No restrictions. This document is available to the public through the National Technical Information Service, Springfield, VA 22161.

19. Security Classif. (of this report)	20. Security Classif. (of this page)	21. No. of Pages	22. Price
Unclassified	Unclassified	44	

Form DOT F 1700.7 (8-69)

EXECUTIVE SUMMARY

REMOVING OBSTACLES FOR PAVEMENT COST REDUCTION BY EXAMINING EARLY AGE OPENING REQUIREMENTS: MATERIAL PROPERTIES

Introduction

The risk of cracking in a concrete pavement that is opened to traffic at early ages is related to the maximum tensile stress, σ_I, that develops in the pavement and its relationship to the measured, age-dependent, flexural strength of a beam, f_r. The pavement stress that develops is due to several factors, including traffic loading and restrained volume change caused by thermal or hygral variations, and also depends on time-dependent mechanical properties, pavement thickness, and subgrade stiffness. There is a strong incentive to open pavements to traffic as early as possible for both construction traffic and the traveling public. However, if pavement is opened to traffic too early, cracking may occur that may compromise the service life of the pavement. The purpose of this report is twofold: (1) to examine the current opening strength requirements for concrete pavements (typically a flexural strength from beams, f_r) and (2) to propose a criterion based on the time-dependent changes of σ_I/f_r which accounts for pavement thickness and subgrade stiffness without adding unnecessary risk for premature cracking. An accelerated pavement testing (APT) facility was used to test concrete pavements that are opened to traffic at an early age to provide data that can be compared with an analytical model to determine the effective σ_I/f_r based on the relevant features of the concrete pavement, the subgrade, and the traffic load. It is anticipated that this type of opening criteria can help decision makers in two ways: (1) it can open pavement sections earlier, thereby reducing construction time, and (2) it may help to minimize the use of materials with overly accelerated strength gain that are suspected to be more susceptible to developing damage at early ages than materials that gain strength more slowly.

Findings

This work examined the criteria that should be used to determine when a concrete pavement can be opened to traffic. The risk of cracking is estimated based on the ratio between the maximum tensile stress developed beneath the wheel and the flexural strength of the concrete (σ_I/f_r). The importance of pavement thickness (h), subgrade reaction modulus (k), time-dependent elastic modulus ($E(t)$), and time-dependent flexural strength (f_r) of the concrete pavement are discussed in relation to the risk of cracking. The theoretical estimation of the maximum stress that develops in the pavement, σ_I, is compared with experimental results obtained from full-scale concrete pavement sections tested at the APT.

The experimental results indicate that when the typical INDOT opening to traffic criterion is used for 10-inch concrete pavement (flexural strength of $f_r = 550\ psi$), the stresses that develop in the pavement are at most 20% of the flexural strength. A similar observation was made for the 10-inch-thick pavement opened to traffic when the flexural strength was 350 psi with the stress-to-strength ratio reaching only 30% of the flexural strength. For thinner concrete pavements (5 inches thick), opening at flexural strength values of 275 psi, 350 psi, and 550 psi resulted in stress-to-strength ratios of 1.09, 0.86, and 0.54, respectively. While a single flexural strength may be the simplest to specify, the results of this study indicate that allowing thicker pavements to be opened at a lower strength may not add substantial risk of cracking due to traffic loading.

Simulations were performed to consider pavements with thickness between 8- and 16-inch depths and different subgrade stiffness between 50 and 400 lb/in^3, and it was determined that traffic loading resulted in stress that was less than 20% of the flexural strength ($\sigma_I/f_r < 0.2$) for any pavement that was more than 10 inches thick (i.e., $h \geq 10$ in). It was observed that the rate of elastic modulus development ($E(t)$) is inversely related to the stress development caused by traffic loading. This implies that stiffer concrete pavement will develop a higher stress. The subgrade stiffness also influences the stress that develops in the concrete pavement, with a greater impact on thinner pavements. It was also observed that the shape of the footprint of the wheel has a minor impact on the estimated stress and strain. On the other hand, considering a perfect bonding condition underestimates the strain development while the frictionless condition has good agreement with experimental measurements of strain due to traffic loading.

CONTENTS

LIST OF TABLES

LIST OF FIGURES

1. INTRODUCTION

1.1 Summary

The risk of cracking in a concrete pavement that is opened to traffic at early ages is related to the maximum tensile stress, σ_I, that develops in the pavement and its relationship to the measured, age-dependent, flexural strength of a beam, f_r. The stress that develops in the pavement is due to several factors, including traffic loading and restrained volume change caused by thermal or hygral variations. The stress that develops is also dependent on the time-dependent mechanical properties, pavement thickness, and subgrade stiffness. There is a strong incentive to open many pavements to traffic as early as possible to allow construction traffic or traffic from the traveling public to use the pavement. However, if the pavement is opened to traffic too early, cracking may occur that may compromise the service life of the pavement. The purpose of this report is twofold: (1) to examine the current opening strength requirements for concrete pavements (typically a flexural strength from beams, f_r) and (2) to propose a criterion based on the time-dependent changes of σ_I/f_r which accounts for pavement thickness and subgrade stiffness without adding unnecessary risk for premature cracking. An accelerated pavement testing (APT) facility was used to test concrete pavements that are opened to traffic at an early age to provide data that can be compared with an analytical model to determine the effective σ_I/f_r based on the relevant features of the concrete pavement, the subgrade, and the traffic load. It is anticipated that this type of opening criteria can help the decision makers in two ways: (1) it can open pavement sections earlier thereby reducing construction time and (2) it may help to minimize the use of materials with overly accelerated strength gain that are suspected to be more susceptible to develop damage at early ages than materials that gain strength more slowly.

This report is divided into eight chapters, including this introduction. Chapter 2 provides a literature review on loading conditions and opening criteria for DOTs and strength development for ready-mix concrete pavements. Chapter 3 presents the experimental program design for this project. Chapter 4 presents an analytical approach for determination of the flexural tensile stress of concrete pavements. Chapter 5 presents a description of a numerical model developed to contrast with the analytical model presented in chapter 4. Chapter 6 presents a proposed numerical model to address early age damage of concrete under restraint conditions. Chapter 7 presents a study of the changes in crack pattern due to changes in degree of hydration (DOH) at early ages. Finally, conclusions and recommendations of this work are presented in chapter 8.

1.2 Background and Problem Statement

When does a pavement develop sufficient strength so that it may be safely opened to traffic? If a pavement is opened to traffic too early the pavement can develop cracks (either visible cracks or invisible microcracks) that result in premature deterioration and shorten the service life of the pavement. If the pavement is opened too late construction delays can result or costly haul roads may be required.

Insuring that the pavement is sufficiently strong before it is open to traffic can result in pavement opening requirements that may overemphasize the need for high early-age concrete strength. This requirement for high early-age strength can delay opening, result in mixtures that optimize performance during the first few days (rather than long-term performance), result in higher pavement costs, and/or reduce the potential for using 'greener' materials (materials with lower CO_2 per cubic yard). Further, it is believed that the high early-age strength requirements can ultimately lead to materials that exhibit higher heats of hydration which may result in increased curling, cracking, and more brittle behavior at later ages. In addition, pavements with high early-age strength may not behave as designed at construction joints leading to premature deterioration.

Currently contractors in Indiana are developing concrete mixtures that gain strength very rapidly to enable these mixtures to be opened to traffic at very early ages. Unfortunately, this leads to pavements that can gain 90% to 95% of their ultimate tensile strength by 18 to 24 hours. This results in pavements that are very brittle at later ages. For example, several mixtures from around the Indianapolis area tend to show that after 18 hours the cracks propagate through the aggregate (Barde, Mozzotta, & Weiss, 2005). This high early strength results in reduced strength gain at later ages and reduced aggregate interlock which reduces the ability to transfer stress across the joint. Further, these pavements have a tendency to crack away from the saw-cuts and longitudinal joints as they are designed to since they gain strength so rapidly. This can lead to random cracking and recent research has suggested that joints that do not crack can accelerate joint deterioration at a later age (Altoubat & Lange, 2001). Research is needed to better understand how design criteria, construction operations, and mixture proportions can be best interrelated to provide cost savings with improved long-term performance.

For example, the reduction in the amount of cement implemented by a specification revision in 2009 may not be fully used because contractors are more concerned with the opening to traffic strength, due to the potential impact on the rate of work that can occur on the project. A reduction in the cost of materials and an improvement in the quality of the concrete may be realized with this reduction of opening to traffic strength.

This research examines the current INDOT requirements for opening a pavement to traffic or for use as a haul road. Specifically, it is believed that changes over the last several decades in the thickness of the pavement sections, the reactivity of the materials used, and the construction speed could enable these opening criteria to be re-evaluated. Improved opening requirements

could result in substantial improvements in the long-term durability performance of the pavement.

1.3 Research Objectives

This project examines early-age concrete pavement opening requirements as they relate to optimizing pavement construction processes. Specifically, the project will examine the role of pavement strength on the time at which the pavement should be opened to traffic. Currently the general rule of thumb is that the stress in the concrete should be kept below 50% of the strength to avoid the potential for fatigue cracking or micro-cracking. Specifically this research will examine the factors surrounding when a pavement can be opened to traffic focusing on:

1. Examining the loading conditions that the concrete is likely to see from environmental loading, construction traffic or public traffic at early ages.
2. Conducting a review of the opening criteria used by other states and the concepts used to develop these values.
3. Using the non-linear fracture based model that considers the effects of material aging and loading on the potential for cracking.
4. Determining the risk of cracking or pavement damage associated with opening to traffic over a range of flexural strengths. This risk data will be used in the evaluation of the current 550 psi specification and the appropriateness of using an alternative opening to traffic criteria.

When completed this research will enable contractors to better time construction operations (i.e., the potential to accelerate construction through material selection or more efficiently time construction operations), reduce the cost of materials and construction (i.e., the potential to reduce construction costs with more efficient use of the most costly materials), and incorporate the sustainable use of materials (i.e., enabling the increased use of recycled, 'greener' and more cost effective materials).

2. LITERATURE REVIEW

2.1 Introduction

At early ages concrete pavements are exposed to loading coming from: (1) construction or user traffic, (2) autogenous and thermal volume changes coming from the hydraulic reaction, and (3) shrinkage and thermal volume changes caused by environmental variations in humidity and temperature. If the stresses caused by these loads are sufficiently high (as compared to the time-dependent strength of concrete) they can impact the potential for cracking. A general rule of thumb is that if the maximum tensile stress remains below 50% of the tensile strength f_r, the concrete can be considered to behave as linear elastically (AASHTO, 2013; ACI Committee 215, 1974; Bangash, 2001) with only limited microcracking. However if the maximum tensile stress exceeds 50% of f_r more substantial microcracking can occur that can lead to nonlinear behavior and fatigue susceptibility which may result in this damage developing over time reducing the service life of the concrete (Lee, Daniel, & Kim, 2000; Rajan, Olek, & Robertson, 2001).

Over the last several decades the rate of strength development of concrete paving mixture has increased (Kosmatka, Panarese, Allen, & Cumming, 2002). This can occur due to an increase in cement content, reduced water to cement ratio (w/c), and the cement being more finely ground (Shah, Wang, & Weiss, 2000; Shah & Weiss, 2000; Shah, Yang, & Weiss, 1998; Weiss, Yang, & Shah, 1998). Higher alkali contents and changes in the relative proportions of the calcium silicate which have increased the proportion tricalcium silicate (when compared to dicalcium silicate) are also frequently suggested to be responsible for the increase of the rate of the strength development. At the same time many DOTs and contractors have worked to develop mixtures with higher early strength to reduce the time it takes to open concrete pavements to traffic, thus reducing the impact of construction delays on the traveling public. As such, it is not uncommon to see concrete mixtures that gain more than 50% of their strength within the first several hours to a day after placement (Wang & Li, 2006). For example, a typical paving mixture in the state of Indiana may develop 60% of its 90 day strength after 18 hours and 90% of its strength after 28 days (Graveen, Falker, Beaver, Weiss, & Gallivan, 2009).

However, the use of concrete with a higher early-age strength can result in higher pavement costs (due to the use of higher cement contents), reduced strength gain at later ages, increased potential for aggregate fracture thus reducing aggregate interlock which helps to transfer stress across the joint (Aïtcin, 2011), and reduced the potential of using mixtures/pavements with lower carbon footprint (Mehta, 2002). Further, pavements that have higher early strengths might be less prone to crack as designed at saw-cuts and longitudinal joints (Raoufi, Their, Weiss, Olek, & Nantung, 2009). This may lead to random cracking (Wiegrink, Marikunte, & Shah, 1996) or joints that do not crack and hold moisture resulting in potential durability issues affecting the life span of the material (Golias et al., 2012).

2.2 Loading Conditions and Opening Criteria

Pavement design theory is based on flexural stress. As a result, it is more common for Agencies to use flexural strength, f_r, as an opening-to-traffic criteria rather than tensile strength, f_r. Two things need to be remembered at this point, neither f_r nor f_r extracted from tests represent the real strength of concrete and second, the geometry of the sample as well as the material affect the computed strength. For quasibrittle materials, like concrete, these two things are gathered in the so-called brittleness number which accounts for characteristic structural dimension and the characteristic material size; both of these are different for different structural types and loadings (Bazant & Planasm, 1997; Hillerborg, Modéer, & Petersson, 1976; Maalej & Li, 1994). Hillerborg et al. (1976) showed that the ratio f_r/f_r of unreinforced concrete

depends on the ratio between the beam depth (H) and the critical crack depth (l_c); ranging from $2 < f_r/f_t < 1$ for $H/l_c \rightarrow 0$ and $H/l_c < 5$ respectively. For a typical bending test specimen (typical ASTM standard testing geometry) f_r/f_r ranges from 1.0 to 1.2 (ASTM C78/C78M-10, 2013).

In the Midwest region, the Departments of Transportation from Michigan (MDOT), Indiana (INDOT) and Illinois (IDOT) define a critical value of flexural strength f_r of 500 psi (3.5 MPa), 550 psi (3.8 MPa) and 600 psi (4.1 MPa) respectively for the time for opening to traffic (Van Dam et al., 2004). However it should be noted that the INDOT requirement of f_r is equivalent to the strength of a simple beam with third-point loading, while MDOT and IDOT requirements of f_r are equivalent to the strength of a simple beam with center point loading. For the same concrete material, the f_r obtained from third-point loading is approximately 15% lower than those from a center-point loading due to the potential for a flaw associated to an extended area subject to damage between loading points (Lamond & Pieler, 2006; Zollinger & Barenberg, 1989). This would imply that the INDOT has the highest opening strength with an estimated value of 630 psi. Research is needed to better understand how design criteria, construction operations, and mixture proportions are related to long-term performance. This work examines the current INDOT requirements for opening a pavement to traffic or for use as a haul road for construction traffic. Specifically, it is believed that changes over the last several decades in the specifications of pavement thickness, the reactivity of the new materials, and the construction speed could enable these opening criteria to be reevaluated. Reexamine opening requirements could result in substantial improvements in the long-term durability performance of the pavement and cost savings in mixture design.

The APT facility of the INDOT Research Division in West Lafayette, Indiana was used in this research (Galal & White, 1999; Saeed & Hall, 2003). This experimental apparatus enables concrete pavements to be loaded with simulated traffic conditions in an environmentally controlled facility.

3. EXPERIMENTAL PROGRAM

3.1 APT Description

The INDOT APT facility is located at the INDOT Research Division in West Lafayette, IN. The APT is housed in an approximately 2,000 ft.^{2} (185 m^2) environmentally controlled building. The APT facility is composed of a testing pit area of 20 feet (6.1 m) wide by 20 feet (6.1 m) long by 6 feet (1.8 m) deep, a loading mechanism, and control and monitoring equipment. The APT carriage (Figure 3.1a) can be equipped with either a full-size, dual-tire truck wheel or a super-single, half-axle assembly (Galal & White, 1999; Saeed & Hall, 2003). The tire can be inflated at various pressures. This setup allows speeds up to 5 mph (8 km/h). The APT loading mechanism uses a system of four air pistons

Figure 3.1 (a) APT carriage; (b) concrete pavement ready to be loaded.

that maintain a constant force up to 20,000 lb. (89 kN). This load can be programmed either in static or dynamic modes. These cylinders also allow the wheels to be raised and returned to the start-up position of the test pad if used in one direction type of testing.

3.2 Mixture Design and Materials

The concrete mixture design chosen was that of a typical concrete pavement used in several sections of the SR-26 in Lafayette, Indiana. The concrete had a water-to-cement ratio (w/c) of 0.42 and 23% of Class C fly ash (by mass) replacing the cement fraction. The fine and coarse aggregates consisted of #23 and #8, respectively, according to INDOT aggregates size specifications. Table 3.1 shows the mixture proportions:

3.3 Maturity Method

The maturity method is frequently used by the construction industry to predict the in-place strength of cementitious materials (Carino, 1991). This is very useful in operations like opening a concrete pavement to traffic or removing the formwork. The concept of the maturity method is based on the idea that strength development in concrete is related to the extent of hydration reaction of the cement and other cementitious materials. This hydration reaction is a function of time and temperature; therefore it is frequently assumed that there is a relationship between strength and the

TABLE 3.1
Mixture proportions for the concrete.

Ingredient	Weight (lb.)	Specific Gravity in SSD	Volume (ft.^{3})
Type I Cement	440	3.15	2.24
Class C Fly Ash	100	2.60	0.62
Fine Aggregate	1412	2.66	8.51
Coarse Aggregate	1750	2.74	10.25
Water	226	1.00	3.62
Air Entrainer	0.125z–4.0 (oz/wct)	—	—
Water Reducer	1.0–3.0 (oz/wct)	—	—
Air	—	—	1.76
TOTAL	3928	—	27.00

product of time and temperature (i.e., time-temperature factor, or TTF).

The flexural strength of the concrete used in this research was determined by means of the maturity method in accordance with ASTM C1074 (Estimating Concrete Strength by the Maturity Method). In this research, the maturity index selected was TTF. Three 6-in (152 mm) wide, 6-in. (152 mm) deep, and 21-in. (533 mm) long concrete beam specimens were tested at five different testing ages (10, 16, 24, 36, and 48 hours). The reason why flexural strength was chosen rather than compressive strength (as stated in ASTM C1074) was due to the mode of failure typically observed in a concrete pavement (i.e., flexural failure at the bottom of the concrete pavement). The temperature history of the specimens was recorded every 5 min from the time of concrete casting by means of thermocouples inserted in the beam specimens. The temperature history is used to calculate the maturity index (i.e., TTF) of the concrete as shown in equation **(1)**:

$$TTF(t) = \sum (T_a - T_0)\Delta t \quad (1)$$

where $TTF(t)$ is the time-temperature factor at age t (degree-hour), Δt is a time interval (h), T_a is the average concrete temperature during the time interval Δt (°C), and T_0 is the datum temperature (°C) taken as -10 °C.

The TTF of the concrete was then determined at each of the testing ages and a plot of the average flexural strength as a function of the logarithm of TTF was made. The resulting curve is fitted to a linear equation used to estimate the TTF at each desired concrete strength (e.g., 550 psi). Knowing the strength-TTF relationship, the strength of the concrete pavement placed at the APT can be estimated by measuring the concrete temperature at all times, and multiplying it by the time. When the particular TTF is reached, the concrete was assumed to have the desired flexural strength.

3.4 Plan of Work and Cross Sections

Four concrete pavements were constructed in the APT using the same concrete mixture design mentioned in Table 3.1. Two different variables were intended to be evaluated: (1) traffic opening time based on the concrete strength, and (2) pavement thickness. The traffic opening times were determined by means of the maturity method described in the previous section.

TABLE 3.2
Summary of the tests performed in this research.

Concrete Lane #	Traffic Opening Time (based on concrete strength)	Thickness
1	18 hours (550 psi [3.8 Mpa])	10 in. (254 mm)
2	13 hours (350 psi [2.4 Mpa])	10 in. (254 mm)
3	13 hours (350 psi [2.4 Mpa])	5 in. (127 mm)
4	8 hours (275 psi [1.9 Mpa])	5 in. (127 mm)

Table 3.2 summarizes the information of each of the concrete pavements tested in this research.

For the 5 in. (254 mm) concrete pavements, an extra 5 in. (127 mm) layer of #23 aggregate had to be added before pouring the concrete pavement, having a final thickness of 8 in. (203 mm). Each layer (except for the concrete) was compacted using a vibration plate compactor machine. Figure 3.2 shows the cross sections used in this research based on the concrete pavement thickness.

Lanes 1 and 2 had a thickness of 10 in. (254 mm), a length of 20 ft. (6 m) and a width of 10 ft. (3 m) each (see Figure 3.3), whereas the two other pavements (Lanes 3 and 4) were 5 in. (254 mm) thick, 20 ft. (6 m) long, and 6.6 ft. (2 m) wide.

3.5 Pavement Instrumentation

Once the aggregate base layers were compacted, the instrumentation for the pavement was placed. This consisted of: (1) strain gages for measuring instantaneous and permanent deformations, (2) thermocouples for measuring concrete temperature, and (3) dowel bars and basket for transferring stresses from one side of the joint to the other.

The strains were measured using embedment gages (Texas Measurement PML-120-2L). The gages were installed in the concrete pavements 1 in. (25.4 mm) below the top surface and at 1 in. (25.4 mm) from the bottom (see Figure 3.4). The exact location of the gages was determined after testing was completed for use in calculations. The gages were oriented in either the longitudinal or transverse direction (in relation to the movement of the APT carriage). The strain gages were

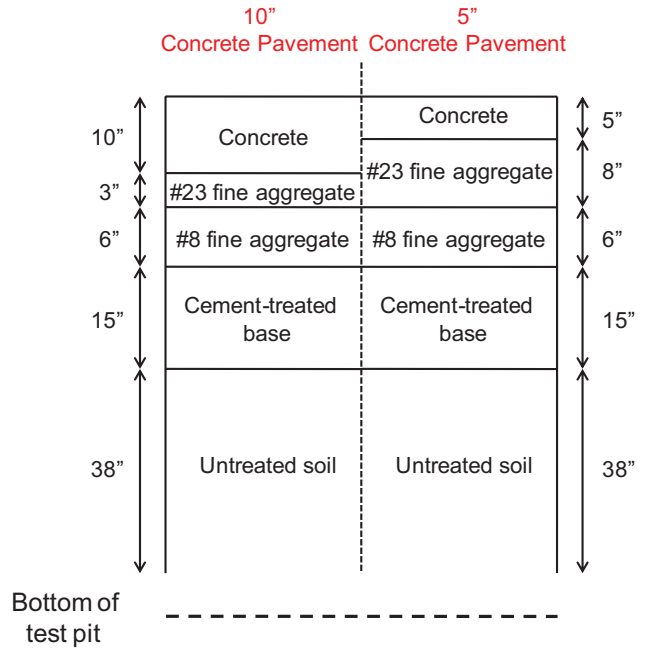

Figure 3.2 Cross sections used: (a) 10 in. (254 mm) concrete pavement; (b) 5 in. (127 mm) concrete pavement.

Figure 3.3 Setup of the two 10 in. (254 mm) thick concrete pavements (Lanes #1 and #2).

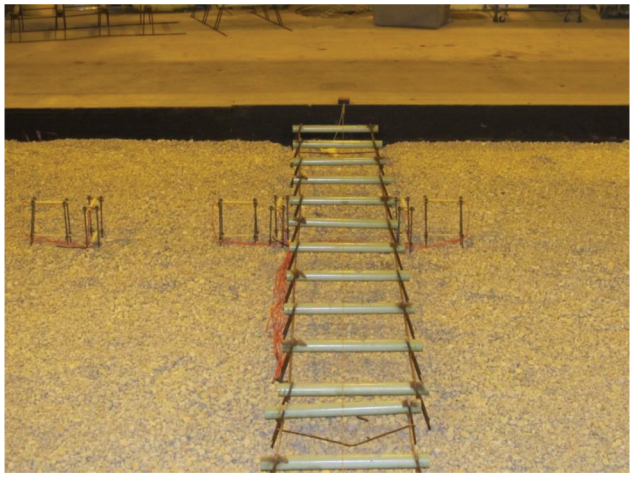

Figure 3.5 Dowel bars, basket, and strain gages installed in one of the concrete pavements prepared in this research.

connected to a data acquisition system (System 6000 manufactured by Vishay Measurements Group) to collect the strain data as a function of time. The thermocouples were placed at varying depth to measure the temperature throughout the cross section of the concrete. A layout of the pavements instrumentation is shown in Figure 3.5.

3.6 Concrete Delivery and Experimental Procedures

As already mentioned, the concrete was delivered by a local ready mix company in 9 $yd.^3$ concrete trucks at the different dates of testing (see section 4.2). Upon arrival of the concrete, a series of test methods were carried out, as well as the preparation of concrete specimens for strength and material characterization. The following sections summarize the test procedures executed for the material characterization.

3.6.1 Slump Test

Upon arrival of the concrete truck, the concrete slump was measured according to ASTM C143 (see Figure 3.6).

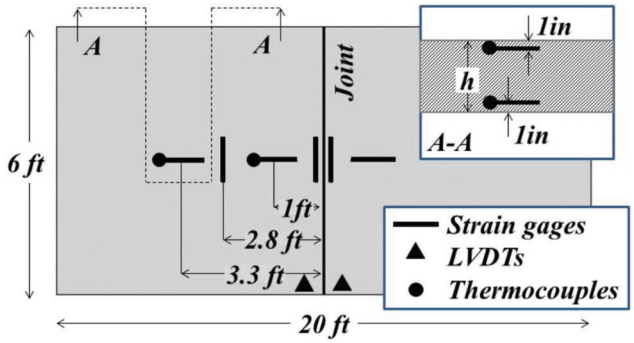

Figure 3.4 A schematic illustration showing the location of the thermocouples, and pairs of longitudinal and transverse strain gages (at the top and the bottom of the pavement) with respect to the transit direction in a 6.6 ft. (2 m) wide concrete pavement.

A slump of 5 in. was targeted for the acceptance of the concrete.

3.6.2 Time of Set

The time of set was measured according to the procedure described in ASTM C403. The resistance of the fresh mortar fraction of the concrete against standard needles with different sizes (1.0, 0.5, 0.25, 0.10, 0.05, and 0.025 $in.^2$) was measured. The needles were placed in a standard penetrometer provided with an analog gage. The fresh mortar was casted in 6×6 in. (153×153 mm) cylindrical molds. Two specimens were used. Initial and final setting times were determined when the resistance reaches 500 and 4000 psi, respectively.

3.6.3 Compressive Strength

Three 4 by 8 in. (102 mm by 204 mm) cylindrical specimens were prepared and tested in accordance with ASTM C39. The specimens were maintained in the molds at the APT for 24 h, moment at which they were demolded. Following demolding, all specimens were sealed in plastic bags and stored in an environmental chamber at a temperature of 23 °C $\pm$ 0.5 °C (73.4 °F $\pm$ 0.9 °F). The cylinders were then tested at several ages: 1, 3, 7, 14, and 28 d.

3.6.4 Static Elastic Modulus

Two of the three specimens prepared for the compressive strength evaluation at each age were used to measure the elastic modulus according to ASTM C469-02. The elastic modulus measurement is based on the theory that the concrete remains in an elastic regime if loaded up to approximately 40% of its ultimate compressive strength at each age. As such, prior to testing the elastic modulus, the compressive strength of a companion specimen was measured. Then, the other two cylinders were fixed in a compressometer provided

Figure 3.6 Slump test performed for quality control.

with an LVDT to measure longitudinal (vertical) deformations. The cylinders were loaded three times at a rate of 35 psi/sec. The following measurements were taken: the load corresponding to a longitudinal strain of 50μ, and the strain corresponding to the load of 40% of the ultimate load. These measurements are needed to calculate the static elastic modulus of the concrete. The first loading was disregarded and the average of the last two loadings was recorded. This was done at the ages of 1, 3, 7, 14, 28 and 90 d.

3.6.5 Split Tensile Strength

The tensile strength of the concrete was assessed in accordance with ASTM C496. The test allows for the determination of the splitting (indirect) tensile strength of a cylindrical concrete specimen. The average result of three specimens was used at various ages: 1, 3, 7, 14, 28 and 90 d.

3.6.6 Flexural Strength

The flexural strength of three 6-in. (152 mm) by 6-in. (152 mm) by 21-in. (533 mm) concrete beams was measured in accordance with ASTM C78 at the early ages up to 48 h. The results of this test were used to determine the concrete maturity, information needed for opening to traffic (see chapter 7.1.3.1 of the report).

3.6.7 Isothermal Calorimetry and Activation Energy

The rate of heat release was measured using an isothermal calorimeter in accordance with ASTM C1702-09 (2009). Immediately after mixing, approximately 15 g of sample was transferred to a 22 mm diameter by 55 mm tall glass vial, sealed, and then placed into a chamber (maintained at 23 $\pm$ 0.1 °C) for approximately 60 hours of testing. Prior to the data collection, the chamber was held in isothermal conditions for 45 min to establish an equilibrium baseline. Calorimetric studies were performed on the cement paste at w/c of 0.42 at 23 $\pm$ 0.5 °C and 38 $\pm$ 0.5 °C.

3.7 Pavement Pouring, Consolidation, and Finishing

After confirming that the consistency (i.e., slump) of the material was in compliant with specification, the concrete was cast at the APT pit by means of wheelbarrows. The construction operations were carefully performed, without disturbing any of the sensors previously installed (strain gages and thermocouples). The concrete was then compacted using a hand-vibrator and finished (Figure 3.7). Special attention was paid to the surroundings of the strain gages, in order to ensure full contact between gages and concrete, so that future strain measurements are reliable.

3.8 Data Collection before Opening

Once the concrete pavement was finally placed, consolidated, and finished, the pavement was covered with plastic to avoid excessive evaporation. At this point, the scanners were started so that strain and temperature measurements could be taken.

3.8.1 Time-Temperature Factor (TTF)

Temperature measurements were taken in the wheel path and at three different heights in order to identify any temperature gradients throughout the cross section. The temperature considered for maturity calculations was that taken at mid-height of the concrete thickness (5 in. and 2.5 in. from the top surface, for the 10-in. and 5-in. thick pavements, respectively). The measured temperature is used to compute the TTF. Once the targeted TTF was reached, the pavement was loaded. (The targeted TTF was based on the maturity results explained in the Results section).

Figure 3.7 Concrete pavement consolidation and finishing.

3.8.2 Early-Age Shrinkage

Strain measurements were taken also before loading the pavement in order to evaluate early age volume changes. These would include drying shrinkage, plastic shrinkage, autogenous shrinkage, and settlement. The strain measurements were taken until the moment of loading the pavement, with a short interruption for the saw-cut operation.

3.9 Saw-Cut

The saw-cutting operation was performed at about 8 hours after pouring the concrete pavement. The saw-cut was performed right at the middle of the concrete pavement, on top of the dowel bars, at a depth of 1/3 of the concrete pavement thickness (Figure 3.8).

3.10 Pavement Loading

As mentioned before, once the targeted TTF was reached, the pavement was loaded. A dual-tire type of wheel was used with a pressure of 90 psi (620 kPa) at a travel speed of 5 mph (8 km/h). The load transmitted to the concrete pavement by the wheel system was 9,000 lb. (40 kN), which would correspond to half of the Indiana legal truck load per axle (i.e., 18,000 lb./axle; INDOT, n.d.). Five thousand load passes per day were performed until a total of 45,000 passes.

Figure 3.8 Saw-cut of the concrete pavements.

4. DETERMINATION OF THE FLEXURAL TENSILE STRESS

The risk of cracking in a concrete pavement that is opened to traffic at early ages is related to the maximum tensile stress, σ_I, that develops in the pavement and its relationship to the measured, age-dependent, flexural strength of a beam, f_r. The stress that develops in the pavement is due to several factors including traffic loading and restrained volume change caused by thermal or hygral variations. The stress that develops is also dependent on the time-dependent mechanical properties, pavement thickness, and subgrade stiffness. There is a strong incentive to open many pavements to traffic as early as possible to allow construction traffic or traffic from the traveling public to use the pavement. However, if the pavement is opened to traffic too early, cracking may occur that may compromise the service life of the pavement. The purpose of this paper is twofold: (1) to examine the current opening strength requirements for concrete pavements (typically a flexural strength from beams, f_r) and (2) to propose a criterion based on the time-dependent changes of σ_I/f_r which accounts for pavement thickness and subgrade stiffness without adding unnecessary risk for premature cracking. An accelerated pavement testing, APT, facility was used to test concrete pavements that are opened to traffic at an early age to provide data that can be compared with an analytical model to determine the effective σ_I/f_r based on the relevant features of the concrete pavement, the subgrade, and the traffic load. It is anticipated that this type of opening criteria can help the decision makers in two ways: (1) it can open pavement sections earlier thereby reducing construction time and (2) it may help to minimize the use of materials with overly accelerated strength gain that are suspected to be more susceptible to develop damage at early ages than materials that gain strength more slowly.

4.1 Analytical Solution of σ_I at the Bottom of an Elastic Pavement as a Result of Traffic Loads

The analytical expression for σ_I (stress at the bottom of the pavement) adopted in this work, was first presented by Westergaard (1926) and subsequently validated through

the years and is still used to this day (Bull & Singh, 1990; Hernández-Olivares, Barluenga, Parga-Landa, Bollati, & Witoszek, 2007; Timoshenko, Woinowsky-Krieger, & Woinowsky, 1959; Young & Budynas, 2001). The estimation of σ_I considers the static equilibrium between a (semi-infinite) homogeneous, isotropic and elastic concrete pavement (slab) and an elastic foundation (subgrade), assuming that there is no friction between the slab and the subgrade. Therefore, the reactions forces of the subgrade are assumed to be normal to the surface of the subgrade and proportional to the deflection of the slab (Yang, Weiss, & Shah, 2000). The traffic load is modeled as a distributed load on a circular area equivalent to the footprint of a dual wheel at the center of an infinite slab (Westergaard, 1926).

The analytical expression for σ_I proposed by Westergaard (1926) can be used considering the changes of the elastic modulus of concrete over time assuming that no history dependent behavior of concrete is induced by the traffic load moving on top. This assumption does not affect the accuracy of σ_I due to the fact that the extension of time that the wheel rest on a single point on top of the pavement moving at 5 mph is significantly smaller than the time needed to produce residual stresses associated with the aging-viscoelastic behavior of concrete at early ages under sustained loads (Antico, Zavattieri, & Weiss, 2015; Bazant & Wu, 1974; Carol & Bazant, 1993). Thermal and shrinkage deformations are not considered in the classical formulation by Westergaard (1926). Therefore, the updated form of σ_I at the bottom of the pavement when the wheel is on top, at the interface with the subgrade is described by equation (2).

$$\begin{cases} \sigma_I(t) = \frac{3(1+v)P}{2\pi h^2}\left(\log_e \frac{l(t)}{b} + 0.6159\right) \\ b = \sqrt{1.6a^2+h^2} - 0.675h \ \text{ for } 4 \le h \le 16\,\text{in} \end{cases} \tag{2}$$

where, t is defined as the age of concrete, v is Poisson's ratio for concrete, P is the total load of the wheel distributed on a circular area of radius a (obtained from P and the wheel pressure (~100 psi (Bollati, Talero, Rodriguez, Witoszek, & Hernandez, 1996) and equal to 5.6 in. in accordance with previous tests (Huang, 1995)) applied on top of a pavement of thickness h.

l(t) is defined as:

$$l(t) = \sqrt[4]{\frac{E(t)h^3}{12(1-v^2)k}} \tag{3}$$

where, $E(t)$ is the elastic modulus of the pavement changing over time t, and k is defined as the modulus of subgrade.

4.2 Experimental Results of σ_I at the Bottom of an Elastic Pavement as a Result of Traffic Loads Obtained from the Tests at the APT

The value of σ_I estimated from the experiments uses the strain measurements from the APT. The pavement is considered as linearly elastic, a good assumption if stress remains below 50% of the strength, and ε_I equal in all directions, in accordance with the values of ε_t in the longitudinal and transverse direction recorded at the tests. An approach proposed by Burmister (1958) is used to determine the stress (σ_z) in the direction perpendicular to the top surface, underneath the wheel load, at the bottom of the pavement based on E(t), k, P and a. The values of σ_z proved to be an order of magnitude less than σ_I for pavements with h≥5 in. for all the pavement configuration and loading conditions presented in this work. The experimental value of σ_I is described by equation (4).

$$\sigma_I(t) = \frac{1}{1-v}(E(t)\varepsilon_I + v\sigma_z(P,h,a,E(t),k)) \sim \frac{1}{1-v}E(t)\varepsilon_I, \tag{4}$$

where $E(t)\varepsilon_I >> v\sigma_z$

According to the values of σ_z obtained from Burmister (1958), $v\sigma_z$ can be neglected introducing only a 3% error in the value of σ_I. This assumption will be validated later on with our finite element calculations. The frictionless condition between the pavement and the subgrade makes possible to determine ε_I by extrapolating the readings of ε_t at the top (compression) and the bottom (tension) of the pavement assuming linear strain distribution underneath the wheel. The shift of the neutral plane with respect to the centroid of the cross section of the pavements (s) is also determined. Values of $s > 0$ could be an indication of damage and inelasticity of the pavement under tension as suggested previously (Bazant & Novak, 2000b). For thick and thin pavements (h = 10 and 5 in. respectively), $0 < s < 0.5$ in. (in direction to the top of the pavement), except for the thin pavement opened at the earliest age of 8 hours where s ~ 1.2 in. indicating the microcracking could occur at the bottom of this pavement. The shift of the neutral plane could be an indication that the effective cross section of the pavement has been reduced due to microcracking on the bottom of the pavement and the remaining part can be still considered as linear elastic (Bazant & Novak, 2000b).

4.3 Finite Element Model (FEM) of the APT Pavement

Three dimensional FEM models have been used to determine the stress and strain distribution that develops in the pavement in the APT underneath the wheel load to address the following points: (1) to evaluate if the assumption of frictionless conditions between the slab and the subgrade is an acceptable condition to model stress development due to traffic loading, (2) if the magnitude of σ_z is sufficiently small such that it can be ignored in equation **(4)**, (3) to evaluate the axisymmetric condition used by Westergaard (1926) for the wheel footprint which was assumed to be circular, (4) to analyze the assumption in the model (equation (1)) which considers an infinite slab while the actual slab tested in the APT has a finite width and, (5) to study whether the wheel in the center of the slab provides

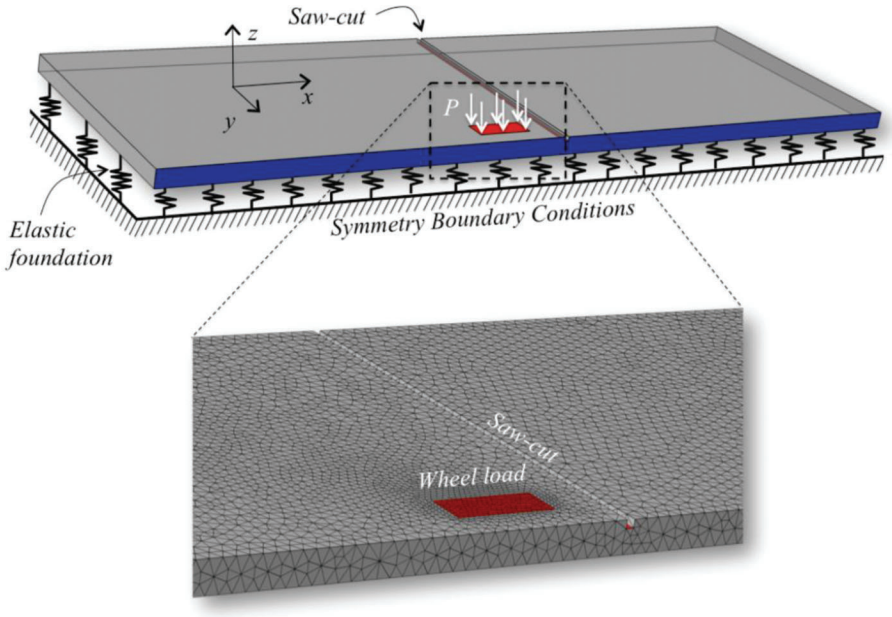

Figure 4.1 (a) A schematic illustration showing saw-cut location, footprint shape, and location (red) in the FE model; symmetry conditions are used to represent half of the slab. (b) A close-up of the location of load and saw-cut to show the finite element mesh using linear tetrahedral elements with four nodes.

the worst case scenario of σ_I. Static loading and the traffic load uniformly distributed on a rectangular area equivalent to the footprint of a dual wheel are considered as well as perfect transfer of loads between adjacent slabs on both sides of the saw-cut (see Figure 4.1). To address points 1, 2, and 3 the wheel load is placed in the center of the slab considering friction and frictionless conditions between the subgrade and the pavement to study how these conditions affect the response of ε_t. In particular for point 3, circular and rectangular footprints are considered to evaluate differences on tensile stress and strain. For point 4, the wheel load is also considered near the corner of a slab. The models are solved in ABAQUS (HKS, 2003) and considered concrete pavement as linear elastic (E(t)) assuming that no history dependent behavior of concrete is induced by the traffic load moving on top and k = 400 lb/in^3 (in accordance to the APT setup).

5. APT RESULTS

5.1 Dates of Concrete Delivery

The concrete mixture was a typical commercially produced INDOT concrete pavement mixture (i.e., it has been used in several sections of the SR-26 in Lafayette, Indiana) with a water-to-cement ratio (w/c) of 0.42, 22% of fly ash replacement of cement by mass, and a fine and coarse aggregate content of 1412 lb/yd^3 and 1750 lb/yd^3 respectively, was provided the local producer IMI. All the lanes were cast between November 2011 and March 2012 at the APT facility under controlled room temperature 73.4 °F.

5.2 Concrete Maturity and Opening Times

Using a Nurse (1949) and Saul (1951) maturity approach, the time-dependent flexural strength was estimated as described in ASTM C1074 (2011). Three values of flexural strength were targeted 275, 350 and 550 psi at 8, 13 and 18 hours respectively.

5.3 Concrete Mechanical Property Development

5.3.1 Slump Test

Upon arrival of the concrete truck, the concrete slump was measured according to ASTM C143. A slump of 5 in. was targeted for the acceptance of the concrete.

5.3.2 Time of Set

The time of initial set was 5.1 hours and 6.4 hours for final set following ASTM C403 (2008). A sample concrete from the batch was sieved to obtain samples of mortar to measure the time of setting. Figure 5.1 shows the experimental recordings of the pressure measured on the mortar samples.

5.3.3 Compressive Strength and Static Elastic Modulus

Concrete cylinders were cast (6 × 12 in.) to obtain the split tensile strength up to 90 days using ASTM C39 (2015). Figure 5.2 shows the compressive strength from Lines 1 and 2 up to 90 days. The compressive elastic modulus was also tested using cylinders of 6 × 12 in.

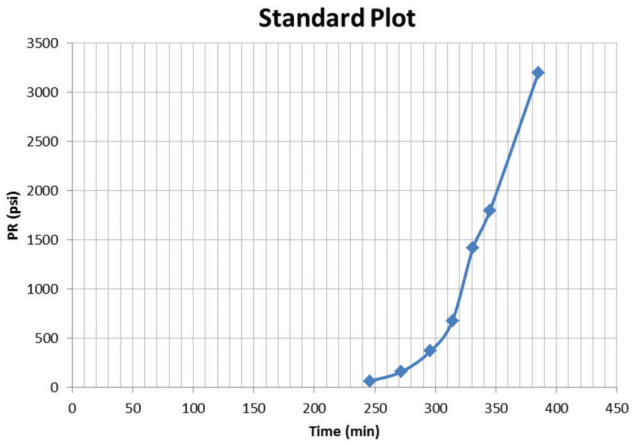

Figure 5.1 Experimental measurement of pressure vs. time using a standardized needle device to determine time of setting using ASTM C403 (2008).

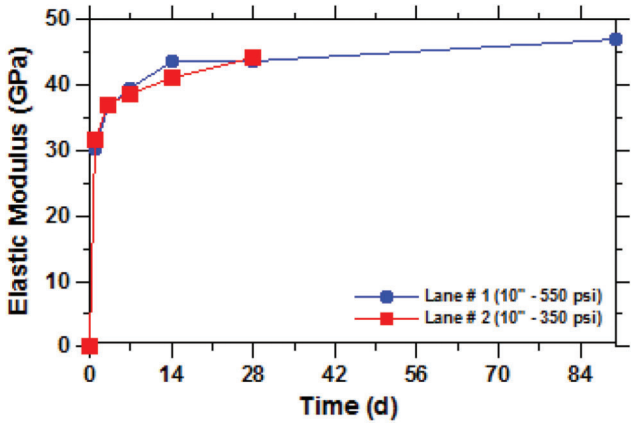

Figure 5.3 Elastic modulus using compressive strength tested for Lanes 1 and 2 using ASTM C39 (2015).

following ASTM C469 (2003). Figure 5.3 shows the compressive elastic modulus from Lines 1 and 2 up to 90 days.

5.3.4 Split Tensile and Flexural Strength

In addition to the concrete used in the casting of the pavements, concrete beams were cast ($6 \times 6 \times 21$ in.) and their flexural strength were tested following AASHTO T 97-10 at the time the opening maturity was reached to confirm the flexural strength (ASTM C78, 2013). Concrete cylinders were also cast (6×12 in.) to obtain the split tensile strength using ASTM C496 (2011) up to 7 days. Figure 5.4 shows both, flexural and split tensile results. The maximum difference recorded (up to 2 days) between flexural and split tensile was approximately 30% at 2 days.

5.3.5 Isothermal Calorimetry or Activation Energy

The rate of heat evolution for the cement used in this research can be seen in Figure 5.5. The results are shown for the same cement paste run at two different temperatures such that the activation energy of the cement could be determined.

Using the calorimetry data, the maximum heat released ($Q\infty$) was calculated to derive the degree of hydration (DOH), defined as the heat at any given time divided by the maximum heat released (Q/Q_∞), as one of the necessary steps to calculate the activation energy (E_a) (Broda, Wirquin, & Duthoit, 2002; Kada-Benameur, Wirquin, & Duthoit, 2000). Q_∞ was calculated using equation (5):

$$Q_\infty = 500P_{C_3S} + 260P_{C_2S} + 866P_{C_3A} + 420P_{C_4AF} + 624P_{SO_3} + 1186P_{FreeCaO} + 850P_{MgO} \quad (5)$$

The calculated maximum heat released for this cement was 430 J/g. Normalizing the cumulative heat released (obtained through integration of the heat flow data presented in Figure 5.6) by the maximum heat released yields the DOH of the cement paste, shown in Figure 5.6 for the test performed at 23 °C.

Using this data, the activation energy (E_a) was able to be estimated for early ages (i.e., lower degree of

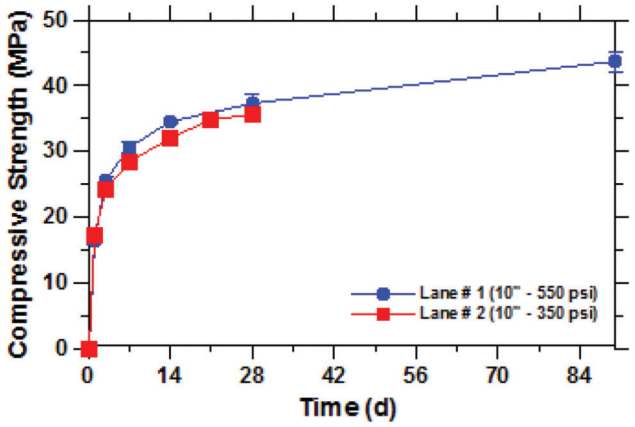

Figure 5.2 Compressive strength tested for Lanes 1 and 2 using ASTM C39 (2015).

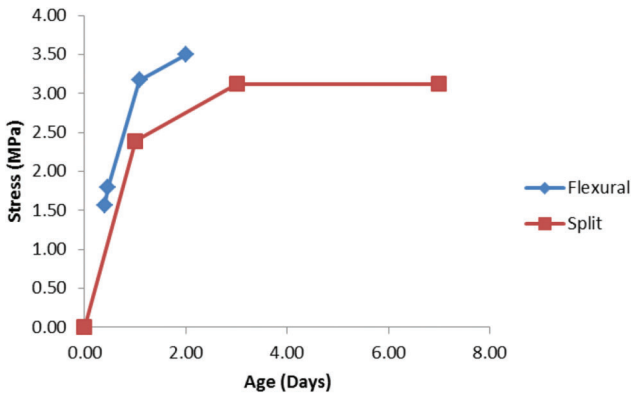

Figure 5.4 Flexural strength and split tensile strengths for the concrete mix tested at the APT.

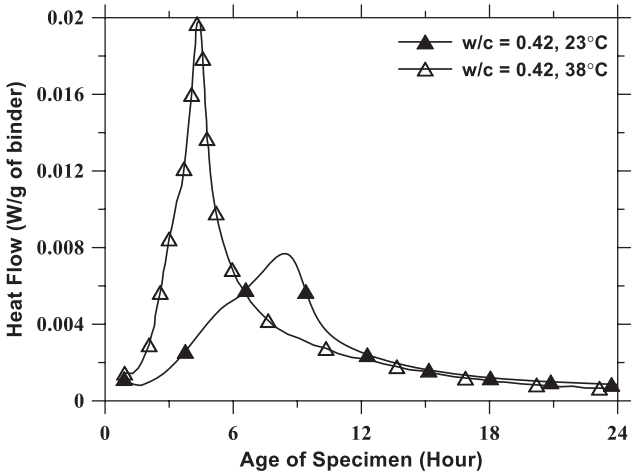

Figure 5.5 Isothermal calorimetry conducted at 23 °C and 38 °C.

hydration) using the Arrhenius approach. The calculated average E_a was 38400 J/mol for DOH up to 0.70.

5.4 ε_t Measurements and Mechanical Linear Response of Thick Pavements

Figure 5.7 provides an example of the type of data obtained in the APT and indicates the strain (measured using the lower strain gage in the wheel path, in the direction of traffic) as a function of the wheel position along the concrete pavement. The strains showed were recorded after 1 and 45K wheel passes (one pass means the whole cycle of moving the wheel back and forth once) on both cases.

It can be observed that for both pavements (Figure 5.7 (a and b)), the magnitude of ε_t varies throughout the test (after 45K wheel passes). Figure 5.8 shows the evolution of ε_t vs. age for all the pavements (5 in. and 10 in. thick) tested for this work. Figure 5.8 shows clearly that thin pavements opened at very early ages (275 and 350 psi) present a high deformation due to traffic loading condition during the first hours after the time to open

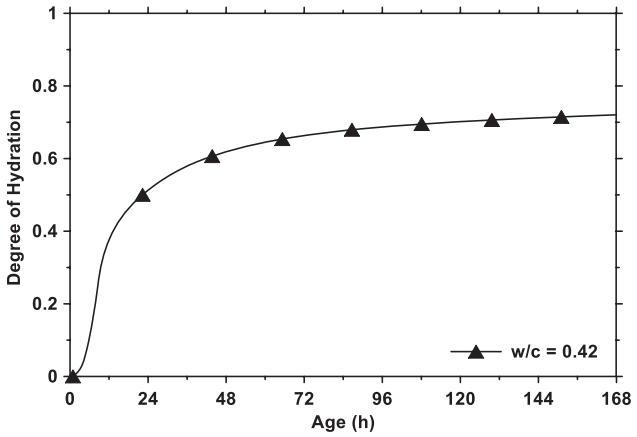

Figure 5.6 Degree of hydration of the cement tested at 23 °C.

to traffic. These higher strains caused by traffic loads after opening to traffic is due to both low elastic modulus associated to the low degree of hydration during the first hours after setting (represented in the FE models using different values of $E(t)$ to determine stress and strain caused by traffic loads at different ages) and it is likely that some microcracking particularly on the earliest pavement opened to traffic ($h = 5$ in. @ $f_r = 275$ psi) in accordance with the extreme values of s described before.

To determine if significant damage occurred in the pavements of $h = 10$ in. tested in this study, one of the thick pavements was loaded after the APT test was finished (45K passes) with a series of incrementally increased and decreased loads in a reduced number of cycles (5K passes) trying to detect non proportional response between the magnitude of P and ε_t which might indicate presence of damage as showed in Figure 5.7 (c). These results show that thick pavements, opened to traffic at an age of 13 and 18 hours had a linear elastic response throughout the entire test (i.e., under loads of 9K pounds for 7 days) and that no residual strain is observed due to damage after loading, confirming that no significant damage is developed in these pavements.

5.5 Finite Element Simulations to Study the Strain Development on Pavements Tested at APT

Figure 5.8 shows a comparison between ε_t measured using the strain gages in the APT pavement in the longitudinal direction, located 1 in. from the bottom the pavement, and from the 3D FEM at the same location. The significant reduction of ε_t in Figure 5.8 (a) and (b) with age is primarily associated with the rapid development of $E(t)$ during the first 24 hours (75% of the value of $E(t)$ at 7 days). The frictionless hypothesis is tested and results are showed in Figure 5.8 for both pavements. To try to mimic the interaction between the pavement and the subgrade a coulomb friction model is used with different levels of friction ranging from frictionless to perfect bonding. The interaction observed for different levels of friction condition (except perfect bonding) are similar to the frictionless case and the latter condition has a good match with experimental data. This indicates that the assumption of no friction appears to not have a major impact on the stress and strain development due to traffic loading. Also, the lack of tangential interaction between the subgrade and the pavement is in accordance with the value of s estimated from experimental data. The extreme case of perfect bonding (no relative displacement between the bottom of the pavement and the subgrade) between the pavement and the subgrade shows a reduction of strain and stress up to 36% and 27% respectively as showed in Figure 5.8 for both pavements.

The shape of the tire footprint (circular or rectangular) has showed an impact in the tensile strain and stress up to 6% development at the bottom of the

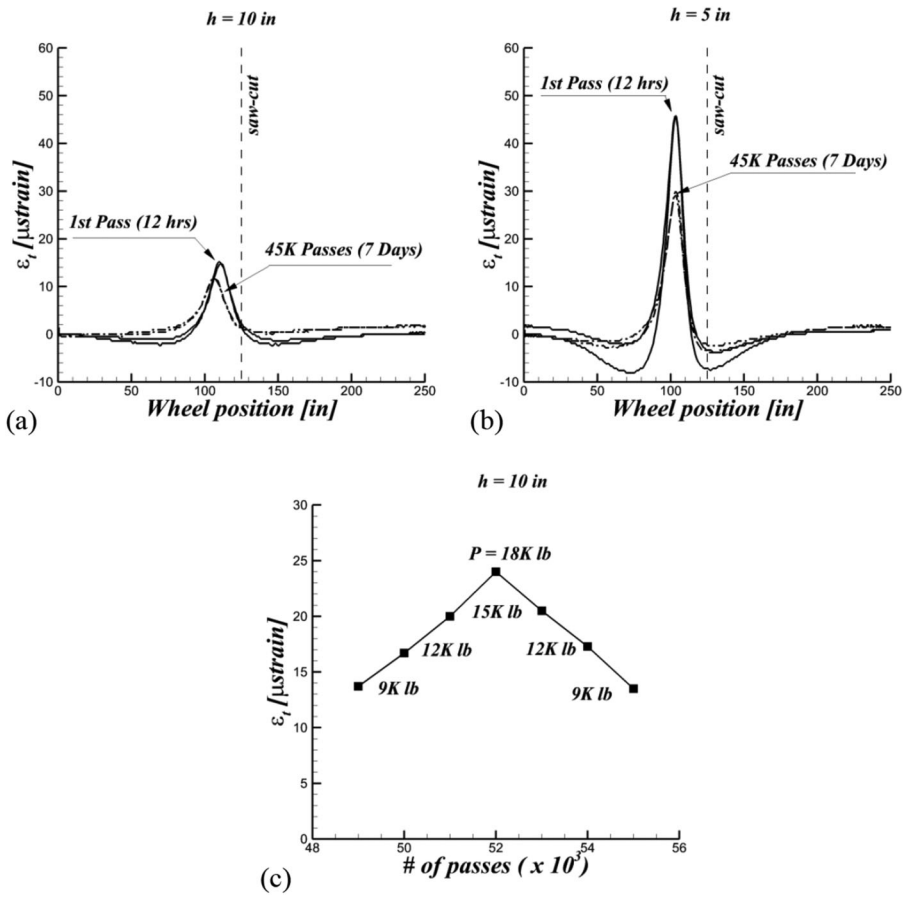

Figure 5.7 Measured ε_t at 1 in. from the bottom with respect to wheel position: (a) Lane 2 (opening at 350 psi for a 10-in. thick pavement); (b) Lane 3 (opening at 350 psi for a 5-in. thick pavement); and (c) ε_t vs. number of passes for one of the thick (10 in.) pavements.

pavement as showed in Figure 5.8 comparing ε_t for the two shapes of footprints with the frictionless condition and perfect bonding for $h = 5$ and 10 in.

According to the values of σ_z obtained from FEM, $\nu\sigma_z$ can be ignored with only a 1% error in the value of σ_I. The error between the approximation of Burmister (1958) and the FE models of this work represents less than 2% of the value of σ_I.

The stress and strain development computed using the FEM of a finite slab with the same dimension to the pavements tested at the APT shows a difference of less than 10% compared with the analytical solution an infinite slab indicating that the solution proposed by Westergaard (1926) provides a good approximation of σ_I even for finite slabs like the ones tested at the APT. In an extreme case where load transfer is negligible through

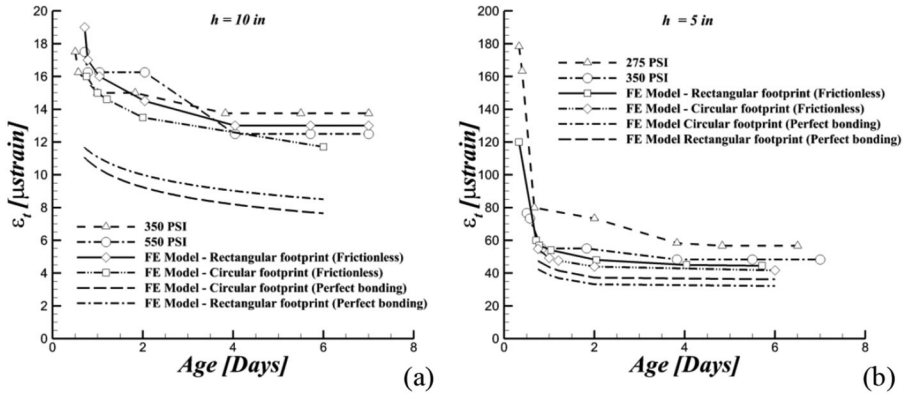

Figure 5.8 ε_t at the strain gage location (1 in. from the bottom) vs. age up to 7 days for two different pavement thicknesses: (a) 10 in. and (b) 5 in. The experimental data and the finite element simulations of this study show good agreement.

the saw-cut (case without dowel bars) the analytical solution of σ_I is up to 15% lower than the FEM results obtained using perfect load transfer to mimic the mechanical contribution of the dowel bars underneath the saw-cut.

Finally, 3D simulations are performed also to determine the values of σ_I near the loading point when the wheel is near a corner of the slab in contact to an adjacent slab, in a similar configuration to the APT test. Under these conditions, it is determined that the maximum σ_I corresponds to the case with the load in the center of the slab.

The takeaway is that each of the assumptions described in this section has a minor impact on the prediction of σ_I. The analytical expression for σ_I proposed by Westergaard can be used considering the changes of the elastic modulus of concrete over time assuming that no history dependent behavior of concrete is induced by the traffic load moving on top. This assumption does not affect the accuracy of σ_I due to the fact that the extension of time that the wheel rest on a single point on top of the pavement moving at 5 mph is significantly smaller than the time needed to produce residual stresses associated with the aging-viscoelastic behavior of concrete at early ages under sustained loads (Antico, Zavattieri, et al., 2015; Bazant & Wu, 1974; Carol & Bazant, 1993). Thermal and shrinkage deformations are not considered in the classical formulation by Westergaard (1926). Therefore, the updated form of σ_I at the bottom of the pavement when the wheel is on top, and at the interface with the subgrade (as described by equations (2) and (4)). are equivalent and can be used conservatively to predict σ_I for real pavements.

5.6 Effect of $E(t)$, k, and h on σ_I/f_r

Figure 5.9 shows the analytical variation of σ_I for pavements with a thicknesses between $4 < h < 16$ in. (showed as lines) for a value of $E(t)$ at very early age (8 h), and at a later age (7 d) and for two extreme values of subgrade reaction modulus (k = 50 lb/in^3 and 400 lb/in^3). Figure 5.9 shows the evolution of σ_I vs. age for the pavements tested at the APT. The increase of $E(t)$ from 8 hours to 7 days resulted in an increase in σ_I of 20% for pavements with $h \leq 10$ in., and less than 15% for pavements with $h \geq 10$ in. as shown in Figure 5.9. As expected, σ_I does not change significantly due to changes of $E(t)$ after 18 hours as showed in the analytical results (dashed –k = 50 lb/in^3- and dashed-dotted – k = 400 lb/in^3- lines) depicted in Figure 5.10 (a) and (b) for the particular cases of the pavements of the APT with h = 5 and 10 in. tested for 7 d. On the other hand, an increment of k from 50 lb/in^3 to 400 lb/in^3 could cause a reduction of σ_I of more than 27% for $h \leq 10$ in. and 20% for $h \geq 10$ in. as showed in Figure 5.9 and Figure 5.10 for pavements of h = 5 and 10 in. The selected range of k is based on values of subgrade reaction modulus described in literature (Hernández-Olivares et al., 2007; Teller & Sutherland, 1943; Westergaard, 1926). Finally, an overall observation

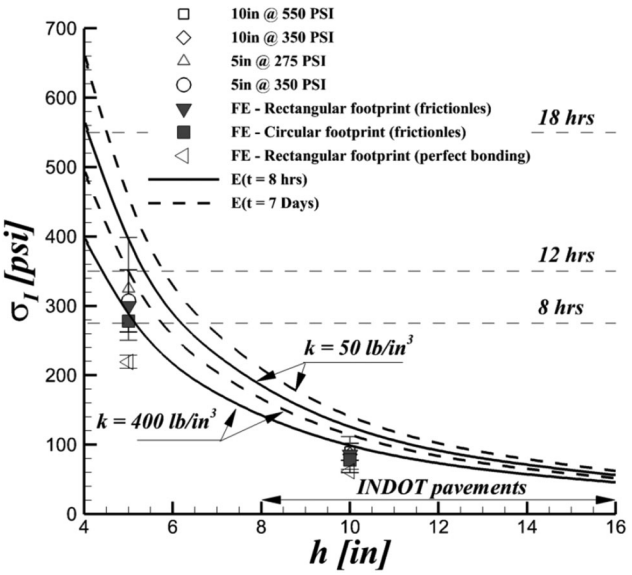

Figure 5.9 σ_I at the bottom of the pavement for two extreme cases of subgrade reaction modulus, k = 50 lb/in^3 and 400 lb/in^3. For each k, σ_I is determined for $E(t)$ at 8 hours (solid lines) and for $E(t)$ at 7 days (dashed lines). Experimental values of σ_I are showed in symbols for h = 5 and 10 in. Horizontal dashed lines indicate f_r at different ages.

of Figure 5.9 reveals that $\sigma_I/f_r < 0.5$ for pavements with thicknesses h $\geq$ 10 in. for any time to open to traffic after the saw-cut (approximately 8 hours after casting) and k.

To support the analytical results presented previously, Figure 5.9 and Figure 5.10 also show the experimental values of σ_I estimated for 5 and 10 in. (showed as discrete points) considering a value of k of 400 lb/in^3 (Newbolds & Olek, 2008). The experimental values of σ_I estimated in this section considered a prescribed traffic load of 9000 lb. (on a dual wheel). The mean value of σ_I over the first 7 days is showed for both 5- and 10-in. thick pavements opened at different ages and the error bars show two standard deviations for each set of the experimental data. The experimental results show good agreement with the analytical models for the σ_I in both 10 in. pavements (i.e., the pavements opened at when the concrete had reached strengths of f_r = 550 or 350 psi). The experimental values obtained for the 10-in. thick pavements indicates that the stress-to-strength ratio, σ_I/f_r was approximately 0.20 and 0.19 for the time to open to traffic at f_r = 350 and 550 psi, respectively. This indicates stress levels that are well below 50% of the peak strength which is a general rule of thumb used to assume elastic behavior. On the other hand, the experimental values of the stress-to-strength ratio in the 5 in. pavements were $\sigma_I/f_r \sim 1.0$ at 8 hours (f_r = 275 psi) and that $\sigma_I/f_r \sim 0.8$ at an age of approximately 12 hours (f_r = 350 psi).

The takeaway is that a rapid increase of σ_I during the first hours after a very early opening is mainly driven by the rapid development of $E(t)$ for high performance concretes (showed in Figure 5.10 (b)). Changes of

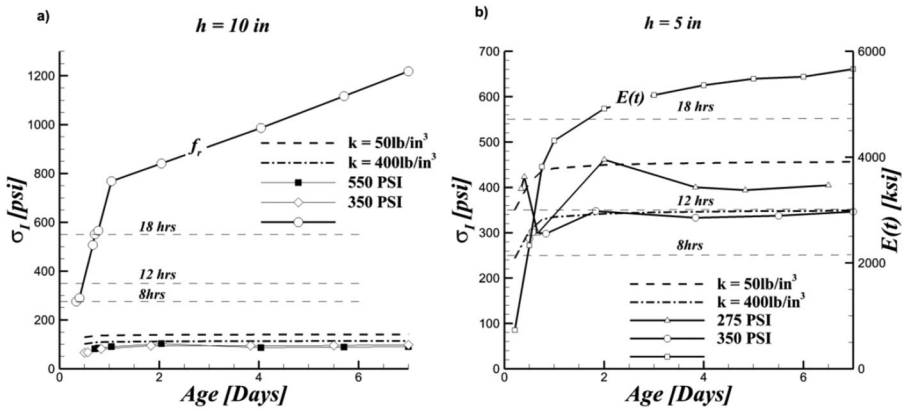

Figure 5.10 Evolution of σ_I, at the bottom of the pavement, vs. age up to 7 days for two different pavement thicknesses: (a) 10 in., and (b) 5 in. σ_I estimated using the analytical and the experimental approximation on both cases. The main source of error in the calculation of σ_I using equation **(4)** comes from the uncertainty of the position of the strain gages. The 5 in. pavements are the most sensitive to this uncertainty. Horizontal dashed lines indicate f_r at different ages.

$E(t)$ are especially important for thin pavements (i.e., 5 in); For this reason, thin pavements opened at earlier ages would benefit from the low values of $E(t)$ and high values of k could to mitigate risk of cracking (27% reduction of σ_I if an increment of k from 50 lb/in^3 to 400 lb/in^3 is achieved).

5.7 Comments on the Permanent Strain, ε_p

ε_p recordings in all the pavements tested at the APT show low to no thermal or shrinkage strain at the bottom and similarly low expansion at the top strain gages during the first hours after setting in a controlled environment of 73.4 °F

The comparison of the pavements with $h = 5$ and 10 in., opened to traffic at the same age (12 hours @ $f_r = 350$ psi) show that the evolution of ε_p during the first 48 hours is similar. This shows that ε_p could be related mainly to the hydration process. After approximately 48 hours, both pavements show the same type of response getting to a steady state of $\varepsilon_p \leq 5\mu strain$ that lasted until the tests were finished. FE simulations consider the thermal gradients to simulate the different temperatures at the top and the bottom of the pavements. σ_I is reached up to 0.9 MPa only under an extreme temperature of 122 °F on the top surface.

5.8 Proposal for a Time of Early Opening to Traffic (EOT) Criterion

Figure 5.11 shows a set of curves, using the theoretical estimation of σ_I, to estimate the time for EOT based on k, h, f_r and $E(t)$. In this chart, the curves are estimated for a low k of 50 lb/in^3 and high k of 400 lb/in^3, for an early $E(t)$ of 1740 ksi (12 Gpa) (@8 h, depicted in short and long dashed lines), and a mature $E(t)$ of 3771 ksi (26 Gpa) (@18 h—INDOT specification of $f_r = 550$ psi, depicted in solid and dashed-dotted lines). At the same time σ_I is estimated for different sets of concrete pavement and subgrade configurations for the maximum loading condition imposed by INDOT (per dual-wheel) of $P = 9$K (40 KN). The selected range of h is according the actual range of thick pavement used by INDOT (10–16 in.) and is extended below the minimum h up to 6 in. The proposed criterion suggests that it may be feasible to tie the strength requirement to pavement thickness and subgrade properties. It is recommended that for pavements less than 8 inches thick that the opening criteria be maintained at 550 psi, for pavements with a thickness between 8 and 10 inches the opening could be reduce to 450 psi to maintain the stress-to-strength ratio at a value of less than 40% and for pavements thicker than 10 inches the opening strength could be reduced to 350 psi to maintain the stress-to-strength ratio at a value of less than 40%.

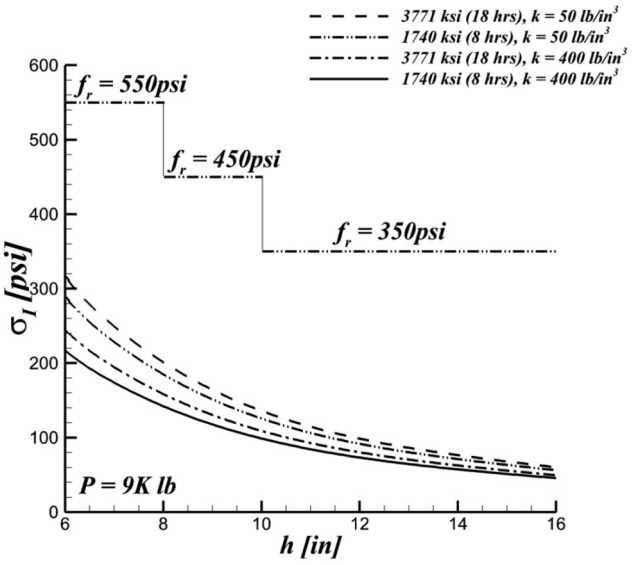

Figure 5.11 Proposed criterion for determination of time of EOT.

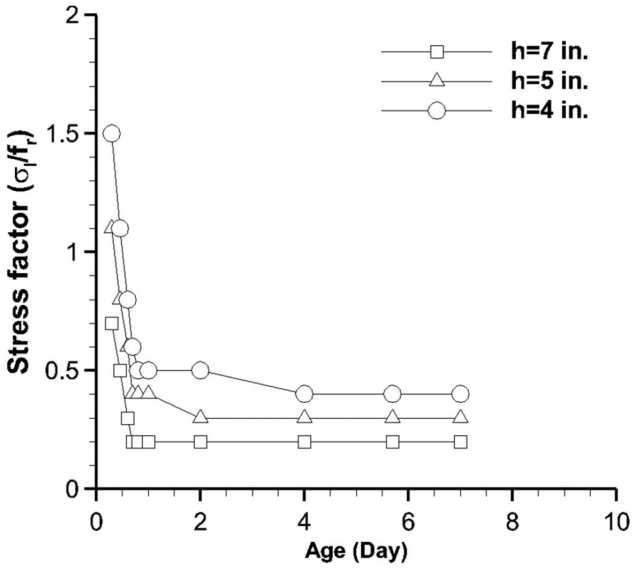

Figure 5.12 Stress factor for thinner pavement assuming $k = 400$ lb/in^3.

5.9 Risk of Cracking on Thin Pavement with High Axle Loads

This work has been focused on thick pavements ($h = 8 - 16$ in.) within the range of INDOT pavements. The risk of cracking could also be addressed for thinner pavements under the same assumptions described for thick pavements. In this section the risk of cracking is evaluated for pavements thickness ranging from 4 to 7 in. using the proposed criterion in this work. Stiffer subgrade reactions reduce the critical value of σ_I. Therefore, a subgrade reaction modulus of 400 lb/in^3 is considered the following results for best performance. A traffic load (P) of 9000 lb. is used to estimate the stress factor (σ_I/f_r) at different ages.

Figure 5.12 shows the estimation of risk of cracking for pavements ranging 4 to 7 in. thick. Assuming that $\sigma_I/f_r \sim 0.3$ is an acceptable risk of cracking, 7- and 5-in. thick pavements could be opened to traffic at 0.7 days (~17 hours), 2 days (48 hours), respectively. On the other hand, the thinner pavement selected in this analysis ($h = 4$ in.) does not reach $\sigma_I/f_r \sim 0.3$ at least for the first 7 days after casting.

6. STRESS-STRAIN ANALYSIS OF RESTRAINT MORTAR AT EARLY AGES USING THE RING TEST

6.1 Introduction

The risk of cracking throughout the life span of cementitious materials, i.e., mortar, is in direct relation to the stress and strain history especially at early ages (days and/or months after casting) when cement is still hydrating. The development of stress and strain of mortar is a consequence of its rheological and aging behavior, defect distribution and growth, and loading conditions.

It is believed that the aging-rheological behavior of cement paste arises mainly from the response of calcium silicate hydrate (C-S-H) to stress and the mechanical interaction between C-S-H particles surrounded by a layers of water, and the formation of hydrated particles that engage to the preexisting load-bearing matter volume (Bazant & Yunping, 1994; Mindess, Young, & Darwin, 2002). The incremental growth of load-bearing matter is proportional to the rise of the elastic modulus and strength (both compressive and tensile) of the material with age (Carol & Bazant, 1993). Many previous investigations have addressed the aging-rheological behavior of early age cement paste or mortar. For instance, Bazant and Wu (1974) compiled a series of previous experimental results of concrete creep tests under low levels of stress and proposed an aging-viscoelastic model to describe them with great success. This rheological model is based on a classical Maxwell chain model with age-dependent properties to represent the linear creep behavior of mortar as an aging viscoelastic, under no damage (Bazant & Wu, 1974). This method has shown to capture the aging-viscoelastic behavior of concrete assuming no damage. However, as it was pointed out by Carol and Bazant (1993), the Maxwell chain model with age-dependent properties has additional difficulties including, the determination of the time-dependent aging material parameters. In response to these difficulties, several aging-viscoelastic approaches have been presented later to overcome the challenges described earlier and also provide an effective approach to be implemented numerically (Bazant, 1977; Carol & Bazant, 1993; Grasley & Lange, 2007; Suter & Benipal, 2006a, 2006b; Vichit-Vadakan & Scherer, 2003). However, there is still a lack of representative models to determine how the time and history dependent behavior of mortar at early ages is coupled with defect formation to address the risk of cracking.

In this section, an approach to characterize the mechanical behavior of mortar at early ages under restrained conditions for the case where defect formation is expected. The role of the time and history dependent mechanical behavior of mortar by means of the approach known as solidification of non-aging constituents (solidification) is considered in this study; and it represents an interesting approach for its physical understanding of the aging-viscoelastic phenomena of cement based materials and its simplicity to be applied as an analytical and numerical tool to predict stress and strain development in mortar and concrete (Bazant, 1977; Bazant & Prasannan, 1989; Grasley & Ambrosia, 2011; Grasley & Lange, 2007). As for the defect distribution and formation, a time-dependent cohesive zone model is implemented to account for the rise of strength as hydration evolves at early ages. This damage model also makes use of a statistical distribution of tensile strength to account for variability effects. This chapter presents a section describing the time and history dependent model used to predict stress and strain development and damage growth of mortar at early ages under restraint conditions. As case of study, this works apply this numerical model to predict the behavior of restraint mortar rings (Hossain & Weiss, 2004)

showed in results section and finally a section with final comments, conclusions and future work is presented.

6.2 Numerical Model of Mechanical Behavior of Restrained Mortar at Early Ages

6.2.1 Free Shrinkage

The role of free shrinkage ($\varepsilon_{SH}(t)$) associated to autogenous, thermal and drying shrinkage which, under a mechanical restraint conditions, are responsible for the stress and strain behavior of cementitious materials has been studied experimentally in detail by many scholars (Dean, Moon, Rajabipour, Pease, & Weiss, 2006; Hossain, 2003; Hossain, Pease, & Weiss, 2003; Hossain & Weiss, 2006; Moon, 2006; Moon, Couch, & Weiss, 2006; Moon, Rajabipour, & Weiss, 2004; Weiss, 1999; Weiss & Shah, 2002). Thermal strains are also included in $\varepsilon_{SH}(t)$ since the temperature of the samples were not controlled during the tests. These works showed how $\varepsilon_{SH}(t)$ is related to the type of cementitious material, described in terms of the water-to-cement ratio (w/c), and the moisture profile, associated to the exposed surface-to-volume ratio under controlled environmental conditions (Hossain et al., 2003). Hossain and Weiss (2004) reported a regression for $\varepsilon_{SH}(t)$ from experimental data for w/c = 0.5 as described by equation (6).

$$\varepsilon_{SH}(t)\begin{cases} -52.83(t-t_0)^{0.59},\ t_0<t<t_d \\ -52.83(t-t_0)^{0.59}-52.01\sqrt{t-t_d}, t\geq t_d \end{cases} \quad (6)$$

where t is the age of the specimen, t_0 is the age of final set and t_d is the age when drying is initiated, $\varepsilon_{SH}(t)$ is measured in microstrains (Hossain & Weiss, 2004).

6.2.2 Constitutive Model

6.2.2.1 The aging-viscoelastic model. When mechanical restraint is exerted to mortar, the time-dependent strain ($\varepsilon(t)$) consist of $\varepsilon_{SH}(t)$ and aging-viscoelastic strain only assuming defects formation is negligible for the magnitude of the mechanical loading (Antico, de la Varga, et al., 2015; Bazant & Wu, 1974; Mindess et al., 2002). The viscous part, is modeled using a Maxwell chain model (Taylor, Pister, & Goudreau, 1970; Zienkiewicz & Taylor, 2005). The aging part is described by solidification theory which departs from the concept that the aging behavior of hydrating cement creep (or relaxation) is due to a stress-free growth of hydrated cement volume fraction, v(t) at the moment of engagement to the preexisting load-bearing material (Bazant & Robert, 1988). The stress-free condition of the incremental solidified material, dv(t), is the key factor to express a non-aging viscoelastic formulation for each differential of solidified matter that engages to the preexisting load-bearing portion of material as shown in Figure 6.1.

The formulation of solidification proceeds from the differential form of stress vs. infinitesimal strain which is consistent with the second law of thermodynamics as stated in a previous work (Bazant, 1979). For the 1D example showed in Figure 6.1, the incremental stress of relaxation ($\Delta\sigma(t)$) associated to a block of solidified matter that engages to the preexisting load-bearing material is described by equation (7).

$$\Delta\sigma(t)=\Delta v_i\int_{t_i}^{t}E(t-\tau)\dot{\varepsilon}\ (\tau)d\tau \quad (7)$$

where Δv_i and $E(t-\tau)$ are the differential volume of solidified matter and the relaxation modulus of solidified matter engaged to the preexisting load-bearing material at time t_i, respectively; $\dot{\varepsilon}(\tau)$ is the strain rate.

The multiaxial representation of the viscoelastic phenomena is commonly expressed in terms of the volumetric and deviatoric stress, $p(t)$, $s(t)$, respectively, and strain, $\theta(t)$, $e(t)$, respectively. Continuum models using viscoelasticity demonstrated high accuracy compared with experimental results as long as stress level is below 50% to avoid the presence of significant microcracking (Bazant & Wu, 1974; Mindess et al., 2002). Therefore, the non-aging viscoelastic stress and strain description, using the integral form of a Maxwell chain (Ferry, 1980; Jirásek & Bazant, 2002; Lakes, 2009; Marques & Creus, 2012), can be coupled with aging effects using solidification theory in the following way:

$$s_{ij}(t)=\int_0^t G(t-t')\dot{e}_{ij}ij(t')v(t')dt' \quad (8)$$

$$p(t)=\int_0^t K\left(\dot{\theta}(t')-3\,\varepsilon\,(t')\right)v(t')dt' \quad (9)$$

where, G(t–t′) and K are the shear relaxation and bulk modulus respectively, and $\dot{e}_{ij}(t')$, $\dot{\theta}(t')$ and $\dot{\varepsilon}(t')$ are the deviatoric, volumetric and total strain-rates as a function of time t respectively. This constitutive model assumes that only the deviatoric stress and strain are involved in

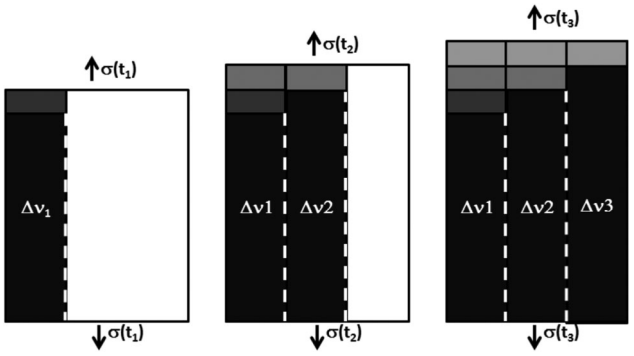

Figure 6.1 1D scheme of the solidification concept. From left to right it is showed how differential blocks of hydrated cement engage to the preexisting load-bearing material. If the material experiences mechanical loading while it solidifies, each block of solidified material will experience different levels of strain.

the viscoelastic process and therefore the bulk modulus, K, and Poisson ratio, η, are constant parameters of the model. For the latter, many works have analyzed the effects and measurement of changes of η in time and the general conclusion is that Poisson ratio can be assumed constant in time in general for concrete (Bazant, 1975; de Borst, Sluys, van den Boogaard, & van den Bogert, 1993; Gopalakrishnan, Neville, & Ghali, 1969; Hannant, 1969; Jones & Grasely, 2011; Jordaan & Illston, 1969). Equations (8) and (9) represent a generalization of a Maxwell material and G(t–t′) can be discretized by means of a Prony Series (Bazant & Wu, 1974; de Borst et al., 1993; Park & Kim, 2001; Raoufi, Pour-Ghaz, Pourasee, & Weiss, 2011; Raoufi, Schlitter, Bentz, & Weiss, 2011; Schapery, 1962; Soussou, Moavenzadeh, & Gradowczyk, 1970):

$$G(t) = G_o\left[\mu_o + \sum_{i=1}^{N} \mu_i \exp\left(-\frac{t}{\lambda_i}\right)\right] \qquad (10)$$

where G_o is the relaxation modulus @ t = 0 and the pairs (μ_i,λ_i) represents the relaxation shear modulus coefficient and the relaxation time respectively (Bazant & Wu, 1974; Taylor & Govindjee, 2008a, 2008b; Taylor et al., 1970). Based on experimental and analytical results (Bazant & Wu, 1974), in this work a N-term (N = 8) Prony series is used to represent the solidification behavior of mortar considering the relaxation time of the eight element of the Maxwell chain as infinite (i.e., a spring with no dashpot).

6.2.2.2 The time-dependent damage model. A cohesive zone model is proposed to model crack formation and propagation from distributed damage. This model has the capability to be adapted to dissimilar fracture behaviors depending on the value of two parameters, $T_{\max}$ and G_c, strength and energy release rate. These two parameters are related through the fracture length scale $\left(l_{fpz} \propto G_c E / {T_{\max}}^2\right)$, where E is the elastic modulus of the composite (Falk, Needleman, & Rice, 2001; Morrissey & Rice, 1998; Rice, 1980). If this quantity is significantly smaller than all of the characteristic geometrical length scales, then the composite behaves in a notch sensitive fashion (Li, Thouless, Waas, Schroeder, & Zavattieri, 2005; Zhou, 1992). On the contrary, the composite will be considered as notch insensitive if l_{fpz} is large compared to any of the characteristic geometrical length scales (Li et al., 2005; Zhou, 1992). Compared with continuum damage models, cohesive zone models are meant to model cracking at interfaces of dissimilar materials. However, under certain assumptions, cohesive zone models can be used to model distributed damage within the bulk of a material. For example, a previous work used this concept to model distributed damage, with good correlation with experimental results, in a solder bump matrix assuming that the size of each cohesive element represent a grain boundary of the underlying microstructure (Abdul-Baqi, Schreurs, & Geers, 2005).

Mortar is random composite materials with the fine aggregate acting as the inclusions and the cement paste acting as the matrix. Typically, the maximum aggregate diameter in a mortar is 1–3 millimeters. Normally, mortar has aggregate volume fractions of up to 70% or so, which implies that the spacing between particle surfaces is on the order of 100 micrometers, as seen by SEM in cross-section (Diamond, Mindess, & Lovell, 1982). Considering these two length scales of the problem this work assumes that the element of the bulk with a characteristic length of an average large aggregate and the cohesive elements length to be representative of the spacing between particles. In this simple two-parameter form of cohesive zone model, no distinction is made between matrix and aggregate cracking (Abdul-Baqi et al., 2005). This is acceptable if the intent of this model is to predict macroscopic performance of a composite (Li et al., 2005). The total strain $\varepsilon(t)$ is decomposed into bulk strain and cohesive strain (de Borst et al., 1993) based on the cohesive zone displacements and bulk elements deformations (Espinosa & Zavattieri, 2003; Tvergaard & Hutchinson, 1992). A potential-based triangular-shaped, initially-elastic cohesive zone model is implemented using four-node, zero-thickness interface elements to represent the quasi-brittle fracture behavior of mortar (Antico et al., 2012; Espinosa & Zavattieri, 2003; Falk et al., 2001; Li, Thouless, Waas, Schroeder, & Zavattieri, 2006; Morrissey & Rice, 1998; Rice, 1980).

An extensive characterization of mode I strength, $T_{max}(t)$, of hydrating paste and mortar has been done before (Hossain & Weiss, 2004; Kovler, 1994; McIntosh, 1956). However, only in late years limited experimental data provided information about changes of the energy release rate in mode I, G_{IC}, at very early ages for paste and mortar (Bassam, Yu, & Ansari, 2007; Hoover, 2013; Yu & Ansari, 1996). In particular, for mortar and concrete specimens G_{IC} showed changes of ~20% within the first 24 hours after casting, reaching a 90% of the maximum G_{IC} before 48 hours (Barde et al., 2005; Bassam et al., 2007; Yu & Ansari, 1996). Normally, the fracture process of laboratory samples of mortar is dominated by strength rather than critical strain energy release rate, this can be quantified by the relative value of l_{fpz} with respect to the characteristic geometrical length scale of the problem. Therefore, G_{IC} is assumed to be constant with age. In this work, $T_{max}(t)$ and constant G_{IC} are considered as a representation of the evolution of the fracture properties at early ages. Also, the tangential stiffness and fracture mode are expected to be stronger and tougher as the normal mode as described in fracture test experiments of mortar and concrete (Bazant & Pfeiffer, 1986). Therefore, deformation and damage in tangential direction of the cohesive zone model will be prevented for the numerical results presented in this work. $T_{max}(t)$ and G_{IC} are related through the normal displacement jump, $\delta_n(t)$, which is described by equation (11).

$$\delta_n(t) = \frac{2G_{Ic}}{T_{\max}(t)} \qquad (11)$$

The formulation of these elements is based on a non-dimensional effective displacement jump $(\lambda = |u_n/\delta_n|)$ that accounts for current normal displacement jump (u_n),

associated with the progression of the irreversible damage within fracture process zone.

The normal traction of the cohesive zone model is defined in equation **(12)**.

$$T_n(t) = \frac{1-\lambda^*}{\lambda^*}\left(\frac{u_n}{\delta_n(t)}\right)\frac{T_{\max}(t)}{1-\lambda_{cr}(t)} \qquad (12)$$

where $\lambda^* = \max(\lambda_{\max},\lambda)$, assuming $\lambda_{\max} = \lambda_{cr}$ if $\lambda < \lambda_{cr}$ and $\lambda_{\max} = \lambda$ if $\lambda > \lambda_{cr}$. The initially elastic behavior of the cohesive element have the same stiffness $(T_{\max}(t)/\delta_n(t)\lambda_{cr}(t))$ adjusting $\lambda_{cr}(t)$ to the changes of $T_{\max}(t)$ and $\delta_n(t)$. A scheme representing the time evolution of the time-dependent cohesive zone model described previously is depicted in Figure 6.2 (b).

6.2.2.3 The defect distribution model. As a random composite material, damage of mortar require a representation of its defects and heterogeneities which affect the strength from point to point in the solid (Carpinteri, 1986; Mihashi & Izumi, 1977; Wittmann & Zaitsev, 1981). A statistical distribution of defects of mortar associated to changes in tensile strength of mortar inside the solid is represented in our model using the classical Weibull (1939) distribution theory updated for this work for time-dependent changes of strength. The Weibull theory for a stochastic representation of defects for quasibrittle materials has been studied in depth and it has been determined to be used only for those cases where failure is expected as soon as a crack initiates somewhere in the structure (Bazant, 1999).

Later, other studies offered theoretical justification of Weibull theory by means of microscopic flaws or microcracks affecting the macroscopic strength response (Freudenthal, 1968; Freudenthal & Gumbel, 1956). Therefore under the conditions described before, the cumulative failure probability, $p(T_{max})$, of the selected test specimen as a function of the average instantaneous failure strength (T_o) and the Weibull parameter, m, is described by equation (13).

$$p(T_{\max}) = 1 - e^{-[T_{\max}(t-t_{set})/T_0(t-t_{set})]^m} \qquad (13)$$

The random spatial distribution of $T_{\max}(t-t_{set})$ depends on the evolution of T_o and m. Figure 6.2 (a) shows a scheme of the time evolution of $T_{\max}(t-t_{set})$ for a specific time evolution of T_o and for two different Weibull parameters (m = 5, 10; Bazant, 1999). Figure 6.2 also shows the distribution of the Weibull probability density function, $f(T_{max}/T_o)$, corresponding to m = 5 and 10, for specific ages. Finally, based on a randomly assigned value of $p(T_{max})$ to each cohesive element, the evolution of $T_{max}(t-t_{set})$ is assigned to determine the time-dependent cohesive zone law (see Figure 6.2 (b)).

6.3 Results

6.3.1 Creep Tests at Early Ages Using Solidification Theory with No Damage

The solidification theory of hydrating cement has the advantage of decoupling viscoelastic and aging behaviors to address the importance of each one in the mechanical response of cementitious materials (Carol & Bazant, 1993). For this purpose, a set of aging-viscoelastic measurements on concrete materials published previously (Bazant & Wu, 1974) are analyzed and some of them are modeled using the solidification theory to provide insights on: (1) the potential for decoupling viscoelastic from solidification parameters extracted from creep tests and (2), the importance of the viscoelastic parameters to address the viscoelastic evolution.

Bazant and Wu (1974) presented an extensive compilation of aging-viscoelastic responses of different mixtures of cementitious materials using creep tests at different ages. For this purpose, they estimated the relaxation modulus ($E_R(t,t')$), accounting for aging effects, to

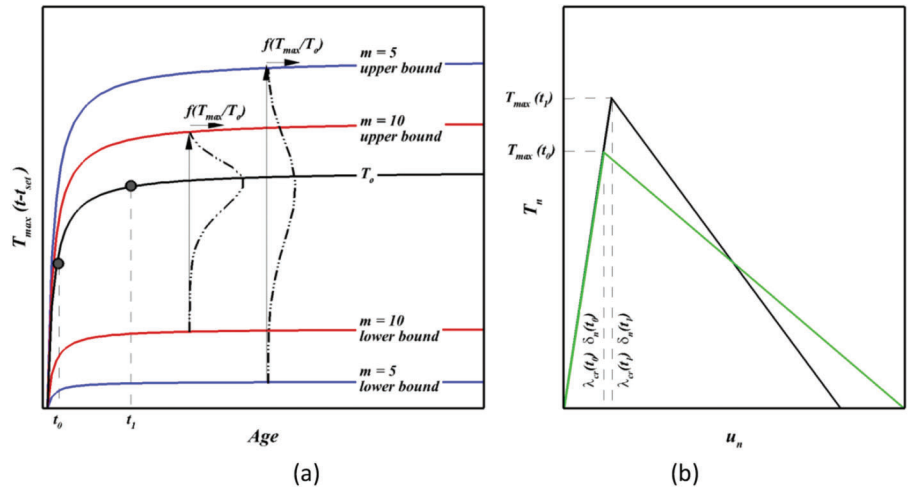

Figure 6.2 (a) Time evolution of $T_{\max}(t-t_{set})$ for a specific time evolution of T_o and for two different Weibull parameters (m = 5, 10), (b) scheme representing the time evolution of the time-dependent cohesive zone model at two different times.

describe the stress in time t caused by a constant unit of strain enforced in time t′ assuming that: (1) the stress is less than about 0.5 of strength in order to avoid significant microcracking, and (2) the water content is constant (Bazant & Wu, 1974).

Within Bazant and Wu's (1974) compilation of experimental results, the creep response of a concrete mixture with Type II cement and w/c of 0.56 is of our interest because of the mix design and the complete characterization of the mechanical response of it in this work. In this work, the creep response of this concrete mixture, enforcing a constant stress at $t' = 1$, 3, 7 and 28 days, is modeled using: (1) the viscoelastic response only using the instantaneous elastic modulus $E_0(t')$ for $t' = 1$ and 28 days and (2) the solidification theory for the same group of viscoelastic parameters as the first group (Figure 6.2) extracted from Bazant and Wu's (1974) work. The results show that for ages up to 20 days approximately, for the same set of coefficients of the Prony Series, the creep response of both viscoelastic only and solidification remains with a relative difference of less than 4%, ~20 days ($t' = 1$ day) either for viscoelastic properties obtained at $t' = 1$ or 28 days. On the other hand, those cases considering an elastic modulus, or solidification, of 28 days to represent the creep behavior early age concrete have a maximum deviation from experimental results of 15% at 20 days ($t' = 1$ day). This can be explained because of the difference between the elastic modulus at 1 and 28 days (<100%) for a Type II cement mixture as showed in Figure 6.3. As a result of the previous, for early ages up to approximately 15 to 20 days, it can be concluded that the viscoelastic response rules the creep evolution and so, it could be possible to adopt viscoelastic properties for early ages (less than 20 days) from a creep test independently of the solidification behavior. On the other hand, results from solidification theory in Figure 6.3 indicate that solidification theory is unable to predict long-term, above approximately 20 days, viscoelastic behavior as pointed out by Grasley and Lange (2001), and earlier by Bazant and Prasannan (1989). The reason for the later was explained by Bazant as an additional effect related to the loss of water (Bazant, Hauggaard, Baweja, & Ulm, 1997).

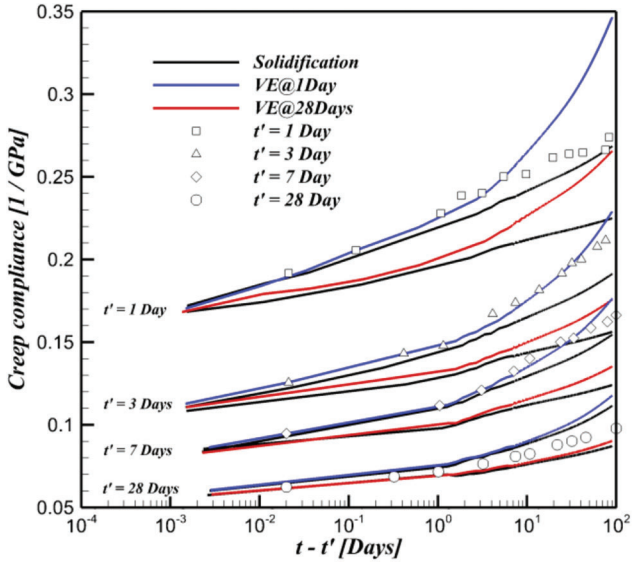

Figure 6.3 Representation of creep response at different ages using viscoelasticity only and solidification of concrete made of Type II cement and w/c of 0.56.

6.3.2 Stress and Strain Behavior of Restrained Mortar at Early Ages Using the Restrained Ring Test

6.3.2.1 Significance of the restrained ring test. The restrained ring test is an experimental tool that can provide insightful information about concrete stress and strain development and age of cracking (AOC) under restrained shrinkage deformation at early ages caused by uniform and non-uniform self-drying and moisture diffusion along its surfaces under different levels of mechanical restraint (Hossain, 2003; Hossain et al., 2003; Hossain & Weiss, 2004, 2006; Moon, 2006; Moon et al., 2006; Moon, Rajabipour, Pease, & Weiss, 2005; Moon & Weiss, 2006; Radlinska, Moon, Rajabipour, & Weiss, 2006). It was demonstrated that the age of cracking is not a material property and is dependent on the geometry of the sample being tested (Raoufi, 2011). In this work, the ring test is modeled because of its potential to provide meaningful information about how the aging-viscoelastic response in addition to defect distribution affect the stress and strain response of cementitious materials at early ages, under restrained conditions.

The test sample of the ring test consists of fresh mixed concrete cast and compacted around a metallic ring. The circumferential strain is measured in the inner radius of the metallic ring as shrinkage of the mortar or concrete evolves up to the point where the sample losses its loading capacity due to the macroscopic cracking of the material which, in general, occurs in an unstable fashion (see Figure 6.4 (a)) (Hossain, 2003; Hossain & Weiss, 2004, 2006). Under uniform moisture content evolving within a specific mixture of cementitious material, the AOC and the evolution of the circumferential tensile stress at the inner radius of mortar are used as indicators of the resistance of a specific mixture to cracking under restrained shrinkage with respect to similar mixtures under the same conditions (Hossain, 2003; Hossain & Weiss, 2004, 2006).

The role of degree of restraint and autogenous and drying shrinkage has been studied experimentally in detail by many scholars (Hossain & Weiss, 2004; Raoufi et al., 2011; Weiss & Shah, 2002; Weiss et al., 1998). These studies provided an estimation of the stress development over time in the mix (mortar or concrete) using continuum (no damage) linear elastic models with homogenous properties. In these works, it was observed that the pressure exerted by mortar on the steel ring before total failure reduces as the level of mechanical restraint increases. Hossain and Weiss (2004) attribute this stress dependence to the history and distribution of damage.

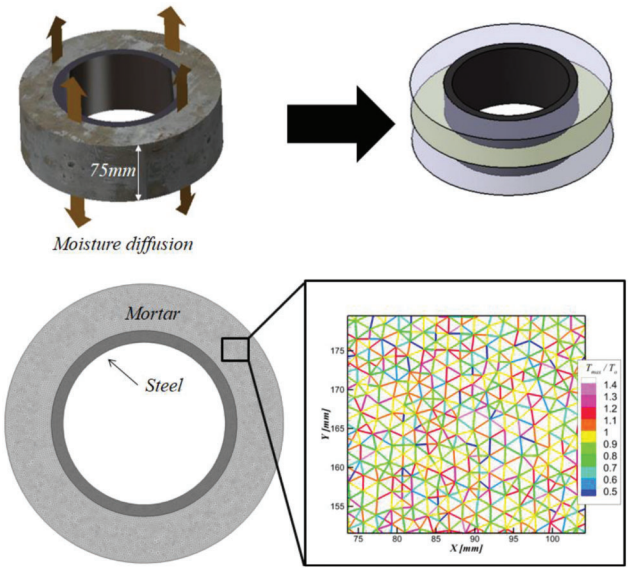

Figure 6.4 (a) Scheme of ring test; (b) finite element model of the ring; (c) detail of models used to represent the steel ring and the mortar; and (d) stochastic distribution of cohesive strength within mortar.

Total failure on the restrained ring tests forms radially, perpendicular to the plane form by the radial and circumferential direction of the ring (Grzybowski & Shah, 1990; Hossain & Weiss, 2004; Krauss & Rogalla, 1996). From the fracture mechanics point of view, this is expected to occur on specimens where the height of the sample, 75 mm, is less than l_{fpz}, typically more than 84 mm which the l_{fpz} for an age of 28 days (Hossain & Weiss, 2004). Taking into consideration the previous description, a 2D finite element (FE) model accounting for damage could be representative of the mechanical behavior of the restrained ring tests. In this work, the restrained ring test is modeled using a 2D plane strain finite element model representing a slice of the ring as showed in Figure 6.4 (b). Both, the steel and the mortar ring are modeled with triangular, constant strain, elements of 3-nodes (see Figure 6.4 (c)). Friction between the steel and the mortar is prevented in experiments. Therefore, the finite element model uses interface elements between the steel and the mortar that prevents friction between these two bodies (Figure 6.4 (c)). Finally, the cohesive zone elements used to represent damage evolution within the mortar are embedded across the finite element mesh, each one of them with a stochastic distribution of its time-dependent properties as described earlier (Figure 6.4 (d)).

Mesh dependence needs to be addressed since the probability of introducing a weak cohesive element is based on the element size and distribution as suggested by Zhou and Molinari (2004). According to this, larger elements are more likely to contain more defects. Therefore, an artificial localization (described in terms of local energy dissipation) may occur and a mesh convergence analysis is required to determine the effective mesh size to avoid mesh dependence on the distribution of defects using a Weibull distribution, avoiding excessive computational costs. Five meshes are tested with three different uniform element size distribution (4, 3, 2, 1, 0.5 mm) in a slice of 10 degree of the restrained ring. Each mesh is tested using three different randomizations to provide a stochastic representation of the total dissipated energy. It is observed that the coarser meshes (3 and 4 mm) show a difference of the average total dissipated energy with respect to the finer mesh of 60%. On the other hand, the average total dissipated energy varies less than 6% between the three finer element size used for this convergence analysis (0.5, 1 and 2 mm) as well as the spatial distribution of dissipated energy. The convergence of these two factors (total dissipated energy and spatial distribution) permits to select a uniform element size of 2 mm to model the restrained rings of mortar selected for this work.

6.3.2.2 Physical variables used to compare numerical and experimental results. Hossain and Weiss (2004) suggested that the residual interface pressure between the steel ring and the mortar, $P_{residual}$, can be computed as the pressure required to cause a strain that is equivalent to the average measured strain in the steel, $\varepsilon_{st}|_{R_{IS}}$ at R_{IS}, as shown in equation (14):

$$P_{residual} = -\varepsilon_{st}|_{R_{IS}} E_S \frac{(R_{OS}{}^2 - R_{IS}{}^2)}{2R_{OS}{}^2} \qquad (14)$$

where R_{os} and R_{IS} are the external and internal radius of the steel ring respectively, E_s is the elastic modulus of the steel. As discussed by Hossain and Weiss (2004), equation (14) illustrates that $P_{residual}$ can be determined using only the mechanical properties and geometry of the steel ring and $\varepsilon_{st}|_{RIS}$ using the electrical resistance strain gages. The only two assumptions are that $P_{residual}$ is uniform and that the steel ring remain elastic at all times.

The recorded $P_{residual}$ is contrasted with the integrated pressure, $P(\theta)$, over the circumference of the inner ring of the mortar (using θ as the angle that describes the circumference) in contact with the steel, called P_{eq}, in a finite element model of a restrained ring using the solidification theory to account for the aging-viscoelastic behavior at early ages of mortar. P_{eq} is estimated considering quasi-static equilibrium between the pressure exerted by the mortar ring and the reaction of the steel ring (assumed as linear elastic) at the interface of both, through the whole external area of the steel ring ($\theta_f - \theta_i = 2\pi$ radians).

6.3.2.3 Model parameters. Hossain and Weiss (2004) provided measurements of the restrained ring tests of mortar under different levels of restraint (Hossain, 2003; Hossain et al., 2003; Hossain & Weiss, 2006). To account for the free shrinkage of this mortar, $\varepsilon_{SH}(t)$, described in equation (1) the time of final set, t_0, adopted is 8 hours and the age when drying is initiated, t_d, as 1 day. The selected experiments to be modeled with the solidification theory in this work are mortars made with Type I cement and water to cement ratios (w/c) of 0.5. As discussed before, it is accepted that the viscoelastic

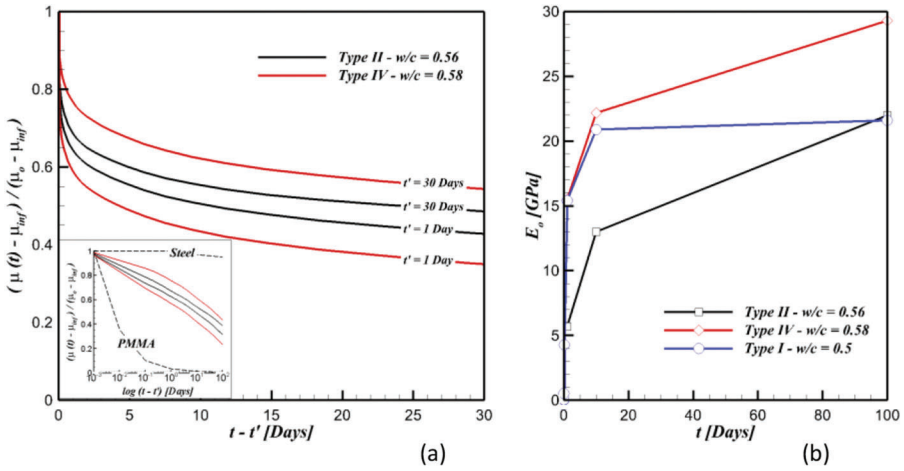

Figure 6.5 (a) Type II—w/c 0.56 and Type IV—w/c 0.58 (Bazant & Wu, 1974), PMMA (Park & Schapery, 1999), Steel (McLean et al., 2010); (b) Type I—w/c 0.5 (Hossain & Weiss, 2004), Type II—w/c 0.56 and Type IV—w/c 0.58 (Bazant & Wu, 1974).

response of cementitious materials is given by the cement paste. It was observed that solidification has minimum effect on the creep response of cementitious materials for short terms at early ages (see Figure 6.5 for Type II cement mixtures) and so, pure viscoelastic responses can be extracted from these tests. Hydrated cements made of Types I and II cements have similar compositions and behavior. For these reasons, the viscoelastic parameters estimated by Bazant and Wu (1974) at t′ 1 and 28 days are used to describe the viscoelastic response of mortar rings.

Table 6.1, presents the coefficients for each set of viscoelastic parameters described in equation **(10)**:

The importance of addressing the solidification for a specific cementitious material could be described by the evolution of $E_0(t)$ as showed in Figure 6.5 (b). The significant differences of $E_0(t)$ between concrete mixtures (up to 200%) indicate that the absolute aging-viscoelastic stress and strain requires $E_0(t)$ to be addressed for each specific concrete mixture. On the other hand, the viscoelastic behavior of cementitious materials could have a well-defined region even for mixes of different types and responses. Figure 6.5 (a) shows the evolution of the normalized relaxation modulus of different mixtures of concrete tested within a range of 28 days. It is observed that even for different cements (e.g., Type II and IV) the decay of the normalized relaxation modulus varies less than 30%. The inset in Figure 6.5 (a) compared these concrete mixtures with respect to other extreme viscoelastic responses (steel and PMMA; McLean, Brown, & Vinci, 2010; Park & Schapery, 1999). This shows that even though it was said that the viscoelastic parameters of concrete are relevant for the aging-viscoelastic response it is clear that a well-defined range for concrete materials could be address with respect to other materials.

The stochastic cohesive zone model implemented for this work requires, the definition of the critical strain energy release rate, $G_{IC} = 50N/m$ (Moon & Weiss, 2006), the Weibull parameter, m, and the average instantaneous failure strength (T_o). The Weibull parameter, m, is completely determined by the experimentally observed scatter of the results of tests of from multiple specimens (Bazant, Pang, Vořechovský, Novak, & Pukl, 2004). For instance, Zech and Wittman (1977) estimate the Weibull modulus for plain concrete using middle range laboratory specimen and estimated a value of m = 12. Later, Bazant and Novak (2000a) extended Zech and Wittman's (1977) analysis using data from multiple previous studies to account for the influence of the Weibull modulus on the flexural strength for a wide range of specimen sizes. Bazant and Novak (2000b) combine an empirical estimation of the deterministic flexural strength of concrete beams associated with the size of the tested samples to the statistical distribution of flexural strength using a Weibull type distribution. From this analysis they show that due to the limited experimental data of Zech and Wittman (1977), their estimation of m correspond to middle range laboratory specimen. In their study, Bazant and Novak (2000a) indicate that m should be larger than 20 and less than 25 to provide the best fitting for the strength of plain mortar and concrete. As $m \to \infty$, $T_{\max}(t-t_{set}) \to T_o(t-t_{set})$, i.e., the strength distribution tends to the deterministic value. The evolution in time of T_o and the instantaneous modulus of elasticity (E_o) of mortar is driven by the growth of hydrated cement volume fraction (Bentur, 2003), v(t), described in equation (15):

$$v(t-t_{setting}) = \frac{C_4 \cdot \lfloor t-t_{setting} \rfloor}{1 - C_4 \cdot \lfloor t-t_{setting} \rfloor} \qquad (15)$$

TABLE 6.1
Coefficients for each set of viscoelastic parameters.

i	0	1	2	3	4	5	6	7
λ_i(Day)	0	0.005	0.05	0.5	5.0	50.0	500.0	5000.0
μ_i@1 Day	0.112	0.128	0.102	0.092	0.114	0.160	0.182	0.110
μ_i@28 Day	0.252	0.078	0.076	0.083	0.096	0.111	0.146	0.158

where C_4 is 2.45 (1/Day) for the mortar modeled in this work (Hossain & Weiss, 2004). The evolution of T_o and E_o are defined respectively as:

$$\begin{cases} T_0 = T_\infty v(t - t_{setting}) \\ E_0 = E_\infty v(t - t_{setting}) \end{cases} \quad (16)$$

where the maximum tensile strength, T_∞, is 4.73 Mpa and the maximum instantaneous elastic modulus, E_∞, is 21.37 Gpa determined for the mortar modeled in this work (Hossain & Weiss, 2004).

As for the linear response of the steel ring, it is considered an elastic modulus of 200 Gpa and a Poisson ratio of 0.3.

6.3.2.4 Aging-viscoelastic behavior of restrained mortar at early ages represented by solidification theory using the restrained ring test with damage. Mortar samples under different levels of restraint ($h = R_{OS}–R_{IS}$ = 3, 6, 9, 14, 19 and 30 mm) are modeled and the mechanical response is presented in this section using previous experimental data (Hossain, 2003; Hossain et al., 2003; Hossain & Weiss, 2004, 2006). The restrained ring of mortar is modeled including the stochastic description of defect distribution presented earlier to account for damage in particular, on those mortar specimens under high level of restraint, which have showed microcracking development in experiments and ultimately sudden failure. P_{eq} is quantified in the models before and at failure and compared with measurements (Hossain, 2003; Hossain et al., 2003; Hossain & Weiss, 2004, 2006). To study the dependence of P_{eq} on the random spatial distribution of $p(T_{max})$ each case with a specific level of restraint is analyzed considering three (3) different randomizations of $p(T_{max})$ separately. Figure 6.6 (a) shows a typical evolution of P_{eq} vs. age for a specific level of restraint (h = 9 mm) for three values of m = 5, 10 and 50. The same evolution of P_{eq} is observed in each case up to failure regardless of m even for an extreme case with a wide spread of defects (m = 5). The evolution of P_{eq} is also independent of random distribution of $p(T_{max})$. On the other hand, the peak value of P_{eq} is driven by m as showed in Figure 6.6 (a). As m reduces (wider spread of T_{max}) the peak value of P_{eq} (and so, $\varepsilon_{st}|_{R_{IS}}$ considering the steel ring as linear elastic) reaches a lower value than those cases that consider high values of m (recall $m \to \infty$ then $p(T_{max}) \to 1$) as showed in Figure 6.6 (a).

The sensitivity of the response of P_{eq} to the constitutive model to describe the mechanical behavior of mortar before the first modeled case fails (~ 9 days) is depicted in Figure 6.6 (b) for the case of h = 9 mm as well as Figure 6.6 for h = 3 and 19 mm using material parameters from a mixture using Type I cement and a w/c = 0.5 similar to the one used for the restraint ring experiments presented in this work (Hossain, 2003; Hossain et al., 2003; Hossain & Weiss, 2004, 2006), except for the viscoelastic parameters which are extracted from a similar mixture using Type II cement and w/c = 0.56 (Bazant & Wu, 1974). For the same age (~ 9 days), mortar considered as linear elastic over predicts the value of P_{eq} at least by 30% for h = 3, 9 and 19 mm. The error bar for P_{eq} estimated with linear elasticity corresponds to the difference between an early elastic modulus ($E_{t=1Day}$) and later one ($E_{t=28Day}$). In the same way, both viscoelasticity (considering $E_{t=1Day}$ and $E_{t=28Day}$), solidification-only (no viscoelasticity) and solidification are also depicted in Figure 6.6 (b) and Figure 6.6. The error bars in these cases (except for solidification-only) corresponds to the use of viscoelastic parameters obtained at $t' = 1$ and 28 days. Mortar considered as viscoelastic could either over predict the value of P_{eq} by at least 25% for $E_{t=28Day}$ a maximum of 15% if $E_{t=1Day}$ is used. The results obtained from the viscoelastic case using $E_{t=1Day}$ for 9 days should be considered carefully knowing that the elastic modulus of this mortar changes more than 400% within 1 and 10 days as showed in Figure 6.7 (b). P_{eq} obtained using solidification-only over predicts the experimental results by a minimum of 25%.

Finally, solidification model shows a maximum difference of 14% with respect to the experimental data for h = 3, 9 and 19 mm. These results show that both,

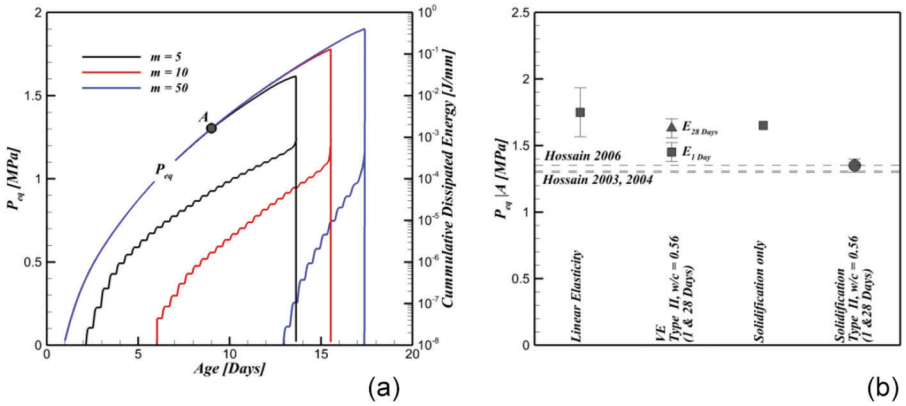

Figure 6.6 (a) Evolution of P_{eq} vs. age for h = 9 mm for a wide range of Weibull parameters; and (b) comparison of P_{eq} from simulations, using different constitutive models, and experiments at 9 days for h = 9 mm.

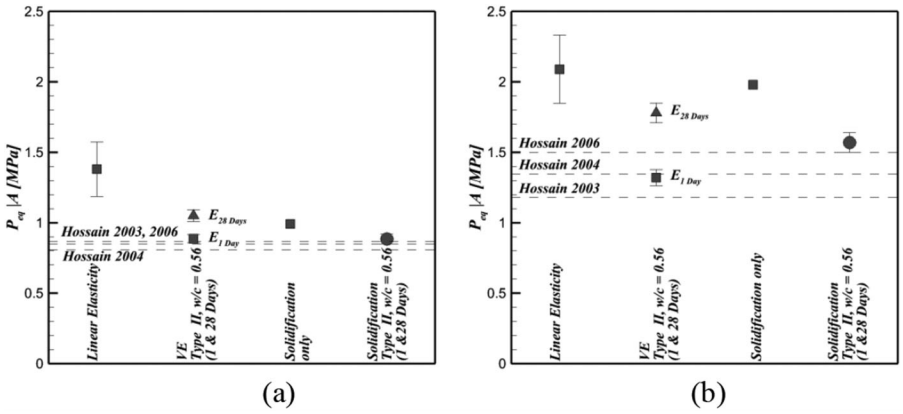

Figure 6.7 Constitutive model sensitivity for (a) $h = 3$ mm; and (b) $h = 19$ mm.

viscoelasticity as well as solidification are important mechanisms to describe the mechanical response of mortar at early ages. Also, the viscoelastic results in Figure 6.6 (b) and Figure 6.7 indicate that assuming a single value of elastic modulus could provide similar results to the results from solidification that uses the real evolution of elastic modulus of mortar. On the other hand, it is important to notice that the impact of using different viscoelastic parameters extracted at early ages from creep tests ($t' = 1$ and 28 days) has a minor impact on the case with solidification rather than the case using viscoelasticity. The impact of using different viscoelastic parameters is 20% less in the estimation of P_{eq} at 9 days in the results using the solidification model. The sensitivity of a shift of the $E_0(t)$ caused by an error determining the time at which this parameter is measured is negligible even if a shift of three hours is committed.

Figure 6.8 shows values of P_{eq} at 9 days vs. h using solidification theory with viscoelastic parameters at $t' = 1$ and 28 days (error bars) from a mixture using Type II cement and a w/c = 0.56 similar to the one used for the restraint ring experiments presented in this work (Hossain, 2003; Hossain et al., 2003; Hossain & Weiss, 2004, 2006). The results from this model is compared to the response obtained from experiments (Hossain, 2003; Hossain et al., 2003; Hossain & Weiss, 2004, 2006). The results in this Figure 6.8 show that there is a good match (less than 10% error) between P_{eq} and $P_{residual}$ for h = 3 and 9 mm. Higher dispersion in the experimental results is observed for h = 19 mm and the solidification model shows an asymptotic behavior as the level of restraint increases similar to Hossain and Weiss (2004).

Figure 6.9 shows an example of a typical curve of P_{eq} vs. age compared with $P_{residual}$ obtained from experiments for the same level of restraint. Figure 6.9 also shows a qualitative comparison of the cumulative dissipated energy vs. age obtained from simulations which is compared with the acoustic emission (AE) measurements performed for the ring tests experiments (Hossain et al., 2003). AE is an important tool to describe microcracking of brittle materials (Landis & Baillon, 2002; Lockner, 1993; Maji, Ouyang, & Shah, 2011; Ohnaka, 1983; Ouyang, Landis, & Shah, 1992). It has been used to describe the evolution of microcracking of quasi-brittle materials like concrete providing good information about the age at which microcracking starts and how it evolves over time (Hossain et al., 2003). Both, AE and the cumulative dissipated energy obtained from the solidification model present good agreement. The model is capable of capturing the age of initiation of microcracking as well as the evolution up to failure for the different levels of restraint.

However, our model shows that the peak stress at failure of the solidification model coincides with experiments for Weibull parameters close to $m = 10$. This is not in accordance with the estimation of the Weibull parameter performed in previous works (Bazant & Novak, 2000a; Zech & Wittmann, 1977). The possible reason is that the proposed model uses a deterministic value of defect distribution, m, associated to the intrinsic variability of the strength of mortar and concrete. A model that could account for strength changes due to the loading history would be necessary to address age of cracking of concrete and mortar.

On the other hand, more information is needed about how damage is spread. It is believed that the distribution of microcracks is uniform across the circumference of the ring but increases close to the inner ring of steel however there is experimental evidence of that up to now. Figure 6.10 and Figure 6.11 shows a sequence of the spread damage within mortar as age evolves confirming what was stated before about the damage distribution of restrained mortar drying from the top and the bottom as the experiments modeled in this work (Hossain, 2003; Hossain et al., 2003; Hossain & Weiss, 2004, 2006).

6.4 Comments and Discussion

The results from creep modeling and tests presented in section 6.3.1 indicate that the creep response of an aging-viscoelastic material like concrete at early ages, for periods of time no longer than approximately a

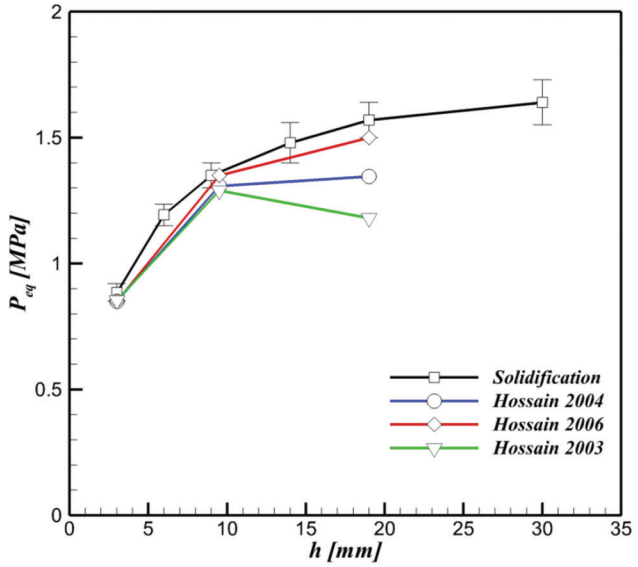

Figure 6.8 Error bars show solidification with VE at 1 and 28 days.

month, depend mostly on the viscoelastic parameters rather the solidification behavior. In other words, the creep response depends on the viscoelastic response of the solidified material up to the time of loading, t'. From these observations, the viscoelastic properties of cementitious materials are extracted from creep tests and used in the solidification model in conjunction with the time evolving solidified volume fraction to describe the aging-viscoelastic behavior of restrained mortar at early ages during short periods of time.

The previous statement is not the case for a general case of mechanical loading of an aging-viscoelastic material, i.e., the restrained ring tests. For the restrained ring test, the expected response (described by P_{eq} and $\varepsilon_{st}|_{R_{IS}}$) is aging-viscoelastic rather than viscoelastic. This could be explained considering that in this case the loading condition evolves over time as the volume of solidified material does. Therefore, each increment of $\varepsilon_{SH}(t)$ is sustained by a material with different volume of solidified matter (i.e., different overall stiffness) affecting the pure viscoelastic stress and strain behavior of mortar.

The results presented in section 6.3.2.4 indicate that the short-term, aging-viscoelastic response of restrained mortar at early ages, before failure, can be described by the solidification theory. For all the levels of restraint, the structural response of the mortar ring described by P_{eq} is independent of the distribution of defects prior to failure. Within the range of viscoelastic parameters of concrete, it is shown that the ring test has less sensitivity to changes of viscoelastic parameters assuming a solidification behavior. The use of more simplified models to describe concrete or mortar (i.e., viscoelasticity) could provide similar results to experiments assuming unrealistic parameters (i.e., constant elastic modulus). For this reason, the evolution of solidification must be addressed carefully. Moreover, the numerical and experimental results show that damage is present a few Hours/Days after set, even for restrained rings with low level of

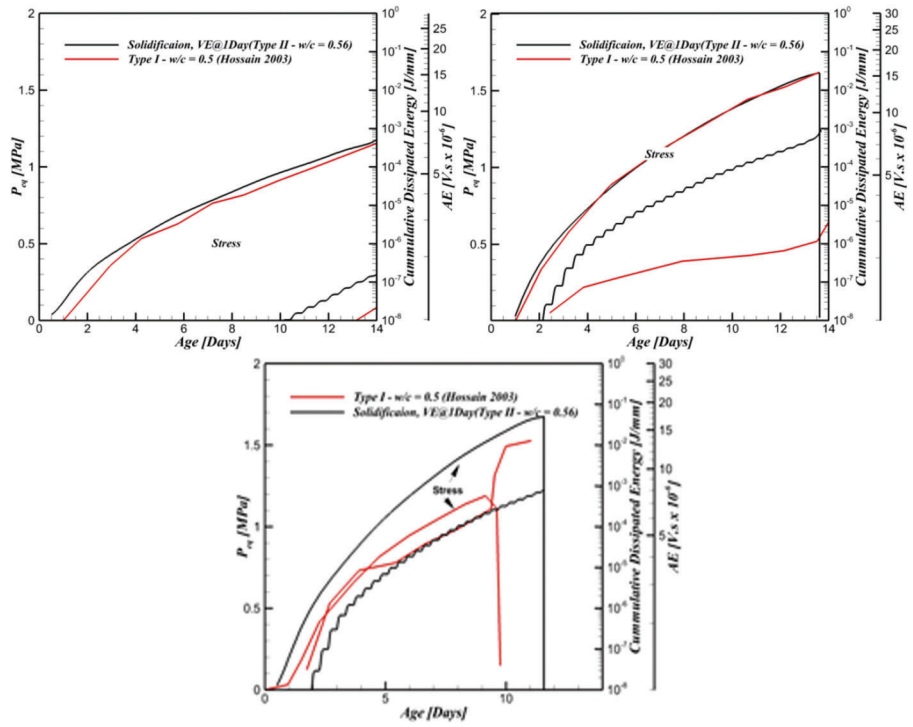

Figure 6.9 Example of a typical curve of P_{eq} vs. age compared with $P_{residual}$ obtained from experiments for the same level of restraint.

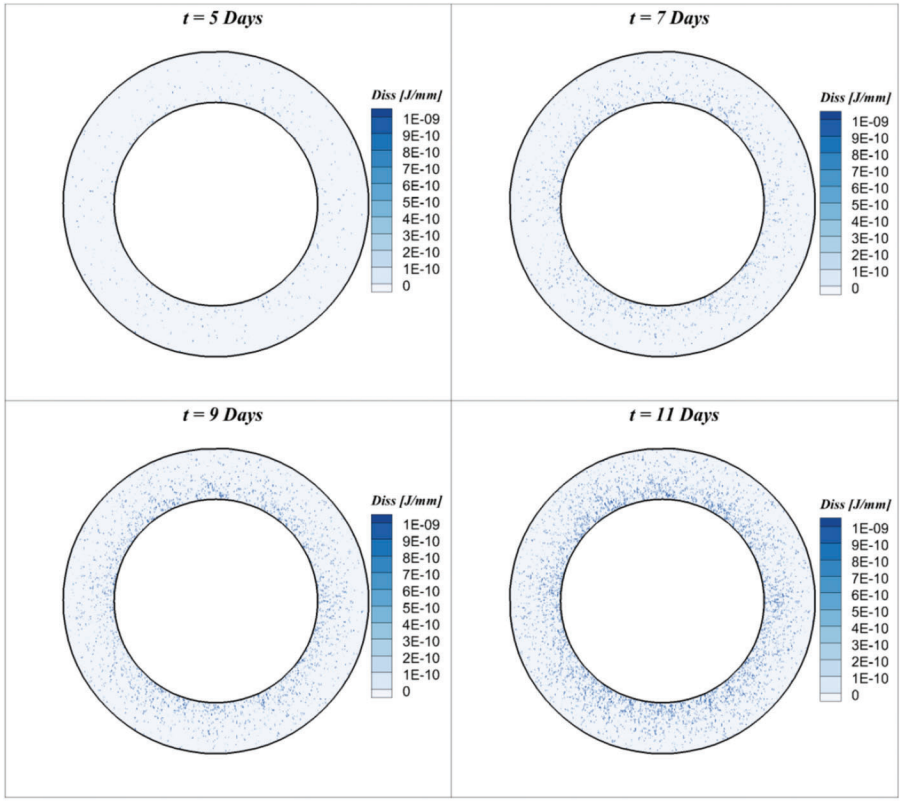

Figure 6.10 Sequence of distributed damage in mortar (h = 9 mm).

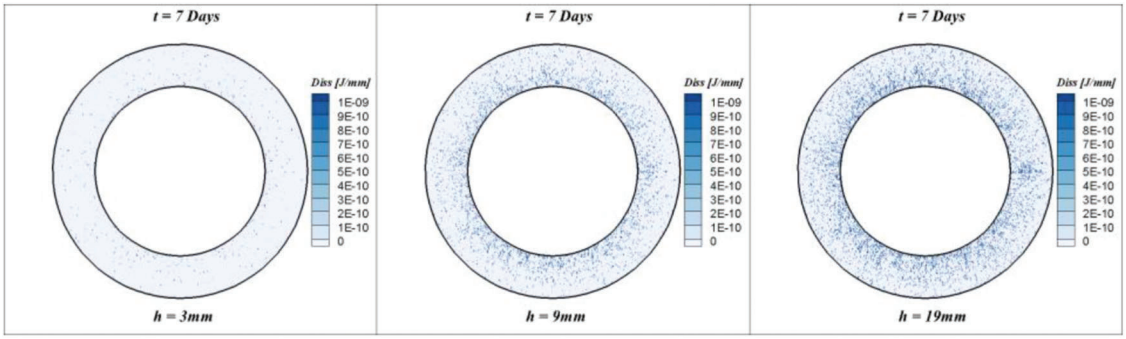

Figure 6.11 Dissipated energy for different levels for restraint at 7 days (same Weibull parameters, m = 5).

restraint (3 mm) indicating that any attempt to extract viscoelastic properties will have to deal with damage evolution as well. In summary, the use of the ring test to determine mechanical parameters of mortar and concrete could have limitations due to the low sensitivity to changes in viscoelastic parameters and the necessity to have a precise measurement of solidification and damage evolution.

The stochastic damage model presented in this work only accounts for preexisting defects in the mortar prior to restraint. The peak values of P_{eq} as a function of the thickness of steel used to enforce mechanical restraint to mortar. This shows that there is only a change of peak P_{eq} of 6% for steel thicknesses between 3 and 30 mm. The dependence on the peak value of P_{eq} on m is nothing more but related to the use of a macroscopic strength-dependent damage model to capture failure. The peak value of $P_{residual}$ reduces for high levels of restraint, and similar $P_{residual}$ development prior to failure due to microcracking that significantly contribute to the relaxation effect (Hossain et al., 2003). The peak P_{eq} and the AOC could be captured with a damage model that account for the microscopic damage progression associated with the loading history.

7. STUDY OF THE CHANGES IN CRACK PATTERN DUE TO CHANGES IN DOH

7.1 Introduction

The rate of mechanical properties development of concrete is strongly influenced by the temperature of the concrete and its surrounding environment. The maturity method has been proposed as an approach to estimate mechanical property development in concrete. This maturity method can be related to mechanical property development (i.e., strength or stiffness) and used to describe strength and stiffness under the specific temperature history to which the structure is exposed.

The precise prediction of strength development using the maturity method requires that the mixture design and constituent materials used to develop the relationship between the maturity and strength are similar to the concrete for which the properties are to be predicted (Barde et al., 2005). It was illustrated that even the slight variations in mixture proportions that can occur during construction should be considered for accurate maturity predictions (Graveen, Weiss, Olek, & Nantung, 2003). Further, it was hypothesized that aggregates play a key role in flexural strength development, and after a specific degree of hydration is achieved the presence of aggregates can alter the maturity–strength gain relationship. To capture the influence of the properties of each phase (i.e., paste, aggregate, and ITZ), researchers have proposed models to explain aggregate stiffness, strength, and interface energy on the properties of concrete (Aquino, Li, & Shah, 1995). It was demonstrated that as the strength of the concrete increases, the aggregates become increasingly important (Wu, Chen, Yao, & Zhang, 2001). In this chapter, an investigation was conducted to illustrate how the mechanical properties and rate of aggregate fracture may be influenced by age of concrete.

Furthermore, a cohesive zone model as a non-linear fracture based model was used to compute the damage in concrete samples at specific ages. The material properties measured in the experimental program will be used as inputs for the finite element model. Extending the non-linear fracture based model considers the effects of material aging and loading on the potential for cracking will be the focus of this portion of work. The results show that the fractured aggregate quantity will be increased at a specific age of concrete.

7.2 Experimental Approach

7.2.1 Materials and Mixture Design

The samples used in this portion of study were a part of a large-scale experiment that was performed using a commercial concrete mixture from a ready-mix concrete truck, prepared with a 0.42 water-to-cementitious material ratio (w/c). Due to weather effects at the time of casting, the research team believes there was a difference between the design mix proportioning and proportioning received from the ready-mix producer. As such, the actual w/c is expected to not be the same as the design w/c which is likely caused by additional aggregate surface moisture. This could have potential to reduce the strength of the samples tested for this study. The fresh concrete was tested and found to have a slump of 6.0" and air content 6.0% (tested in accordance with ASTM C143/C143M – 12 ASTM C231/C231M – 10, respectively). The coarse aggregate is AP #8 aggregate from U.S. Aggregates in Delphi, IN. The fine aggregate is #23 Swisher Road from Vulcan Aggregates in West Lafayette, IN. The mixture proportions are shown in Table 7.1.

7.2.2 Testing Methodologies

Maturity development for the mixture was tested for flexural strength, compression and elastic modulus. The data was obtained over a 28 day period, taking measurements every 3h, starting at 10h from the time of water-to-cement contact for the next 24 hours (34 hours from the time of water-to-cement contact). Strength measurements were taken at after these times: 40 hours, 2 days, 4 days, 7 days, 14 days, and 28 days. For the flexural beam testing, the number of fractured aggregates was determined over time in order to evaluate the strength development. In conjunction with the maturity testing, additional beams were cut and tested from a restrained slab as shown in Figure 7.1. Fresh concrete was placed into the forms in which the deeper section on each end provides restraint to the middle section. More information regarding the restrained beams can be found by referencing Section 7.2.3. The flexural strength of these restrained beams were tested at ages of 7 days and 14 days to evaluate the role of micro-cracking as it pertains to possible strength reduction directly due to restraint.

7.2.3 Experimental Mechanical Properties of Concrete Beams

7.2.3.1 Flexural strength. The flexural strength of the concrete was determined in accordance with ASTM C78-10, standard test method for flexural strength of concrete using third-point loading. Simple beams with approximate dimensions of 6 in. tall $\times$ 6 in. deep $\times$ 21 in. long beams were cast to study the flexural strength. The exact dimensions were recorded at the time of experiment and used in the flexural strength calculations.

TABLE 7.1
Design quantities of materials used in concrete test specimens.

Material	Design Quantity	Units
#8 Coarse Agg., SSD	1800	lb/yd^3
#23 Fine Agg., SSD	1275	lb/yd^3
Buzzi Cement	440	lb/yd^3
Class C Fly Ash	100	lb/yd^3
Water	226.6	lb/yd^3
Water Reducer	2.0	oz/cwt
Air Entrainer	1.3	oz/cwt

Figure 7.1 Restrained slab mold (left) in which the deeper end sections provide restrained to the 6 in. deep middle section. The mold filled with concrete (right) has a divider to enable cutting 6 in. by 6 in. beams to tested in flexure.

These samples are assumed free of restraint during set and are therefore considered in an 'undamaged' condition upon testing. In addition, specimens were cut from restrained slab to have the approximate dimensions of the six beam samples ($6 \times 6 \times 21$ in.) as shown in Figure 7.2.

These slabs are designed to provide restraint (and to induce damage). The beam specimens were cast in two lifts, vibrated, and rodded after each lift. The concrete beams remained in molds, under damp burlap and a plastic sheet until the time of testing. The samples were maintained in a temperature controlled environment at 23 $\pm$ 0.5 °C. The flexural strength of the mixture was determined at various ages under third-point loading, loaded at a rate of 35 $\pm$ 5 lb/s as shown in Figure 7.3. The internal temperature of the beam specimens was monitored from placement throughout the duration of testing.

7.2.3.2 Compressive strength. The compressive strength of cylindrical concrete specimens was determined in accordance with ASTM C39-12. Sets of three, 4 in. diameter by 8 in. tall (100 mm by 200 mm), cylinders were cast to study the compressive strength of the mixture. The cylinders were cast in two lifts, being vibrated and rodded 25 times after each lift. The concrete cylinders remained in molds (a sealed condition), placed in a temperature controlled environment at 23 $\pm$ 0.5 °C. Three cylinders per testing age were used to determine an average compressive strength of the mixture at each age. The cylinders were loaded at a

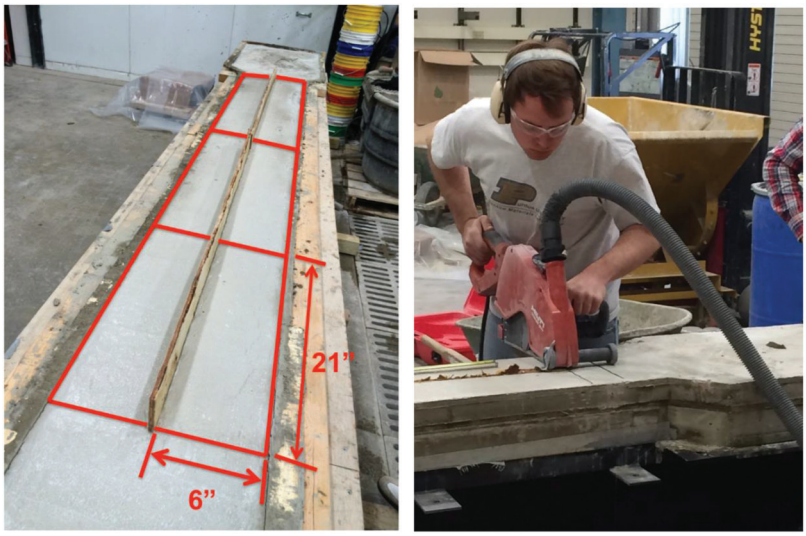

Figure 7.2 Total of 6 beams cut from the restrained slab (left) and picture of cutting beams from the middle section of the slab (right).

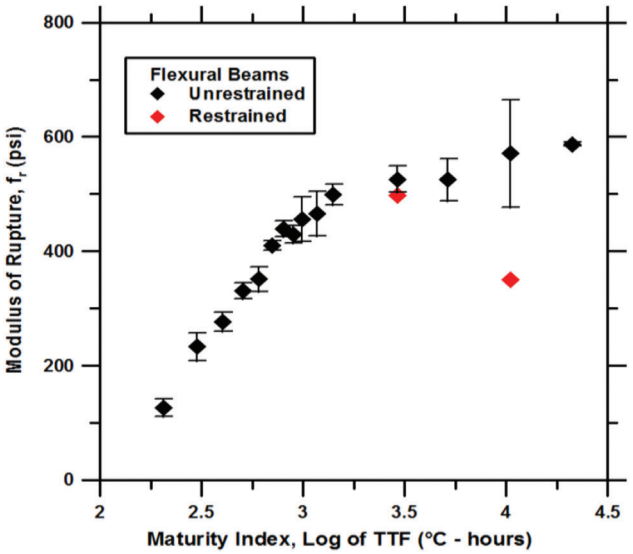

Figure 7.3 Modulus of rupture (flexural strength) vs. maturity index (equation **(1)**) plot demonstrating the maturity response of the mixture in flexure. Also presented is a plot of restrained flexural beams, demonstrating the role of micro-cracking in a reduction of strength.

rate of 35 ± 2 psi/s (0.25 ± 0.05 MPa/s) in a 700 kip (3100 KN) hydraulic compression machine, utilizing neoprene end caps. The resulting data was used in developing a strength-age relationship as shown in Figure 7.4.

7.2.4 Elastic Modulus

The static modulus of elasticity (Young's modulus of elasticity) was determined using a procedure similar to that in ASTM C469-10. Sets of two, 4 in. diameter by 8 in. tall (100 mm by 200 mm), cylinders were cast to study the elastic modulus of the mixture. The cylinders were cast in two lifts, being vibrated and rodded 25 times after each lift. The concrete cylinders remained in molds (a sealed condition), placed in a temperature controlled environment at 23 ± 0.5 °C. Upon testing, the cylinders were fitted with a compressometer, equipped with a linear variable differential transformer (LVDT) displacement transducer. The cylinders were then loaded to 40% of their ultimate strength two separate times. The resulting slope of the stress-strain curve from the second loading was taken as the static modulus of elasticity. For each age of testing, two cylinders were tested for elastic modulus as displayed in Figure 7.5.

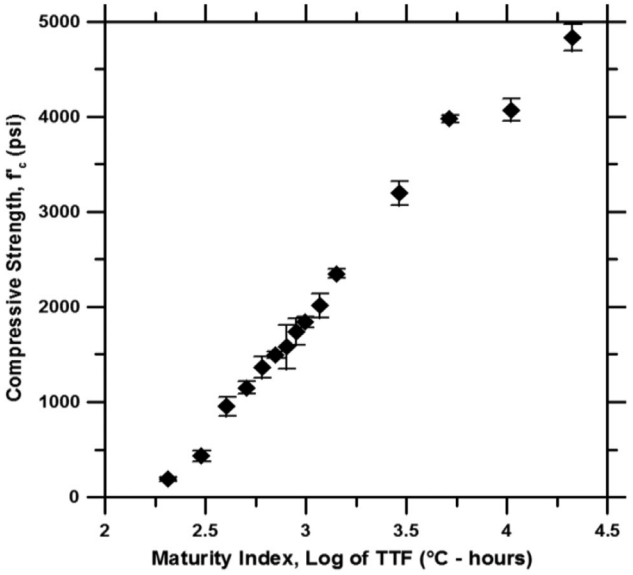

Figure 7.4 Compressive strength vs. maturity index shown in equation **(1)** plot demonstrating the maturity response of the mixture in compression.

7.2.5 Experimental Results and Analysis

The maturity method is a procedure in which the strength development of concrete can be estimated by considering the effects of time and temperature for different curing methods. It originated with work done relating to accelerated curing methods (McIntosh, 1949; Nurse, 1949; Saul, 1951) using equation (3).

Figure 7.6 presents the number of fractured aggregates in the flexural beams (obtained after the beam is tested). Figure 7.7 also presents results for flexural beams cut from a restrained slab. 6 beams were tested to obtain the data at each specific maturity index. Two of the beams tested at a maturity index of 4.0 °C-hours (14 days' real time) fractured prior to testing, resulting in zero strength, as displayed in Figure 7.7.

7.3 Numerical Approach

7.3.1 Fracture Mechanics Approach

This section discusses the feasibility of using a non-linear fracture mechanics based model to quantify the development of flexural strength of early age concrete. Specifically, the role of aggregates is examined in determining the strength development of maturing concrete. The maturity method is based on the concept that there is a proportional relationship between the material strength development and the extent of the hydration reaction that has occurred. A fracture mechanics approach is employed in this study to examine the role of aggregate (size, shape and distribution) on how it can impact this relationship.

A cohesive crack model is proposed to describe and quantify the damage in a mature concrete. This cohesive model is a phenomenological discrete damage model based on a traction-separation law that characterizes the fracture process zone. Such cohesive zone approach differs from the more traditional linear elastic fracture mechanics (LEFM) theory in the sense that there is no need to assume linear elasticity that leads to unrealistic square-root singularity around a sharp crack-tip. A prescribed cohesive surface traction-separation relation is used to adapt fracture characteristics of the materials as displayed

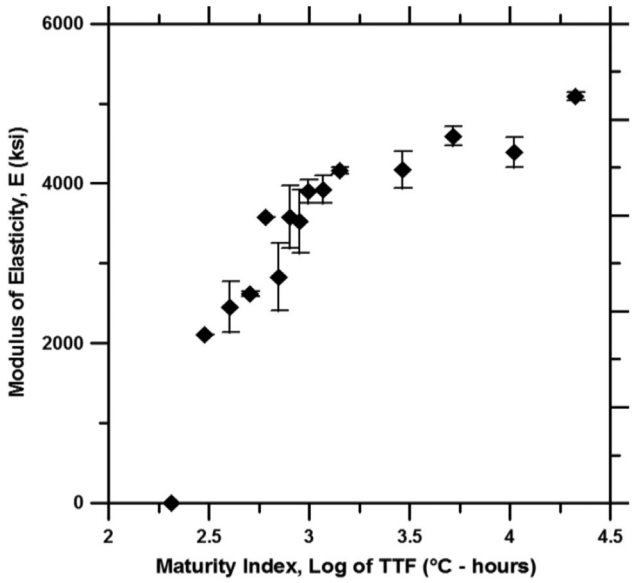

Figure 7.5 Modulus of elasticity vs. maturity index plot demonstrating the maturity response of the elastic modulus for the mixture.

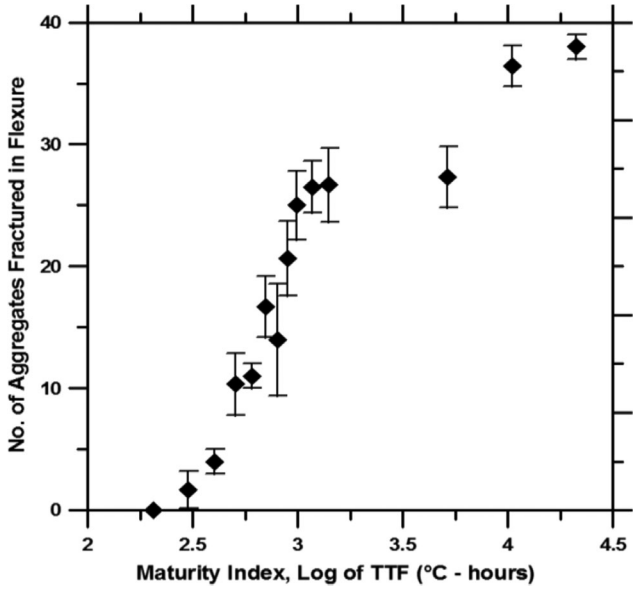

Figure 7.6 Number of fractured aggregates vs. maturity index (equation **(1)**) plot demonstrating the role of aggregate in concrete as it relates to concrete paste development.

in Figure 7.8 (a) (Camacho & Ortiz, 1996; Xu & Needleman, 1995). In a finite element framework, additional nodes are introduced along predefined interface inserted between volumetric elements. In this intrinsic approach, the failure criterion is incorporated within the constitutive model of the cohesive elements as a traction-separation law (Espinosa & Zavattieri, 2003). The damage in the cohesive zone takes place after the cohesive tractions reach a maximum value. Subsequent damage gradually decreases the cohesive traction to zero value at a point where the interface point is considered to fail as shown in Figure 7.8 (b). The area under the curve in Figure 7.8 (b) represents the separation critical strain energy release rate G_{Ic}.

Due to inherent complexity of the problem, it is not possible to find closed-form analytical solution for the present problem. As such, a finite element analysis is adopted (1) to understand the physical behavior of a third-point bending test and (2) to predict the failure of the beam as material discontinuity modeling accurately. This test method evaluates the flexural performance of concrete beam using parameters derived from the load-deflection curve obtained by testing a simply supported beam under third-point loading. The determined peak load and its corresponding stress are calculated by inserting them in the formula for modulus of rupture given in equation **(17)**.

$$f = \frac{PL}{bd^2} \tag{17}$$

where f is the flexural (third point) strength (MPa), P is the load (N), L is the span length (mm), b is the average width of the specimen at the fracture (mm), and d is the average depth of the specimen at the fracture.

A microstructure containing cohesive elements to predict the fracture was embedded in the middle of concrete beam as shown in Figure 7.9 (a). Figure 7.9 (b) illustrates the loading force applied by means of two loading pin with a distance between them equal to a half of the distance between the supporting pin on a mesh generated beam with span of 457.2 (mm) and height of 152.4 (mm). Since the loading is applied along with XY plane and no certain amount of stress concentration or nodal displacement is anticipated in the z direction, a plane strain analysis is selected to solve the problem.

However, the analysis shown in this chapter was made for concrete material in which initial flaws and strength distribution are inserted within a microstructure as shown in Figure 7.10 (a). This microstructure is embedded in the middle of concrete beam's span to (1) quantify the peak applied load value to the pavement to identify flexural strength of concrete beam before its complete failure state; (2) reduce the computational time by decreasing number of inserted cohesive elements within discretized finite element beam.

Figure 7.10 illustrates the density of the generated mesh within microstructure imposed within concrete beam. Since the prediction of crack path depends on the size and the orientation of mesh elements based on the criterion of cohesive zone model, the number of elements inside the microstructure is increased. One of the main objectives of this numerical analysis is to assess the role of aggregate on crack nucleation, evolution, and maximum peak load that composite cementitious material may withstand. Thus, the microstructure is presumed to be composed of cement paste and aggregate, as shown in Figure 7.10.

The configuration and distribution of aggregates are derived from a cut cross-section surface of test cylinder. While two more microstructures containing random distribution of aggregates with same area fraction were built and simulations were performed on them, the final

Figure 7.7 Crack in the middle section of the slab, induced from restrained in 14 day samples (left) at a distance of approximately 22 inches from the restraining ends (right).

results did not vary noticeably. As such, the results are related independent of aggregate distribution. Since the cohesive zone model for fracture is only used to insert the damage to the microstructure in the middle of beam as shown in Figure 7.10 (a), the interface elements are inserted these elements to represent the traction-separation law and to reduce the simulation time. The magnitude of these forces is a function of relative separation and shear displacement between the two surfaces. The compressive tractions at the contact zone of two rollers at top of concrete beam as loading conditions and two stationary rollers at bottom part of concrete beam as fixed displacement boundary conditions are calculated through impenetrability condition employed in the contact model. Since all the simulation are performed in two dimensional configuration, the description for the formulation of the interface elements presented based on four-nodded linear finite element as shown in Figure 7.10.

7.3.2 Identification of Mechanical Properties of Components in Composite Cementitious Material

7.3.2.1 Mechanical parameters. The variation of the mechanical properties of concrete at early ages is strongly influenced by maturity. Using this information, one can predict the strength and stiffness of concrete for a specific temperature history. One of the challenges is to quantify the flexural strength of the concrete beam by considering the independent mechanical properties for each components of composite material.

However, the elastic modulus of concrete at early ages is obtained from results of modulus of elasticity testing operated on cylindrical specimen. The elastic modulus of Indiana dolomite aggregate is derived from Schmidt (1976), and Young's modulus of cement paste is thus calculated by performing numerical uniaxial tension on this composite material for different ages to obtain desired

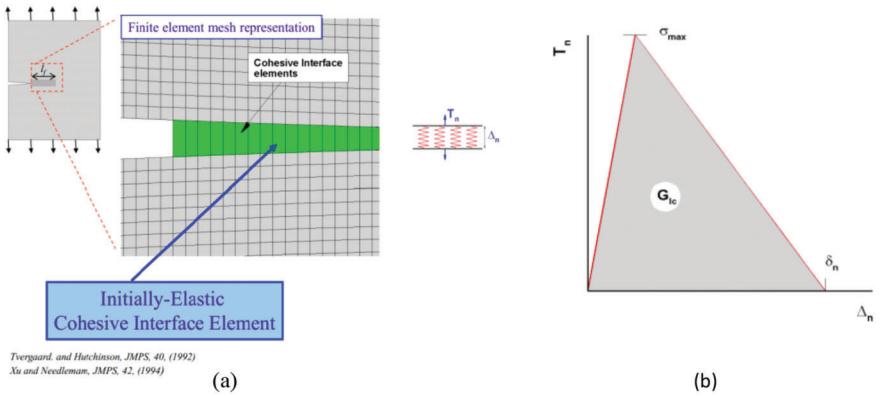

Figure 7.8 (a) Cohesive interactions approximate progressive nonlinear fracture behavior, named as the cohesive zone model, (b) the CZM is characterized by the two parameters of cohesive strength, T_{max}, and separation energy, G_{Ic} (shown only mode I-opening for simplicity).

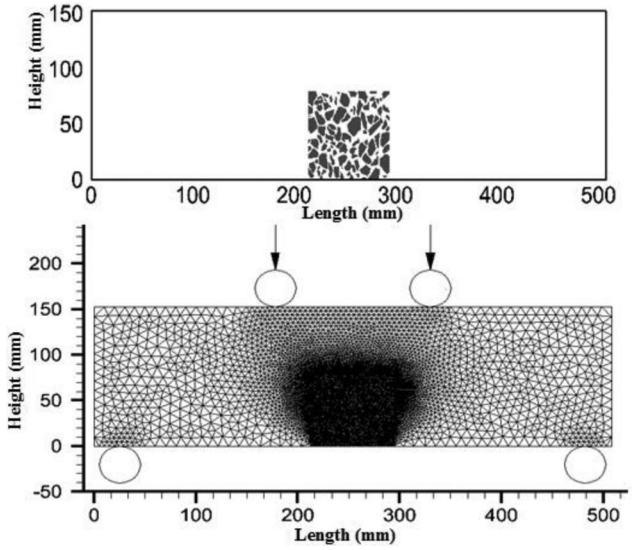

Figure 7.9 Discretized domain of beam element with triangular finite elements interconnected with nodal points.

elastic modulus for composite system reported in chapter 7.2.3.3 as shown in Figure 7.11. Poisson's ratio of all constitutive is assumed to be equal to 0.2.

7.3.2.2 Fracture parameters. A previous work (Barde et al., 2005) proposed that the flexural strength development for cement paste can be described as a linear function of its maturity age. However, this response is bilinear for mortar and concrete specimen since this change in response may be attributed to the presence of aggregate. Barde et al. (2005) demonstrate that the weaker response after a specific time may be correlated to either the presence of very weak aggregates or weaker mechanical properties developed within interfacial transition zone (ITZ). In the numerical approach used in this chapter, it is hypothesized that the aggregate particles initially start to fail after a specific time and crack also begins to grow through these particles since they possess less flexural strength than both cement paste and ITZ particles. Therefore, aggregate particles have a role on flexural strength of early-age concrete. In addition, it is assumed that cement paste and ITZ elements have the same fracture properties to simplify the simulation of role of aggregate in our numerical approach. Fracture toughness of three constitutive materials is considered to be unchanged during maturity period of concrete. The merely mechanical parameter which is variable over maturity time is flexural strength parameter of each constituent of concrete. This results in study the effect of individual flexural strength development of each component on overall flexural strength of concrete beam. Figure 7.12 shows the evolution in critical strain energy release of cement paste particles while the critical strain energy release of aggregate particles is unchanged. These values are derived from equation (18).

$$G_{IC} = \frac{K_{IC}^2}{E} \tag{18}$$

where G_{IC} is the critical strain energy release rate in mode I, K_{IC} is fracture toughness, and E is Young's modulus of material.

It is assumed that the initial slope or stiffness of the interface elements is compared to the stiffness of the material. An identical slope is selected for all cohesive elements with different fracture parameters as shown in Figure 7.13. Figure 7.13 displays the evolution of bilinear traction-separation relation of cohesive elements inserted within microstructure.

One of aspect of this work is to quantify the flexural strength of concrete beam by identifying the independent mechanical and fracture parameters for each individual constitutive material. Cohesive strength of

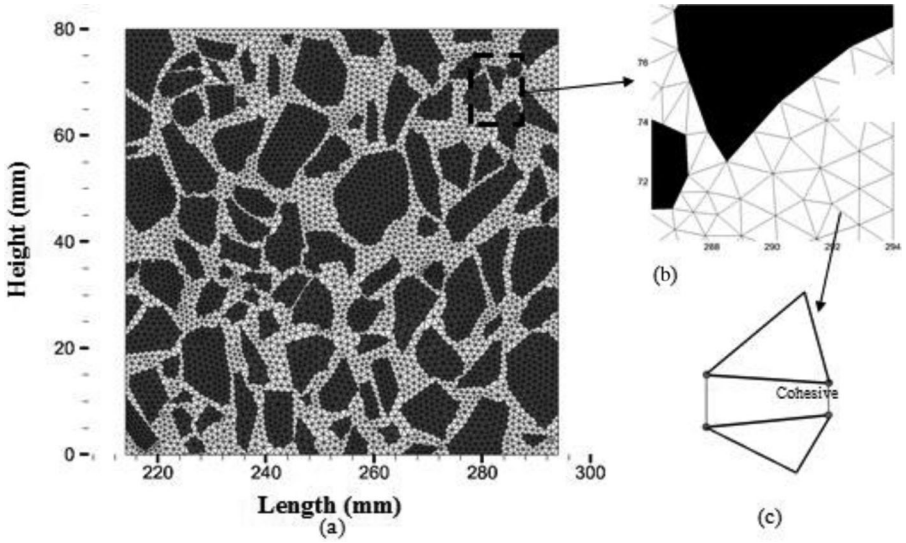

Figure 7.10 (a) Schematic of Concrete microstructure composed of three different constitutive material as cement paste, aggregate and Interfacial transition zone as a heterogeneous composite material; (b–c) illustration of interface element insertion within microstructure.

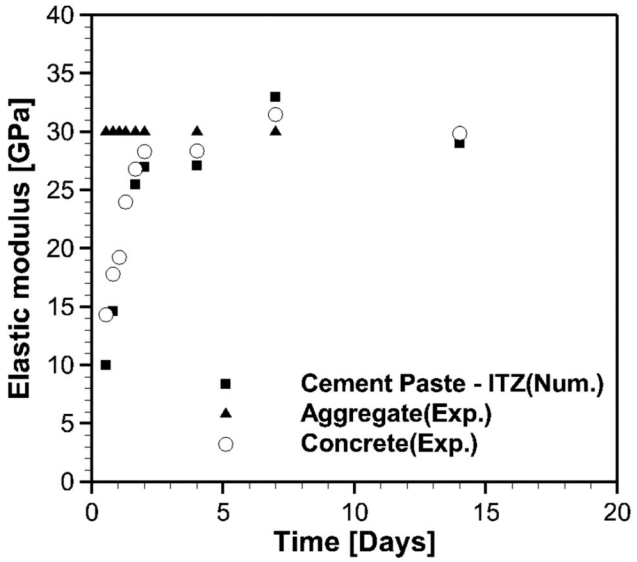

Figure 7.11 Young's modulus of concrete, cement-paste, ITZ, and aggregate as a function of their age.

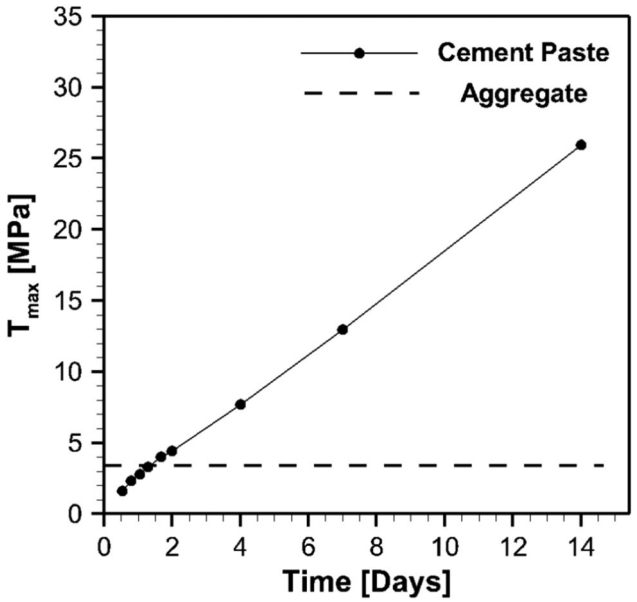

Figure 7.12 Critical strain energy release rate evolution of cement paste and aggregate as a function of maturity age.

cohesive element, T_n, and separation of undergoing cohesive element, $delta_n$, of cement paste was determined to be linear as a function of maturity (Barde et al., 2005); however, the cohesive strength of the aggregate is assumed to be unchanged with maturity as one would expect as shown in Figure 7.13.

Therefore, it is anticipated that at early ages (i.e., low degree of hydration) the crack will grow through cohesive elements inserted within cement paste or ITZ particles that have lower T_{max} and K_{IC} respect to aggregate particles. After a certain time, i.e., 2 days, crack path will alter and starts to propagate through aggregate particles since they possess lower T_{max}. This change in crack path has been observed in experimental study (Barde et al., 2005) since aggregates initiate to fractures in flexural test after aforementioned certain time.

7.3.2.3 Stochastic damage model. The strength distribution curve for a brittle solid material is wide. The tail of this curve covers a broad range of strength while this distribution is very narrow if a large number of identical samples were to be experimented. This distribution curve may be explained by a statistical distribution named as the Weibull (1951) distribution. Since there is only one interfacial strength parameter that can be varied, one distribution will be considered: varying T_{max} and keeping K_{IC} unchanged.

The Weibull (1951) distribution to define T_{max} of each interfacial element is:

$$f(T_{\max}) = \frac{m(T_{max})^{m-1}}{T_{max}^{0} m} \exp\left[\left(\frac{T_{max}}{T_{max}^{0}}\right)^{m}\right],\ T_{max} > 0 \qquad (19)$$

where T_{max}^{0} is cohesive strength of material which is unchanged and m is the measure of the variability in the strength of the material. A broad range of strength values are randomly generated on each interface elements defined by the Weibull (1951) distribution. Generally,

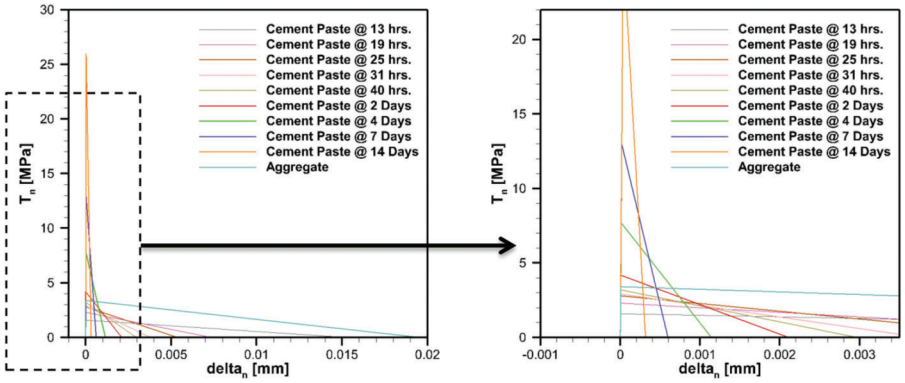

Figure 7.13 Evolution of traction-separation relation of cement paste and aggregate particles as a function of maturity age.

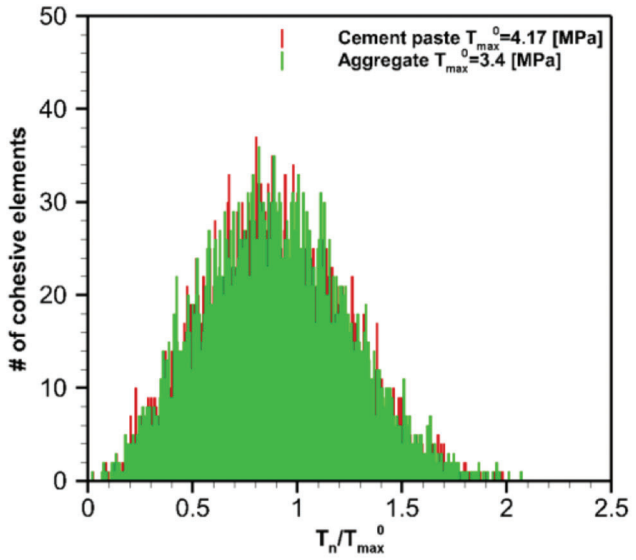

Figure 7.14 Example of Weibull strength distribution for interface elements of microstructure of (a) cement paste material; (b) aggregate material.

m = 3~10 is assumed for the case of brittle cement paste and aggregate material. Histogram of strength distribution curves for T_{max} of cement paste and aggregate material after 2 days as shown in Figure 7.14.

7.4 Comparison of Numerical and Experimental Results

An explicit integration scheme is used to integrate the system of spatially discretized the ordinary differential equations in time. This method is being used to verify the obtained numerical flexural strength results with experimental data.

Figure 7.15 displays that crack pattern as a function of maturity. The sequence of crack growth within the microstructure after 31 hours is shown in Figure 7.15 (a–c). This crack pattern shows that the numerical hypothesis that that before the certain time of change in fracture behavior, i.e., after 31 hours, cracks are most likely initiate to propagate through the interfacial transition zone and cement paste interface element which assess lower tensile strength rather than aggregate particles. ITZ in concrete is the region of cement paste around aggregate particles, which is perturbed by the presence of the aggregate. However, once the age of concrete reaches to the corresponding time of maturity, the crack starts to nucleate through the aggregate particles first as shown in Figure 7.15 (d–f). This fracture behavior confirms the proposed fact that aggregate has influence on developing of flexural strength of concrete at early ages.

Figure 7.16 compares the flexural strength results from the numerical simulations and experimental results obtained. The numerical results are in a good agreement with the results experimentally determined strength at early ages. However, it is observed that flexural strength in numerical simulations is slightly higher than what recorded in experimental program. This difference can be derived from (1) the higher flexural strength values for cement paste; (2) the proposed shape parameter in stochastic damage model.

7.5 Summary

This chapter described the early age mechanical behavior of paste, mortar, and concrete. The role of aggregate in determining the flexural strength of concrete as a function of maturity was investigated.

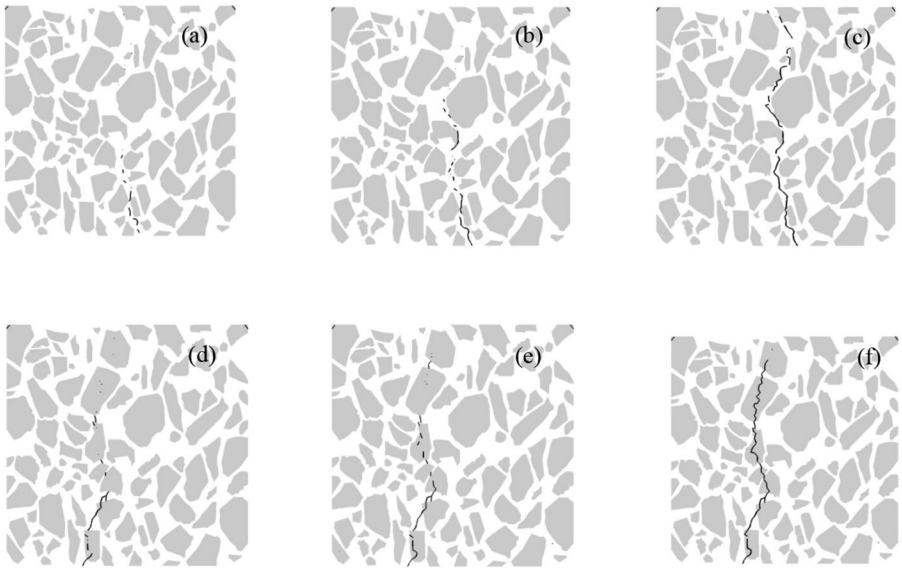

Figure 7.15 Sequential crack pattern within established microstructure due to third-point bending load at the fracture point (top) after 31 hours; (bottom) after 96 hours.

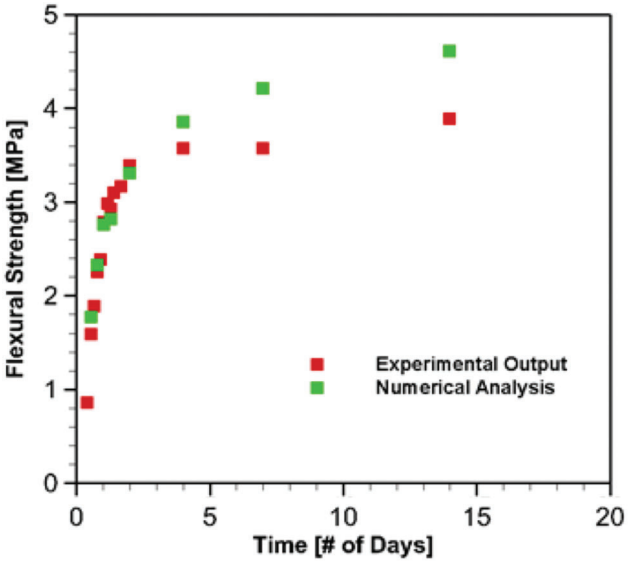

Figure 7.16 Numerical flexural strength of concrete beam under third-point bending test compared to experimental test results.

This influence of aggregates after a certain maturity age were investigated since the paste dominates failure at very early ages; however, at later ages the aggregates dominate the failure response. The rate of development of elastic modulus differs from that of flexural strength. Aggregates do not affect the elastic modulus in the same way they affect the flexural strength development.

8. SUMMARY, CONCLUSIONS, AND RECOMMENDATIONS

8.1 Summary and Conclusions

This work examined the criteria that should be used to determine when a concrete pavement can be opened to traffic. The risk of cracking is estimated based on the ratio between the maximum tensile stress developed beneath the wheel and the flexural strength of the concrete (σ_I/f_r). The importance of pavement thickness (h), subgrade reaction modulus (k), time-dependent elastic modulus ($E(t)$), and time-dependent flexural strength (f_r) of the concrete pavement are discussed in relation to the risk of cracking. The theoretical estimation of the maximum stress that develops in the pavement, σ_I, is compared with experimental results obtained from full-scale concrete pavement sections tested at the APT.

The experimental results indicate that when the typical INDOT opening to traffic criterion is used for 10-inch concrete pavement (flexural strength of f_r = 550 *psi*), the stresses that develop in the pavement are at most 20% of the flexural strength. A similar observation was made for the 10-inch-thick pavement opened to traffic when the flexural strength was 350 psi with the stress-to-strength ratio reaching only 30% of the flexural strength. For thinner concrete pavements (5 inches thick), opening at flexural strength values of 275 psi, 350 psi, and 550 psi resulted in stress-to-strength ratios of 1.09, 0.86, and 0.54, respectively. While a single flexural strength may be the simplest to specify, the results of this study indicate that allowing thicker pavements to be opened at a lower strength may not add substantial risk of cracking due to traffic loading. It should also be mentioned that the pavement thickness employed in the APT does not correspond to a typical INDOT cross section.

Simulations were performed to consider pavements with thickness between 8- and 16-inch depths and different subgrade stiffness between 50 and 400 lb/in^3, and it was determined that traffic loading resulted in stress that was less than 20% of the flexural strength ($\sigma_I/f_r < 0.2$) for any pavement that was more than 10 inches thick (i.e., $h \geq 10$ in). It was observed that the rate of elastic modulus development ($E(t)$) is inversely related to the stress development caused by traffic loading. This implies that stiffer concrete pavement will develop a higher stress. The subgrade stiffness also influences the stress that develops in the concrete pavement, with a greater impact on thinner pavements. It was also observed that the shape of the footprint of the wheel has a minor impact on the estimated stress and strain. On the other hand, considering a perfect bonding condition underestimates the strain development while the frictionless condition has good agreement with experimental measurements of strain due to traffic loading.

8.2 Recommendations

This work however suggests that it may be feasible to tie the strength requirement to pavement thickness and subgrade properties. It is recommended that for pavements less than 8 inches thick that the opening criteria be maintained at 550 psi, for pavements with a thickness between 8 and 10 inches the opening could be reduce to 450 psi to maintain the stress-to-strength ratio at a value of less than 40% and for pavements thicker than 10 inches the opening strength could be reduced to 350 psi to maintain the stress-to-strength ratio at a value of less than 40%. This analysis however assumes minimal additional stress due to moisture or thermal gradients. It was estimated that only under extreme cases of temperature during the summer, thermal gradients could cause an increase of the estimated σ_I up to 0.9 MPa.

REFERENCES

AASHTO. (2013). *AASHTO LRFD bridge design specifications* (6th ed.). Washington, DC: American Association of State Highway Transportation Officials.

Abdul-Baqi, A., Schreurs, P. J. G., & Geers, M. G. D. (2005). Fatigue damage modeling in solder interconnects using a cohesive zone approach. *International Journal of Solids and Structures*, *42*(3–4), 927–942. http://dx.doi.org/10.1016/j.ijsolstr.2004.07.026

ACI Committee 215. (1974). Considerations for design of concrete structures subjected to fatigue loading. *ACI Journal*

Proceedings, *71*(3), 97–121. http://dx.doi.org/10.14359/11172

Aïtcin, P.-C. (2011). *High-performance concrete*. Boca Raton, FL: CRC Press.

Altoubat, S. A., & Lange, A. D. (2001). Creep, shrinkage, and cracking of restrained concrete at early age. *ACI Materials Journal*, *98*(4), 323–331. http://dx.doi.org/10.14359/10401

Antico, F. C., de la Varga, I., Esmaeeli, H. S., Nantung, T. E., Zavattieri, P. D., & Weiss, W. J. (2015). Using accelerated pavement testing to examine traffic opening criteria for concrete pavements. *Construction and Building Materials*, *96*, 86–95. http://dx.doi.org/10.1016/j.conbuildmat.2015.07.177

Antico, F. C., Zavattieri, P. D., Hector, L. G., Jr., Mance, A., Rodgers, W. R., & Okonski, D. A. (2012). Adhesion of nickel–titanium shape memory alloy wires to thermoplastic materials: theory and experiments. *Smart Materials and Structures*, *21*(3). http://dx.doi.org/10.1088/0964-1726/21/3/035022

Antico, F., Zavattieri, P., & Weiss, W. (2015). *Time-dependent properties of concrete at early ages: Strain and stress development under restrained conditions*. Manuscript in preparation.

Aquino, M. J., Li, Z., & Shah, S. P. (1995). Mechanical properties of the aggregate and cement interface. *Advanced Cement Based Materials*, *2*(6), 211–223. http://dx.doi.org/10.1016/1065-7355(95)90040-3

ASTM C39/C39M-14a. (2015). *Standard test method for compressive strength of cylindrical concrete specimens*. West Conshohocken, PA: ASTM International.

ASTM C78/C78M-10. (2013). *Standard test method for flexural strength of concrete (using simple beam with third-point loading)*. West Conshohocken, PA: ASTM International.

ASTM C403/403M-08. (2008). *Time of setting of concrete mixtures by penetration resistance*. West Conshohocken, PA: ASTM International.

ASTM C469–02e1. (2003). *Standard test method for static modulus of elasticity and Poisson's ratio of concrete in compression*. West Conshohocken, PA: ASTM International.

ASTM C496/C496M-11. (2011). *Standard test method for splitting tensile strength of cylindrical concrete specimens*. West Conshohocken, PA: ASTM International.

ASTM C1074-11. (2011). *Standard practice for estimating concrete strength by the maturity method*. West Conshohocken, PA: ASTM International.

Bangash, M. Y. H. (2001). *Manual of numerical methods in concrete: Modelling and applications validated by experimental and site-monitoring data*. London, UK: Thomas Telford Ltd.

Barde, A., Mazzotta, G., & Weiss, J. (2005). Early age flexural strength: The role of aggregates and their influence on maturity predictions. In F. Young & J. P. Skalny (Eds.), *Materials science of concrete VII* (pp. 247–264). New York, NY: Wiley.

Bassam, S. A., Yu, B.-J., & Ansari, F. (2007). Fracture energy of concrete by maturity method. *ACI Materials Journal*, *104*(1), 77–85. http://dx.doi.org/10.14359/18498

Bazant, Z. (1975). I.—Theory of creep and shrinkage in concrete structures: A précis of recent developments. In S. Nemat-Nasser (Ed.), *Mechanics today, Volume 2* (pp. 1–93). Elmsford, NY: Pergamon Press Inc. http://dx.doi.org/10.1016/B978-0-08-018113-4.50007-0

Bazant, Z. (1977). Viscoelasticity of solidifying porous material—Concrete. *Journal of Engineering Mechanics*, *103*(6), 1049–1067. Retrieved from http://trid.trb.org/view.aspx?id=72013

Bazant, Z. (1979). Thermodynamics of solidifying or melting viscoelastic material. *Journal of the Engineering Mechanics Division*, *105*(6), 933–952. Retrieved December 3, 2012, from http://cedb.asce.org/cgi/WWWdisplay.cgi?9166

Bazant, Z. (1999). Size effect on structural strength: A review. *Archive of Applied Mechanics*, *69*(9), 703–725. http://dx.doi.org/10.1007/s004190050252

Bazant, Z. P., Hauggaard, A. b., Baweja, S., & Ulm, F. (1997). Microprestress-solidification theory for concrete creep. I: Aging and drying effects. *Journal of Engineering Mechanics*, *123*(11), 1188–1194. http://dx.doi.org/10.1061/(ASCE)0733-9399(1997)123:11(1188)

Bazant, Z. P., & Novak, D. (2000a). Energetic-statistical size effect in quasibrittle failure at crack initiation. *ACI Materials Journal*, *97*(3), 381–392. http://dx.doi.org/10.14359/9879

Bazant, Z., & Novak, D. (2000b). Probabilistic nonlocal theory for quasibrittle fracture initiation and size effect. *Journal of Engineering Mechanics*, *126*(2), 166–174. http://dx.doi.org/10.1061/(ASCE)0733-9399(2000)126:2(166)

Bazant, Z. P., Pang, S. D., Vořechovský, M., Novák, D., & Pukl, R. (2004). Statistical size effect in quasibrittle materials: Computation and extreme value theory. In V. C. Li, K. Y. Leung, K. J. William, & S. L. Billington (Eds.), *Fracture Mechanics of Concrete Structures (Proceedings of the 5th International Conference on Fracture Mechanics of Concrete and Concrete Structures)*, Vol. 1 (pp. 189–196). Ia-FraMCos.

Bazant, Z., & Pfeiffer, P. (1986). Shear fracture tests of concrete. *Materials and Structures*, *19*(2), 111–121. http://dx.doi.org/10.1007/BF02481755

Bazant, Z., & Planasm, J. (1997). *Fracture and size effect in concrete and other quasibrittle materials*. Boca Raton, FL: CRC Press.

Bazant, Z., & Prasannan, S. (1989). Solidification theory for concrete creep. I: Formulation. *Journal of Engineering Mechanics*, *115*(8), 1691–1703. http://dx.doi.org/10.1061/(ASCE)0733-9399(1989)115:8(1691)

Bazant, Z., & Robert, L. (1988). Material models for structural creep analysis. In Z. Bazant (Ed.), *Mathematical modeling of creep and shrinkage of concrete* (pp. 99–215). New York, NY: John Wiley & Sons, Ltd. Retrieved December 3, 2012, from http://www.civil.northwestern.edu/people/bazant/PDFs/Backup of Papers/S21.pdf

Bazant, Z. P., & Wu, S. T. (1974). Rate-type creep law of aging concrete based on maxwell chain. *Matériaux et Construction*, *7*(1), 45–60. http://dx.doi.org/10.1007/BF02482679

Bazant, Z., & Yunping, X. (1994). Drying creep of concrete: constitutive model and new experiments separating its mechanisms. *Materials and Structures*, *27*(1), 3–14. http://dx.doi.org/10.1007/BF02472815

Bentur, A. (Ed.). (2003). *Early age cracking in cementitious systems—Report of RILEM Technical Committee 181-EAS—Early age shrinkage induced stresses and cracking in cementitious systems*. Bagneaux, France: RILEM.

Bollati, M. R., Talero, R., Rodriguez, M., Witoszek, B., & Hernandez, F. (1996). Porous high performance concrete for road traffic. In *Concrete for infrastructure and utilities* (pp. 589–599). London, UK: E&FN Spon.

Broda, M., Wirquin, E., & Duthoit, B. (2002). Conception of an isothermal calorimeter for concrete—Determination of the apparent activation energy. *Materials and Structures*, *35*(7), 389–394. http://dx.doi.org/10.1007/BF02483141

Bull, J., & Singh, A. (1990). A comparison between the stresses computed for finite sized precast concrete pavement units using westergaards equations and a numerical design

method. *Computers and Geotechnics*, *9*(4), 325–340. http://dx.doi.org/10.1016/0266-352X(90)90045-W

Burmister, D. (1958). *Evaluation of pavement systems of the WASHO road test by layered system methods* (Highway Research Board Bulletin No. 177). Washington, DC: Transportation Research Board.

Camacho, G., & Ortiz, M. (1996). Computational modelling of impact damage in brittle materials. *International Journal of Solids and Structures*, *33*(20–22), 2899–2938. http://dx.doi.org/10.1016/0020-7683(95)00255-3

Carino, N. (1991). The maturity method. In V. M. Malhotra & N. J. Carino (Eds.), *CRC handbook on nondestructive testing of concrete* (pp. 101–144). Boca Raton, FL: CRC Press.

Carol, I., & Bazant, Z. (1993). Viscoelasticity with aging caused by solidification of nonaging constituent. *Journal of Engineering Mechanics*, *119*(11), 2252–2269. http://dx.doi.org/10.1061/(ASCE)0733-9399(1993)119:11(2252)

Carpinteri, A. (1986). *Mechanical damage and crack growth in concrete*. Dordrecht: Springer Netherlands. http://dx.doi.org/10.1007/978-94-009-4350-6

de Borst, R., Sluys, L. J., van den Boogaard, A. H., & van den Bogert, P. A. J. (1993). Computational issues in time-dependent deformation and fracture of concrete. In Z. Bazant & I. Carol (Eds.), *Creep and shrinkage of concrete* (pp. 309–326). London, UK: E&FN Spon.

Dean, S., Moon, J. H., Rajabipour, F., Pease, B., & Weiss, J. (2006). Quantifying the influence of specimen geometry on the results of the restrained ring test. *Journal of ASTM International*, *3*(8). 100436. http://dx.doi.org/10.1520/JAI100436

Diamond, S., Mindess, S., & Lovell, J. (1982). On the spacing between aggregate grains in concrete and the dimension of the Aureole de Transition. In *International RILEM Colloquium, Liaisons Pâtes de Ciment/Matériaux Associés, Toulouse, France* (pp. C42–C46). Bagneaux, France: RILEM.

Espinosa, H. D., & Zavattieri, P. D. (2003). A grain level model for the study of failure initiation and evolution in polycrystalline brittle materials. Part I: Theory and numerical implementation. *Mechanics of Materials*, *35*(3–6), 333–364. http://dx.doi.org/10.1016/S0167-6636(02)00285-5

Falk, M. L., Needleman, A., & Rice, J. R. (2001). A critical evaluation of cohesive zone models of dynamic fracture. *Journal de Physique IV France*, *11*, Pr5-43–Pr5-50. http://dx.doi.org/10.1051/jp4:2001506

Ferry, J. D. (1980). *Viscoelastic properties of polymers* (3rd ed.). New York, NY: John Wiley & Sons, Inc.

Freudenthal, A. M. (1968). Statistical approach to brittle fracture. In H. Liebowitz (Ed.), *Fracture* (Vol. 2, pp. 591–619). New York, NY: Academic Press.

Freudenthal, A. M., & Gumbel, E. (1956). Physical and statistical aspects of fatigue. In *Advances in applied mechanics* (Vol. 4, pp. 117–158). New York, NY: Academic Press.

Galal, K. A., & White, T. D. (1999). *INDOT–APT test facility experience*. Paper presented at the 1st International Conference on Accelerated Pavement Testing, Reno, Nevada, October 18–20. Retrieved from https://sites.google.com/site/afd40web/apt-conferences/reno-nevada-october-18-20-1999/post-conference-presentations

Golias, M., Castro, J., Peled, A., Nantung, T., Tao, B., & Weiss, W. J. (2012). Can soy methyl esters improve concrete pavement joint durability? *Transportation Research Record*, *2290*, 60–68. http://dx.doi.org/10.3141/2290-08

Gopalakrishnan, K. S., Neville, A. M., & Ghali, A. (1969). Creep Poisson's ratio of concrete under multiaxial compression. *ACI Journal Proceedings*, *66*(12), 1008–1019. http://dx.doi.org/10.14359/7451

Grasley, Z. C., & Ambrosia, M. D. D. (2011). Cement & Concrete Composites Viscoelastic properties and drying stress extracted from concrete ring tests. *Cement and Concrete Composites*, *33*(2), 171–178. http://dx.doi.org/10.1016/j.cemconcomp.2010.10.014

Grasley, Z. C., & Lange, D. A. (2007). Constitutive modeling of the aging viscoelastic properties of portland cement paste. *Mechanics of Time-Dependent Materials*, *11*(3), 175–198. http://dx.doi.org/10.1007/s11043-007-9043-4

Graveen, C., Falker, E., Beaver, M., Weiss, W. J., & Gallivan, L. (2009). *Performance related specifications (PRS) for concrete pavements in Indiana, Volume 1: Executive summary* (Joint Transportation Research Program Publication No. FHWA/IN/JTRP-2004/13-1). West Lafayette, IN: Purdue University. http://dx.doi.org/10.5703/1288284314213

Graveen, C., Weiss, W. J., Olek, J., & Nantung, T. (2003). Implications of maturity and ultrasonic wave speed measurements in QC/QA for concrete. In A. M. Brandt, V. C. Li, & I. H. Marshall (Eds.), *Brittle Matrix Composites 7* (pp. 457–472). Cambridge, UK: Woodhead Publishing Limited.

Grzybowski, M., & Shah, S. P. (1990). Shrinkage cracking of fiber reinforced concrete. *ACI Materials Journal*, *87*(2), 138–148. http://dx.doi.org/10.14359/1951

Hannant, D. (1969). Creep and creep recovery of concrete subjected to multiaxial compressive stress. *ACI Journal Proceedings*, *66*(5), 391–394. http://dx.doi.org/10.14359/7366

Hernández-Olivares, F., Barluenga, G., Parga-Landa, B., Bollati, M., & Witoszek, B. (2007). Fatigue behaviour of recycled tyre rubber-filled concrete and its implications in the design of rigid pavements. *Construction and Building Materials*, *21*(10), 1918–1927. http://dx.doi.org/10.1016/j.conbuildmat.2006.06.030

Hillerborg, A., Modéer, M., Petersson, P. (1976). Analysis of crack formation and crack growth in concrete by means of fracture mechanics and finite elements. *Cement and Concrete Research*, *6*(6), 773–781. http://dx.doi.org/10.1016/0008-8846(76)90007-7

HKS. (2003). ABAQUS (Version 6.4-1) [Computer software]. Providence, RI: Hibbitt, Karlsson & Sorensen, Inc.

Hoover, C. (2013). Experimental determination of early age fracture toughness and fracture process zone size in cement pastes. In U. Franz-Josef, J. M. Hamlin, & R. J.-M. Pellenq (Eds.), *Mechanics and Physics of Creep, Shrinkage, and Durability of Concrete: A Tribute to Zdeněk P. Bazant* (pp. 364–371). http://dx.doi.org/10.1061/9780784413111.043

Hossain, A. B. (2003). *Assessing residual stress development and stress relaxation in restrained concrete ring specimens* (Doctoral dissertation). West Lafayette, IN: Purdue University. Retrieved from http://docs.lib.purdue.edu/dissertations/AAI3113817/

Hossain, A, Pease, B., & Weiss, J. (2003). Quantifying early-age stress development and cracking in low water-to-cement concrete: Restrained-ring test with acoustic emission. *Transportation Research Record*, *1834*, 24–32. http://dx.doi.org/10.3141/1834-04

Hossain, A. B., & Weiss, J. (2004). Assessing residual stress development and stress relaxation in restrained concrete ring specimens. *Cement and Concrete Composites*, *26*(5), 531–540. http://dx.doi.org/10.1016/S0958-9465(03)00069-6

Hossain, A. B., & Weiss, J. (2006). The role of specimen geometry and boundary conditions on stress development and cracking in the restrained ring test. *Cement and Concrete Research*, *36*(1), 189–199. http://dx.doi.org/10.1016/j.cemconres.2004.06.043

Huang, H. (1995). *Analysis of accelerated pavement tests and finite element modeling of rutting phenomenon* (Doctoral

dissertation). West Lafayette, IN: Purdue University. Retrieved from http://docs.lib.purdue.edu/dissertations/AAI9601511/

INDOT. (n.d.). *Oversize/Overweight Vehicle Permitting Handbook*. Indianapolis, IN: Indiana Department of Transportation. Retrieved from http://www.in.gov/dor/files/osowhandbook.pdf

Jirásek, M., & Bazant, Z. (2002). *Inelastic analysis of structures*. West Sussex, England: John Wiley & Sons, Ltd.

Jones, C. A., & Grasely, Z. C. (2011). Short-term creep of cement paste during nanoindentation. *Cement and Concrete Composites*, *33*(1), 12–18. http://dx.doi.org/10.1016/j.cemconcomp.2010.09.016

Jordaan, I., & Illston, J. (1969). The creep of sealed concrete under multiaxial compressive stresses. *Magazine of Concrete Research*, *21*(69), 195–204. http://dx.doi.org/10.1680/macr.1969.21.69.195

Kada-Benameur, H., Wirquin, E., & Duthoit, B. (2000). Determination of apparent activation energy of concrete by isothermal calorimetry. *Cement and Concrete Research*, *30*(2), 301–305. http://dx.doi.org/10.1016/S0008-8846(99)00250-1

Kosmatka, S. H., Panarese, W., Allen, G., & Cumming, S. (2002). *Design and control of concrete mixtures*. Stokie, IL: Portland Cement Association.

Kovler, K. (1994). Testing system for determining the mechanical behaviour of early age concrete under restrained and free uniaxial shrinkage. *Materials and Structures*, *27*(6), 324–330. http://dx.doi.org/10.1007/BF02473424

Krauss, P. D., & Rogalla, E. A. (1996). *Transverse cracking in newly constructed bridge decks* (NCHRP Report 380). Washington, DC: Transportation Research Board.

Lakes, R. (2009). *Viscoelastic materials*. Cambridge, UK: Cambridge University Press. http://dx.doi.org/10.1017/CBO9780511626722

Lamond, J. F., & Pieler, J. H. (2006). *Significance of tests and properties of concrete and concrete-making materials, STP 169D*. West Conshohocken, PA: ASTM International.

Landis, E. N., & Baillon, L. (2002). Experiments to relate acoustic emission energy to fracture energy of concrete. *Journal of Engineering Mechanics*, *128*(6), 698–702. http://dx.doi.org/10.1061/(ASCE)0733-9399(2002)128:6(698)

Lee, H., Daniel, J. & Kim, Y. (2000). Continuum damage mechanics-based fatigue model of asphalt concrete, Journal of Materials in Civil Engineering, 12(2), 105–112. http://ascelibrary.org/doi/abs/10.1061/(ASCE)0899-1561(2000)12:2(105)

Li, S., Thouless, M. D., Waas, A. M., Schroeder, J. A., & Zavattieri, P. D. (2005). Use of a cohesive-zone model to analyze the fracture of a fiber-reinforced polymer—matrix composite. *Composites Science and Technology*, *65*(3–4), 537–549. http://dx.doi.org/10.1016/j.compscitech.2004.08.004

Li, S., Thouless, M. D., Waas, A. M., Schroeder, J. A., & Zavattieri, P. D. (2006). Mixed-mode cohesive-zone models for fracture of an adhesively bonded polymer–matrix composite. *Engineering Fracture Mechanics*, *73*(1), 64–78. http://dx.doi.org/10.1016/j.engfracmech.2005.07.004

Lockner, D. (1993). The role of acoustic emission in the study of rock fracture. *International Journal of Rock Mechanics and Mining Sciences & Geomechanics Abstracts*, *30*(7), 883–899. http://dx.doi.org/10.1016/0148-9062(93)90041-B

Maalej, M., & Li, V. (1994). Flexural strength of fiber cementitious composites. *Journal of Materials in Civil Engineering*, *6*(3), 390–406. http://dx.doi.org/10.1061/(ASCE)0899-1561(1994)6:3(390)

Maji, A. K., Ouyang, C., & Shah, S. P. (2011). Fracture mechanisms of quasi-brittle materials based on acoustic emission. *Journal of Materials Research*, *5*(1), 206–217. http://dx.doi.org/10.1557/JMR.1990.0206

Marques, P. C., & Creus, G. J. (2012). *Computational viscoelasticity*. Dordrecht: Springer Netherlands.

McIntosh, J. D. (1949). Electrical curing of concrete. *Magazine of Concrete Research*, *1*(1), 21–28. http://dx.doi.org/10.1680/macr.1959.1.1.21

McIntosh, J. D. (1956). The effects of low-temperature curing on the compressive strength of concrete. *Proceedings of the RILEM Symposium on Winter Concreting*. Copenhagen: Danish National Institute for Building Research.

McLean, M., Brown, W. L., & Vinci, R. P. (2010). Temperature-dependent viscoelasticity in thin au films and consequences for MEMS devices. *Journal of Microelectromechanical Systems*, *19*(6), 1299–1308. http://dx.doi.org/10.1109/JMEMS.2010.2076787

Mehta, P. (2002). Greeningof the concrete industry for sustainable development. *Concrete International*, *24*(7), 23–28. Retrieved June 19, 2015, from http://maquinamole.net/EcoSmartconcrete.com/docs/trmehta02.pdf

Mihashi, H., & Izumi, M. (1977). A stochastic theory for concrete fracture. *Cement and Concrete Research*, *7*(4), 411–421. http://dx.doi.org/10.1016/0008-8846(77)90069-2

Mindess, S., Young, J. F., & Darwin, D. (2002). *Concrete* (2nd ed.). Upper Saddle River, NJ: Prentice Hall, 2002.

Moon, J. H. (2006). *Shrinkage, residual stress, and cracking in heterogeneous materials* (Doctoral dissertation). West Lafayette, IN: Purdue University. Retrieved from http://docs.lib.purdue.edu/dissertations/AAI3232114/

Moon, J. H., & Weiss, J. (2006). Estimating residual stress in the restrained ring test under circumferential drying. *Cement and Concrete Composites*, *28*(5), 486–496. http://dx.doi.org/10.1016/j.cemconcomp.2005.10.008

Moon, J. H., Couch, J., & Weiss, W. J. (2006). Preliminary numerical assessment of microcracking caused by autogenous shrinkage in a heterogeneous system. In M. S. Konsta-Gdoutos (Ed.), *Measuring, monitoring and modeling concrete properties* (pp. 317–323). Dordrecht: Springer Netherlands.

Moon, J. H., Rajabipour, F., Pease, B., & Weiss, J. (2005). Autogenous shrinkage, residual stress, and cracking in cementitious composites: The influence of internal and external restraint. In B. Persson, D. Bentz, & L.-O. Nilsson (Eds.), *Self-desiccatin and its important in concrete technology* (pp. 1–20). Lund, Sweden: Lund Institute of Technology.

Moon, J. H., Rajabipour, F., & Weiss, W. J. (2004). Incorporating moisture diffusion in the analysis of the restrained ring test. In B. H. Oh, K. Sakai, O. E. Gjorv, & N. Banthia (Eds.), *Concrete Under Severe Conditions: Environment and Loading (CONSEC'04)*, Vol. 2 (pp. 1973–1980). Seoul, Korea: Seoul National University, Korea Concrete Institute.

Morrissey, J. W., & Rice, J. R. (1998). Crack front waves. *Journal of the Mechanics and Physics of Solids*, *46*(3), 467–487. http://dx.doi.org/10.1016/S0022-5096(97)00072-0

Newbolds, S., & Olek, J. (2008). *Evaluation of performance and design of ultra-thin whitetopping (bonded concrete resurfacing) using large-scale accelerated pavement testing* (Joint Transportation Research Program Publication No. FHWA/IN/JTRP-2008/14). West Lafayette, IN: Purdue University. http://dx.doi.org/10.5703/1288284314322

Nurse, R. W. (1949). Steam curing of concrete. *Magazine of Concrete Research*, *1*(2), 79–88. http://dx.doi.org/10.1680/macr.1949.1.2.79

Ohnaka, M. (1983). Acoustic emission during creep of brittle rock. *International Journal of Rock Mechanics and Mining Sciences & Geomechanics Abstracts*, *20*(3), 121–134. http://dx.doi.org/10.1016/0148-9062(83)91302-5

Ouyang, C., Landis, E. N., & Shah, S. P. (1992). Damage assessment in concrete using quantitative acoustic emission. *Journal of Engineering Mechanics*, *117*(11), 2681–2698. http://dx.doi.org/10.1061/(ASCE)0733-9399(1991)117:11(2681)

Park, S., & Kim, Y. (2001). Fitting Prony-series viscoelastic models with power-law presmoothing. *Journal of Materials in Civil Engineering*, *13*(1), 26–32. http://dx.doi.org/10.1061/(ASCE)0899-1561(2001)13:1(26)

Park, S. W., & Schapery, R. A. (1999). Methods of interconversion between linear viscoelastic material functions. Part I—A numerical method based on Prony series. *International Journal of Solids and Structures*, *36*(11), 1653–1675. http://dx.doi.org/10.1016/S0020-7683(98)00055-9

Radlinska, A., Moon, J. H., Rajabipour, F., & Weiss, J. (2006). The ring test: A review of recent developments. In O. M. Jensen, P. Lura, & K. Kovler (Eds.), *International RILEM Conference on Volume Changes of Hardening Concrete: Testing and Mitigation* (pp. 205–214). Bagneaux, France: RILEM.

Rajan, S., Olek, J., & Robertson, T. (2001). *Analysis of performance of the ultra-thin whitetopping subjected to slow moving loads in an accelerated pavement testing facility*. Paper presented at the 7th International Conference on Concrete Pavements, Orlando, FL, September 9–13. Retrieved from http://rebar.ecn.purdue.edu/apt/pdf/s16-p4-rajan.pdf

Raoufi, K. (2011). *Restrained shrinkage cracking of concrete: The influence of damage localization* (Doctoral dissertation). West Lafayette, IN: Purdue University. Retrieved from http://docs.lib.purdue.edu/dissertations/AAI3477734/

Raoufi, K., Pour-Ghaz, M., Pourasee, A., & Weiss, J. (2011). Restrained shrinkage cracking in concrete elements: Role of substrate bond on crack development. *Journal of Materials in Civil Engineering*, *23*(6), 895–903. http://dx.doi.org/10.1061/(ASCE)MT.1943-5533.0000247

Raoufi, K., Schlitter, J., Bentz, D., & Weiss, J. (2011). Parametric assessment of stress development and cracking in internally cured restrained mortars experiencing autogenous deformations and thermal loading. *Advances in Civil Engineering*, 2011, 1–16. http://dx.doi.org/10.1155/2011/870128

Raoufi, K., Their, T., Weiss, W. J., Olek, J., & Nantung, T. E. (2009). Saw-cutting guidelines for concrete pavements: examining the requirements for time and depth of saw-cutting (Joint Transportation Research Program Publication No. FHWA/IN/JTRP-2007/05). West Lafayette, IN: Purdue University. http://dx.doi.org/10.5703/1288284313449

Rice, J. R. (1980). The mechanics of earthquake rupture. In A. M. Dziewonski & E. Boschi (Eds.), *Physics of the Earth's Interior* (pp. 555–649). Bologna, Italy: Società Italiana di Fisca. Retrieved December 6, 2012, from http://esag.harvard.edu/rice/088_Rice_MechEarthquRupt_80.pdf

Saeed, A., & Hall, J. W. (2003). *Accelerated pavement testing: Data guidelines* (NCHRP Report 512). Washington, DC: Transportation Research Board.

Saul, A. G. A. (1951). Principles underlying the steam curing of concrete at atmospheric pressure. *Magazine of Concrete Research*, *2*(6), 127–140. http://dx.doi.org/10.1680/macr.1951.2.6.127

Schapery, R. A. (1962). Approximate methods of transform inversion for viscoelastic stress analysis. In R. M. Rosenberg (Ed.), *Proceedings of the Fourth U.S. National Congress of Applied Mechanics* (Vol. 2, pp. 1075–1085). Elmsford, NY: Pergamon Press Inc.

Schmidt, R. A. (1976). Fracture-toughness testing of limestone. *Experimental Mechanics*, *16*(5), 161–167. http://dx.doi.org/10.1007/BF02327993

Shah, S. P., Wang, K., & Weiss, W. J. (2000). Mixture proportioning for durable concrete: Challenges and changes. *Concrete International*, *22*(9), 73–78.

Shah, S. P., & Weiss, W. J. (2000). High performance concrete: Strength, permeability, and shrinkage cracking. In L. S. Johal (Ed.), *PCI/FHWA/FIB International Symposium on High Performance Concrete* (pp. 331–339). Chicago, IL: Precast/Prestressed Concrete Institute.

Shah, S. P., Yang, W., & Weiss, W. J. (1998). Shrinkage cracking—Can it be prevented? *Concrete International*, *20*(4), 51–55.

Soussou, J. E., Moavenzadeh, F., & Gradowczyk, M. H. (1970). Application of Prony series to linear viscoelasticity. *Journal of Rheology*, *14*, 573. http://dx.doi.org/10.1122/1.549179

Suter, M., & Benipal, G. S. (2006a). Time-dependent behaviour of reacting concrete I: Mechanism and theory. *Mechanics of Time-Dependent Materials*, *10*(1), 51–62. http://dx.doi.org/10.1007/s11043-006-9008-z

Suter, M., & Benipal, G. S. (2006b). Time-dependent behaviour of reacting concrete II: Applications and discussion. *Mechanics of Time-Dependent Materials*, *10*(1), 63–81. http://dx.doi.org/10.1007/s11043-006-9012-3

Taylor, R., & Govindjee, S. (2008a). *FEAP—A Finite Element Analysis Program: Version 8.2 Parallel User Manual*. Berkeley, CA: University of California, Berkeley.

Taylor, R., & Govindjee, S. (2008b). *FEAP—A Finite Element Analysis Program: Version 8.2 Theory Manual*. Berkeley, CA: University of California, Berkeley.

Taylor, R. L., Pister, K. S., & Goudreau, G. L. (1970). Thermomechanical analysis of viscoelastic solids. *International Journal for Numerical Methods in Engineering*, *2*(1), 45–59. http://dx.doi.org/10.1002/nme.1620020106

Teller, L. W., & Sutherland, E. C. (1943). The structural design of concrete pavements: Part 5-An experimental study of the Westergaard analysis of stress conditions. *Public Roads*, *23*(8), 167–212. Retrieved from http://trid.trb.org/view.aspx?id=97656

Timoshenko, S., Woinowsky-Krieger, S., & Woinowsky, S. (1959). Theory of plates and shells. *PersianGig*. Retrieved July 3, 2013, from http://nmoslemi.persiangig.com/58209_fm.pdf

Tvergaardm V., & Hutchinson, J. W. (1992). The relation between crack growth resistance and fracture process parameters in elastic-plastic solids. *Journal of the Mechanics and Physics of Solids*, *40*(6), 1377–1397. http://dx.doi.org/10.1016/0022-5096(92)90020-3

Van Dam, T. J., Peterson, K. R., Sutter, L. L., Panguluri, A., Sytsma, J., Buch, N., Desaraju, P. (2004). *Guidelines for early-opening-to-traffic Portland cement concrete for pavement rehabilitation* (NCHRP Report 540). Washington, DC: Transportation Research Board.

Vichit-Vadakan, W., & Scherer, G. W. (2003). Measuring permeability and stress relaxation of young cement paste by beam bending. *Cement and Concrete Research*, *33*(12), 1925–1932. http://dx.doi.org/10.1016/S0008-8846(03)00168-6

Wang, S., & Li, V. (2006). High-early-strength engineered cementitious composites. *ACI Materials Journal*, *103*(2), 97–105. http://dx.doi.org/10.14359/15260

Weibull, W. (1939). *The phenomenon of rupture in solids*. Stockholm, Sweden: Generalstabens litografiska anstalts förlag.

Weibull, W. (1951). A statistical distribution function of wide applicability. *Journal of Applied Mechanics*, *18*, 293–297.

Weiss, W. J. (1999). *Prediction of early-age shrinkage cracking in concrete elements* (Doctoral dissertation). Evanston, IL: Northwestern University. Retrieved December 1, 2012, from http://adsabs.harvard.edu/abs/1999PhDT.....219W

Weiss, W. J., & Shah, S. P. (2002). Restrained shrinkage cracking: the role of shrinkage reducing admixtures and specimen geometry. *Materials and Structures*, *35*(2), 85–91. http://dx.doi.org/10.1007/BF02482106

Weiss, W., Yang, W., & Shah, S. (1998). Shrinkage cracking of restrained concrete slabs. *Journal of Engineering Mechanics*, *124*(7), 765–774. http://ascelibrary.org/doi/abs/10.1061/(ASCE)0733-9399(1998)124:7(765)

Westergaard, H. M. (1926). Stresses in concrete pavements computed by theoretical analysis. *Public Roads*, *7*(2), 25–35. Retrieved from http://trid.trb.org/view.aspx?id=97833

Wiegrink, K., Marikunte, S., & Shah, S. P. (1996). Shrinkage cracking of high-strength concrete. *ACI Materials Journal*, *93*(5), 440–415. http://dx.doi.org/10.14359/9844

Wittmann, P. H., & Zaitsev, Yu.V. (1981). Crack propagation and fracture of composite materials such as concrete. *Proceedings of the 5th International Conference on Fracture (ICF5)* (pp. 2261–2274). Retrieved April 21, 2014, from http://www.gruppofrattura.it/ocs/index.php/ICF/ICF5/paper/view/2924/7726

Wu, K.-R., Chen, B., Yao, W., & Zhang, D. (2001). Effect of coarse aggregate type on mechanical properties of high-performance concrete. *Cement and Concrete Research*, *31*(10), 1421–1425. http://dx.doi.org/10.1016/S0008-8846(01)00588-9

Xu, X., & Needleman, A. (1995). Numerical simulations of dynamic crack growth along an interface. *International Journal of Fracture*, *74*(4), 289–324. http://dx.doi.org/10.1007/BF00035845

Yang, Y., Weiss, W., & Shah, S. P. (2000). Predicting shrinkage stress field in concrete slab on elastic subgrade. *Journal of Engineering Mechanics*, *126*(1), 35–42. http://dx.doi.org/10.1061/(ASCE)0733-9399(2000)126:1(35)

Young, W., & Budynas, R. (2001). *Roark's formulas for stress and strain* (7th ed.). New York, NY: McGraw-Hill. Retrieved June 18, 2015, from http://materiales.azc.uam.mx/gjl/Clases/MA10_I/Roark's%20formulas%20for%20stress%20and%20strain.pdf

Yu, B.-J., & Ansari, F. (1996). Method and theory for nondestructive determination of fracture energy in concrete structures. *ACI Structural Journal*, *93*(5), 602–613. http://dx.doi.org/10.14359/9719

Zech, B., & Wittmann, F. H. (1977). *A complex study on the reliability assessment of the containment of a PWR. Part II. Probabilistic approach to describe the behavior of materials*. Paper presented at the 4th International conference on Structural Mechanics in Reactor Technology, San Francisco, California. Retrieved from http://www.iasmirt.org/transactions/04/J1-11.pdf

Zhou, F. P. (1992). *Time-dependent crack growth and fracture in concrete* (Doctoral dissertation). Lund, Sweden: Lund University. Retrieved from http://lup.lub.lu.se/luur/download?func=downloadFile&recordOId=1272876&fileOId=1651582

Zhou, F., & Molinari, J. F. (2004). Dynamic crack propagation with cohesive elements: a methodology to address mesh dependency. *International Journal for Numerical Methods in Engineering*, *59*(1), 1–24. http://dx.doi.org/10.1002/nme.857

Zienkiewicz, O. C., & Taylor, R. L. (2005). *The finite element method* (6th ed.). Butterworth-Heinemann: Elsevier.

Zollinger, D., & Barenberg, E. (1989). *Proposed mechanistic based design procedure for jointed concrete pavements* (Publication No. FHWA/IL/UI-225). Urbana, IL: University of Illinois at Urbana-Champaign. Retrieved June 18, 2015, from http://ict.illinois.edu/Publications/report files/TES-057.pdf

About the Joint Transportation Research Program (JTRP)

On March 11, 1937, the Indiana Legislature passed an act which authorized the Indiana State Highway Commission to cooperate with and assist Purdue University in developing the best methods of improving and maintaining the highways of the state and the respective counties thereof. That collaborative effort was called the Joint Highway Research Project (JHRP). In 1997 the collaborative venture was renamed as the Joint Transportation Research Program (JTRP) to reflect the state and national efforts to integrate the management and operation of various transportation modes.

The first studies of JHRP were concerned with Test Road No. 1—evaluation of the weathering characteristics of stabilized materials. After World War II, the JHRP program grew substantially and was regularly producing technical reports. Over 1,500 technical reports are now available, published as part of the JHRP and subsequently JTRP collaborative venture between Purdue University and what is now the Indiana Department of Transportation.

Free online access to all reports is provided through a unique collaboration between JTRP and Purdue Libraries. These are available at: http://docs.lib.purdue.edu/jtrp

Further information about JTRP and its current research program is available at: http://www.purdue.edu/jtrp

About This Report

An open access version of this publication is available online. This can be most easily located using the Digital Object Identifier (doi) listed below. Pre-2011 publications that include color illustrations are available online in color but are printed only in grayscale.

The recommended citation for this publication is:

Antico, F. C., Esmaeeli, H. S., De la Varga, I., Jones, W., Barrett, T., Zavattieri, P., & Weiss, W. J. (2015). *Removing obstacles for pavement cost reduction by examining early age opening requirements: Material properties* (Joint Transportation Research Program Publication No. FHWA/IN/JTRP-2015/18). West Lafayette, IN: Purdue University. http://dx.doi.org/10.5703/1288284316003